UNIVERSITY OF
KWAZULU-NATAL

INYUVESI
YAKWAZULU-NATALI

THE UNIVERSITY OF KWAZULU-NATAL

RAIN CELL SIZE ATTENUATION MODELLING FOR TERRESTRIAL AND SATELLITE RADIO LINKS

Peter Odero Akuon

2011

RAIN CELL SIZE ATTENUATION MODELLING FOR TERRESTRIAL AND SATELLITE RADIO LINKS

By Peter Odero Akuon

Submitted in completion of the academic requirements
for the degree of M.Sc. Engineering
in the Faculty of Engineering
at the University of KwaZulu-Natal, Durban, South Africa

December 2011

As the supervisor for the candidate, I have approved this dissertation for submission.

Signed: _____

Name: Professor Thomas J. O. Afullo

Date: 2nd December 2011

Declaration

I, Peter Odero Akuon, declare that

i.   Except where otherwise indicated, the report in this thesis, is my original work.

ii.   This thesis has not been submitted for any degree or examination in any other university.

iii. This thesis does not contain other persons' data, pictures, graphs or other information, unless specifically acknowledged as being sourced from other persons.

iv.   This thesis does not contain other persons' writing, unless specifically acknowledged as being sourced from other researchers.

Where other written sources have been quoted, then:

   a) their words have been re-written but the general information attributed to them has been referenced;

   b) where their exact words have been used, their writing has been placed inside quotation marks, and referenced.

v.   Where I have reproduced a publication of which I am an author, co-author or editor, I have indicated in detail which part of the publication was actually written by myself alone and have fully referenced such publications.

vi.   This thesis does not contain text, graphics or tables copied and pasted from the Internet, unless specifically acknowledged, and the source being detailed in the thesis and in the References sections.

Signed: _____

Acknowledgements

I must express my sincere gratitude to my supervisor, Professor Thomas J. O. Afullo, for his adept contribution towards the completion of this degree. His continual synergy in the research topic and reviewing of the topics in this dissertation was unyielding.

The unrivalled patience from my family especially my able wife, Rebecca and son Mae has been great during the course of this degree. The unvoiced but insuperable contributions from Mano have been enormous.
 I make a clean breast that your filial care has been incredibly inspiring. *Erokamano Nyar Ranalo*!

To all my neighbours, both at school and home I am grateful for your upbeat contributions.

Much approval to be associated with my current employer: The University of Nairobi, Kenya.

Thank you Almighty God in Heaven for the favour you offered me to complete this work successfully.

Abstract

There is need to improve prediction results in rain attenuation in order to achieve reliable wireless communication systems. Existing models require improvements or we need fresh approaches.

This dissertation presents a model of rain attenuation prediction for terrestrial and satellite radio links based on a novel approach. This approach postulates that the difference in rain attenuation for various locations is attributed to the dissimilar rain drop sizes and rain cell diameter sizes and that cell sizes derived from local measurements would depict the true nature of rain cells better than the cells derived from long term rain data gathered from different climates. Therefore all other link parameters used in the attenuation equation are presented by the use of mathematical analysis; but the rain cell size is derived from local rain rate measurements.

The physical link aspects considered in the mathematical attenuation model are: the Fresnel ellipsoid of the link path, the effect of elevation angle, the rain cell diameter size and the shape of growth of rain rates in the cell. The effect of the elevation angle of the link on the scale of attenuation is accounted for through the proposed coefficient of elevation equation. The coefficient of elevation is considered to modify the size of the rain cell diameter in proportion to the elevation angle of the link and the rain rate growth is taken to be of the truncated-Gaussian form. On the other hand, the rain cell diameter is derived from rain rate measurements as a power law model and substituted in the attenuation expression.

The rain cell size model evaluated in this dissertation is based on point rain rate measurement data from the disdrometer located at the University of KwaZulu-Natal, South Africa. The "Synthetic Storm" technique is applied to develop the rain cell diameter distributions and the rain cell diameter model. In addition, the impact of the rain cell diameter size model in site diversity and cellular network-area planning for the region is discussed.

To validate the model for terrestrial links, attenuation data collected from Durban, South Africa is used while that for satellite links, attenuation data from 15 links which are located in tropical climatic zones are used. In each case, the new model is tested against some well-known global rain attenuation prediction models including the standard ITU-R models. The performance of the proposed models for the sampled radio links based on error estimations shows that improvements have been achieved and may be regarded as a universal tropical model especially for satellite links.

Table of Contents

List of Figures

List of Tables

List of Acronyms

ACCF	accumulation time factor
BER	bit error rate
C-band	4 - 8 GHz
CCDF	complementary cumulative distribution function
CD	cumulative distribution
CDF	cumulative distribution function
COST-255	European concerted research action
dB	decibels
EIRP	equivalent isotropically radiated power
EXCELL	exponential cell
FSL	Free-space loss
GHz	giga-Hertz
GSM	global system for mobile communications
HYCELL	hybrid exponential cell
IDW	inverse distance weighting
IP	Internet Protocol
ITU-R	international telecommunications union-radio communication
Ka-band	26.5 – 40 GHz
km	kilometers
Ku-band	12 – 18 GHz
LOS	line of sight
LTE	long term evolution
NGN	next generation networks
PDF	probability density function
Q-band	30 – 50 GHz
RADAR	radio detection and ranging
RCDD	rain cell diameter distribution
SAWS	South African Weather Service
UPC	uplink power control
V-band	50 – 75 GHz

CHAPTER ONE

Introduction

1.1 Theory of Wave Propagation

Wave propagation paths used in communication systems are classified broadly as terrestrial and satellite links. As the waves propagate along these paths, they interact with propagation fade phenomena which can be divided into two broad classes: clear air and precipitation mechanisms. These mechanisms include: absorption, scattering, refraction, diffraction, multipath, scintillation and frequency dispersion. Various signal parameters are affected by these fade mechanisms which include the signal amplitude, phase, polarization, frequency, bandwidth and angle of arrival. For example, at 60 GHz, oxygen attenuation is very high in the order of tens of decibels per km (dB/km) and at 23 GHz, water vapour resonance results in signal absorption thus poses a major problem. The signal attenuation increases with frequency and therefore most high frequency bands only find applications in short range links [1–3].

With the knowledge of these signal properties, it is easier to plan microwave links which find applications in many spheres of modern technology. Microwave radio link application is considered in this work and the next section elaborates more on the link system design.

1.1.2 Microwave Radio Link Design

Many upcoming technologies today require frequency usage to achieve their intended goals. The growth in mobile telephone networks, smart phones and other radio communication systems has resulted in high demand for frequency resource. Nevertheless, there is imminent scarcity in frequency bandwidth to meet the increased demand. This drawback has seen the increase in other technologies that do not depend on radio frequencies e.g. optic fibre links. Despite this alternative solution, the advantages reaped from microwave links seem to encourage continuous research in utilizing higher frequency bands. In order to aid in the problem of scarcity, frequency spectrum management is exercised by governmental bodies to ensure secure use and healthy competition by network operators. The frequency spectrum is divided into different bands based on the signal wavelength. Today, many technologies e.g. The Global System for Mobile Communications, GSM utilize the Ka, KU and Q-bands. When the same frequency bands are used in the same area by different network operators, interference occurs and the communication integrity is lost. Also, for example, when less signal power is transmitted in a radio link, then the propagation losses may

Figure 1-1 Representation of radio link planning process

exceed the signal power and the carried message will be of poor quality or not available at the receiver. To solve this problem of under-provision or over-provision of frequency bandwidth, high precision is needed in radio link planning exercise. Fig. 1-1 is a summary of the steps involved in decision making for the best possible frequency bandwidth allocation. When the operator's licence is initially issued, frequency planning is managed in such a way as to solve the interference problem [4–6].There are some measurable or near-universal expected signal losses that occur in link systems; these may include the branching losses, equipment efficiencies, losses in transmission lines, waveguides, filters and splitters. They can be regarded as hardware system losses. Others are propagation losses through the clear-air and other forms of precipitation like snow, clouds and fog or mists. On the other hand, there are some path losses that require fade level predictions known as fade margin predictions. Examples in this class include rain attenuation, multipath, refraction and diffraction losses. Depending on the supported application, link planners need to strike the balance between availability of clear-air signal level and the quality of the transmitted signal in order to make the best provision for the fade margin. One of the methods employed by most radio link engineers is to make provision by considering the required link availability level. In some countries, this has become a licence requirement. For example, the link can be planned in such a way that if the hardware system remains in the on-status, the outage on the link is expected to occur only for 0.01% of the time in a year [5–6].
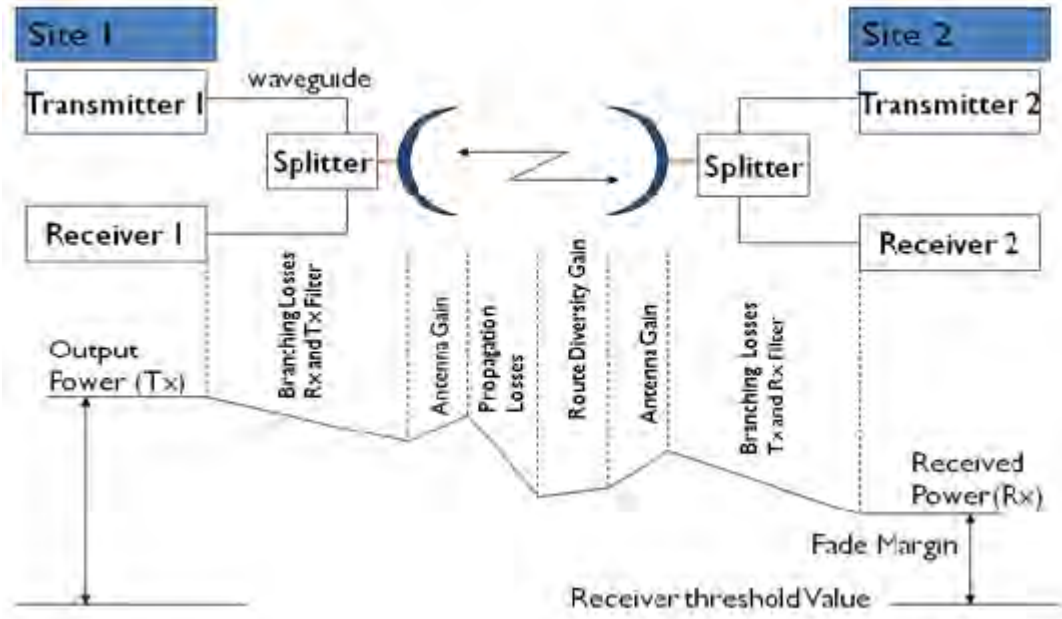
Figure 1-2 Sample attenuation margin allocations

This means that the desired received signal power level will be available 99.99% of the time in a year period despite the occurrence of the largest fade phenomena on the link. Fig. 1-2 summarises the fade margin calculations that are often met in link planning process. The receiver threshold value is set so that the radio equipment runs a constant bit error rate, BER. A typical value for BER is 10^{-6}. Another solution to this is the employment of forward error-correction methods. The transmitted power suffers branching and propagation path losses but the gain of the transmitting antenna and the receiving antenna provide for some of the losses. Various mitigation methods have been suggested that are used so as to achieve higher power levels on the receiver. Route or site diversity is used to increase the effective fade margin. Uplink power control, UPC or automatic transmitter power control are also some of the useful as mitigation techniques but their bandwidth of operation is limited due to the non-linear amplifier characteristics under increased power levels [3,7–8].

Besides, the major contribution of the fade margin depletion comes from rain attenuation especially for shorter wavelengths or frequencies higher than 10 GHz [9 –12]. The next section reviews some of the effects of rainfall on microwave links.
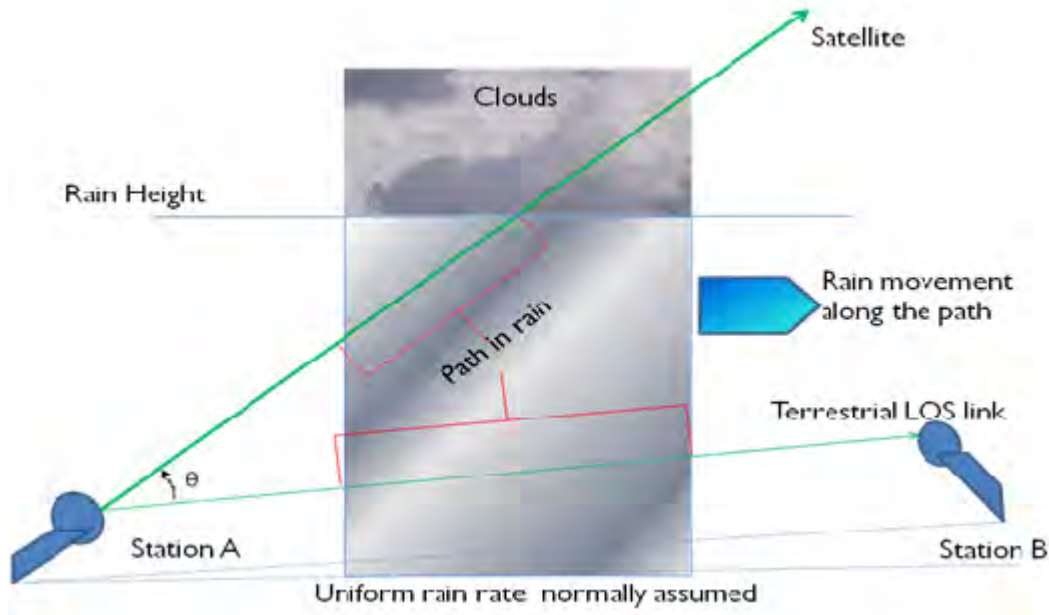
Figure 1-3 Description of the signal path through a single rain cell

1.1.3 Effects of Rainfall on Microwave Links

When rain occurs in a signal path and the received signal power reduces as compared to the transmitted one then that reduction in the power level is caused by that rain phenomenon and is referred to as rain fade or rain attenuation. Fig. 1-3 is a description of how a signal path may be represented by an occurrence of a single rain cell. There are various time varying occurrences that lead to rain attenuation: the rain drop number, rain drop water temperature, and the drop size distribution; spatial variation of rain and wind advection velocity of the rain form. The individual contribution of the rain drops can be summed up over a path length to compute the total attenuation or summed up as a distribution to compute the specific attenuation as a function of rain rate [12].

The rain attenuation increases when higher frequencies are used in transmission links though there is a desire for the higher data rates that are offered by those frequencies [3, 5–6, 12]. Rain attenuation in the C-band and Ku-bands is minimal and is easily accommodated in radio link planning. However at higher frequencies e.g. the Ka-band or even V-band, the signal degradation is so high that more compensation for signal loss needs to be provided. This is simply because the electromagnetic waves are scattered thereby causing diffusion or absorbed by liquid rain drops thus losing energy through molecular resonance [5–6]. Attenuation through absorption increases with frequency: high frequency waves have smaller wavelengths in the order of rain drop sizes.

For example, rain drops from measurements from disdrometer exhibit size ranges in the order of 0.5 to 5 mm [13]; a V-band frequency of 40 GHz has a wavelength of 7.5 mm. These sizes are comparable thus increasing the extent of absorption. It is therefore imperative to estimate the actual magnitude of attenuation expected from rain absorption and scattering mechanisms. On the other hand, path attenuation is caused when the radio wave propagation path is intersected by a rain cell(s). It is noted that by angular orientation, the path intersection for a satellite link differs from that of the terrestrial microwave link. The intersection occurs in the form of deep fades when rain-cell(s) fills a fairly significant part of the Fresnel's ellipsoid (or simply the path) between the transmitting radio and the receiving radio through absorption and significantly by scattering processes [1,12–13]. Rayleigh scattering is caused mainly by drizzle rain form (for Ku-band signal, average drop size ≤ 0.4 mm) while Mie scattering is caused by average to heavy rain forms (drop size>0.4 mm) [1]. This attenuation scenario therefore necessitates accurate results for predicting the rain attenuation magnitudes in order to eliminate the possibilities of a signal degradation or eventual loss.

Today, the question still is, what should be the appropriate fade margin and at which site locations? A method with a global applicability could be the answer. This question has led to continual development of rain attenuation prediction models.

1.2   Rain Fade Prediction Modelling

Presently, various analyses have been employed to estimate the effects of propagation through rain. Physical modelling involving theoretical formulations have been attempted that require complete knowledge of the rain medium and all the boundaries, though this is not readily feasible. Other quasi-empirical methods are used today to address this uncertainty. The methods make use of assumptions of propagation physics that affect the attenuation magnitudes and derive parameters from rain meteorological statistics but does not compare with attenuation statistics to adjust the derived parameters. On the other hand, empirical models use a summary of statistics of the path performance sourced from a collection of measurements which has always been from mid latitude and continental climate locations. The method involves extrapolating them with given occurrence probabilities to different frequencies and sites by using measured attenuation and rain rate statistics to set the model parameters. This is called modelling by regression. Regression modelling can be applied in attenuation prediction by using existing attenuation measurements and applying them in any attenuation equation to derive the regression coefficients [3,5–6], and is useful if large data base of attenuation measurements is available and accessible like those maintained by the ITU-R.

Also, some sites like those found in tropical regions lack these large attenuation databases. The other method is to use a physical randomly-occurring scenario with similar characteristics of rainfall to model the parameters of attenuation or to use a semi-empirical approach.

Several approaches have been suggested that are used in prediction of rain attenuation: we have analytical models used for determination of the specific attenuation [12, 14–16], effective path length models [5–6, 17–20] and "Synthetic Storm" models [21–24]. Other ways of modelling include rain cell-shape profile models [25–32] and path-average rain rate models [3]. The variation in the methods depends on how the effective path length is computed. But, more specifically the accuracy of the approaches varies in whether or not attenuation is assumed to grow uniformly or not along the path. It has been observed that the growth of rain attenuation with rain rates is not uniform in a given rain event [3, 5–6]. Some other models give predictions at some percentage of time e.g. the ITU-R model while others give predictions based on the full rain rate. Another class of models are improvements on the existing ones. The next section is a review of rain-fade modelling classes: specific attenuation, effective path length, rain cell-shape profiling methods and the "Synthetic Storm" technique.

1.2.1   Specific Attenuation due to Rain

The absorption and scattering effects of rain drops depend on the relation between the rain drop size and the wavelength of the transmitted energy. Several rain drops constitute a rain cell. The sum of the contribution of these drops for each rain rate causes attenuation on the transmitted signals. Based on Mie scattering theory, the specific attenuation is computed by considering several factors: the complex refractive index of water at the drop temperature, terminal drop-velocity and the rain drop diameter distribution [12–15]. The specific attenuation is then expressed as:

$$\gamma = 4.343 \int_{0}^{\infty} Q_{t}(D) N(D) \, dD \qquad (1\text{-}1)$$

where $Q_t(D)$ is the extinction cross-section, $N(D) \, dD$ is the raindrop number density with equivalent drop diameter D in the interval dD.

$Q_t(D)$ is a theoretical result determined from classical scattering theory developed by Mie for frequencies above 3 GHz. Normally, Rayleigh approximation is used for frequencies in the range 1-3 GHz. The total Qt (D) is the sum of the contribution from absorption and scattering. In the calculations, it is normally assumed that: (1) rain drops are spherical (or oblate spherical) in shape, (2) rain drops are uniformly distributed in the area bound by the field of the waves and (3) rain

drops are sufficiently separated from each other to avoid mutual interaction. The $N(D)$ is estimated from measurements or by application of rain drop size distribution prediction models. Many prediction models have been proposed so far to model rain drop size distribution but variations are seen to exist according to the climate of the location of interest. Currently, attempts are being made to describe rain drop size distributions in Southern Africa from measurements made in Durban [13]. Some models of the distribution include negative exponential, Gama, log-normal, power law and Weibull models. The rain rate and drop size relationship used in the disdrometer measurement equipment is expressed as:

$$R = 6\pi \times 10^{-4} \int_0^\infty D^3 N(D)V(D)d(D) \qquad (1\text{-}2)$$

where R is the rain rate and $V(D)$ is the terminal velocity of rain drops [13].

In an attempt to simplify (1-1), Olsen *et al.* expressed specific attenuation in to take the form:

$$\gamma = kR^\alpha \qquad (1\text{-}3)$$

where k is a factor that depends on the wave frequency for a given model of the rain microstructure and the α-factor depends on the polarization at a given tilt angle [12-15].

Also, based on the work of Fedi, 1979 and Maggiori, 1981 the values k and α were calculated for frequencies between 1 and 400 GHz for oblate spheroid rain drop shapes at 20^0C temperature by the use of 1943 Laws and Parsons drop size distribution; terminal drop velocity following Gunn and Knizer's 1949 work and the refractive index values according to the model of Ray, 1972. These values were adopted by ITU-R [12] and are currently used to compute specific attenuation the world over where site-specific measurements are not available.

1.2.2   Effective Path Length and Path Reduction Factor

Rain is characterized by horizontal variability and appears to be more convective in tropical regions. In actual estimation of the total attenuation due to rain in a given link, the effective path length is determined to account for the non-uniformity of rain rate along the path of propagation.

The path length reduction factor (r) is a general concept used in many rain attenuation modelling methods to cater for the non-uniformity of precipitation (in this case rain) rate along the propagation link between two stations [5–6, 17–20]. It is defined as the ratio of an effective path

length, L_E on which the rain rate intensity, R is considered uniform to the actual path length, L between the two terminals. To evaluate this path length reduction factor, the measured or predicted rain attenuation, A [dB] exceeded for any given percentage of time is divided by the specific attenuation for that same percentage of time:

Thus, the attenuation is expressed as the product of specific attenuation and the effective path length:

$$A = \gamma L_E \qquad (1\text{-}4)$$

where L is the actual path length and the effective path length is the product of the actual distance between the transmitter and the receiver stations and the path reduction factor:

$$L_E = rL \qquad (1\text{-}5)$$

However, the path intersection for a satellite link is considered different and normally referred to as slant path due to the vertical variability of rain structure and the difference in elevation [6].

1.2.3 Path-Average Rainfall Rate Attenuation Analysis

A path-averaged rain rate is calculated based on the point rain rate. The average rain rate is related to the point rain rate by [3].

$$\bar{R} = f_1(d)R^{1+f_2(d)} \qquad (1\text{-}6)$$

where d denotes the path length, while f_1 (d) and f_2 (d) are derived empirically.

This Global Crane model is summarized in the following set of equations:

$$A= aR^b[(e^{-ubd} - 1)/ub] \quad (\text{for } 0\leq d \leq D_0) \qquad (1\text{-}7)$$

$$A=aR^b\left[\frac{(e^{-ubd}-1)}{ub} - \frac{B^b e^{cb}D_0}{cb} + \frac{B^b e^{cbd}}{cb}\right] \qquad (1\text{-}8)$$

$$(D_0 \leq d \leq 22.5 \ km) \qquad (1\text{-}9)$$

where $D_0 = 3.8 - 0.6\ln(R)$ [km] , $B = 2.3R^{-0.17}$, $c = 0.026 - 0.03\ln(R)$,

$$u = \ln[Be^{cD_0}]/D_0$$

and A (dB) is the rain attenuation, R (mm/hr) is point rain rate, and d (km) is path distance. a and b parameters are functions of frequency and polarization respectively which are tabulated for the different global zones [5].

1.2.4 Rain Cell Profile Attenuation Analysis

In rain cell profile modelling, the shape, rain rate intensity profile, motion, size and the spatial density of rain cells in a given area are considered. Rain cell is an intense rainfall structure whose spatial dimensions is about 5-10 km and appears to be imbedded in the areas of highest widespread rainfall [33]. The cell tends to last around 30 minutes and to produce a peak precipitation rate of about 50–100mm/h in New England [34].

From radar reports [30, 35], rain cells show the distribution of the precipitation about the intensity peak. Various shapes have been proposed in the past: cylindrical, circular, elliptical, basic top-hat profiles [25], Power-law [26], Gaussian [27–28], or exponential shapes (EXCELL) [29]. In a concerted effort to parameterize the actual shapes, rain events have been defined as regions where the rain rate exceeds some threshold. This phenomenon has been so because of the prominent difficulty in modelling the rain rate horizontal variation within the cells through a single physical mathematical function. Observations made from radar [35] show that the horizontal rain rate distribution about the rain cell peak decays as Gaussian rather than the abrupt exponential function. A precise rain-cell profile needs to be defined by various elements that include the rainfall volume (radius of the cell), local geology, climate and the maximal rain intensity R_{max} at the centre of the rain cell to achieve accurate prediction results. Nonetheless, where rain accumulation is the parameter of interest, the profiling based on constant rain rate within cell has been useful in hydrological modelling. Allowing smoother variation of rain rate within cells is expected to yield better second order statistics, for example, correlating rain fade effects on two links. The point rain intensity value, R, for various rain cell models can be derived from the basic rain cell specification and the distance, d, being from the centre of the rain cell along the specified path by the following relations:

a) Cylindrical rain cell model:

$$R= R_{max} \quad \text{constant, where } d< \text{Radius, } \rho \tag{1-10}$$

Figure 1-4 Cylindrical rain cell shape model

b) Gaussian rain cell model,

$$R = R_{max} . e^{-\frac{1}{2}(\frac{3d}{0.8\ Radius})^2} \tag{1-11}$$

where $d < \rho$

c) Exponential (EXCELL) rain-cell profile,

$$R = R_{max} . e^{\frac{4d}{\rho}} \tag{1-12}$$

where $d < \rho$

A physical approach, hybrid cell (HYCELL), has been used to model rain cells depending on a hybrid distribution of the rain rate profile: a Gaussian distribution for the inner convective core and an exponential distribution for the stratiform outer part of the cell [30].This HYCELL model produces annual fade distributions and is suitable in the description of the small scales rain rate spatial variability which has been important. The EXCELL model was later refined by Paraboni *et al.* [31] that extended its use to very minimal rates, R, where:

$$R = R_{\mathrm{M}} + R_{low} e^{-\rho/\rho_0} - R_{low} \tag{1-13}$$

$$\rho_{\max} = \rho_0 \ln \left[\frac{R_{\mathrm{M}} + R_{low}}{R_{low}} \right] \tag{1-14}$$

where ρ is a path distance from the peak, R_{M} being the peak rain rate, ρ_0, is a cell radius at R_M/e as shown in the Fig. 1-5.
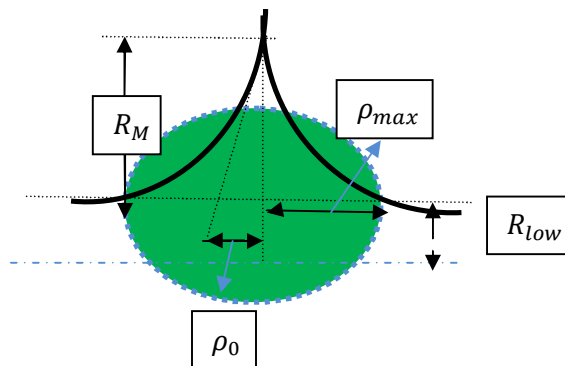
Figure 1-5 Diagrammatic representation of the modified EXCELL model [31]

Other developments include truncated exponential rain cell, combining the exponential shapes with the cylindrical shapes and conversely avoids the limits of path length factor greater than one, which is inherent in other rain cell prediction methods. This has been discussed by Assis *et al*. [32] and the symmetry is defined by:

$$R(x) = R_m / e \quad \text{for } |x| \leq \rho \tag{1-15}$$

$$R(x) = R_m \, e^{-x/\rho} \quad \text{for } \rho \leq |x| \leq d \text{ where } d = 2\,\rho \tag{1-16}$$

Then the calculation of rain attenuation across a rain cell can be computed by using the equation:

$$A_{incell} = \int_0^l k . R^\alpha(x) \, dx \tag{1-17}$$

where $R(x)$ being the rain rate at any position x along the path, k and α are the respective frequency and polarization dependent parameters , see ITU-R P.838 [12].

Even though the methods based on the rain rate profiles in the rain cell can easily be adopted for horizontal variability in terrestrial links, the calculation in (1-17) may not apply for satellite link due to the nature of vertical variability of rain forms.

Another method is to generate the rainfall rate-dependent equivalent rain cell size and use it in determining the effective path length which is consequently applied in attenuation prediction.
The following section describes the method used in transforming time series point rainfall rate into the spatial rain cell size distribution. The technique applied is called "Synthetic Storm".

1.2.5 "Synthetic Storm" Technique

Theoretically, the attenuation due to rain along a path of length, L would be expressed in terms of specific attenuation per unit length as [36]:

$$A = \lim_{n \to \infty} . \sum_i^n a \, R_i^b \, \frac{L}{n} \tag{1-18}$$

where R_i is the distribution of rain rate in space along the path, n is the number of rain cells, a and b are coefficients dependent on frequency and polarization respectively.

But the application of (1-18) as it is in predicting the attenuation statistics may not be practical since it would require several rain gauges in the area to accurately measure the spatial distribution.
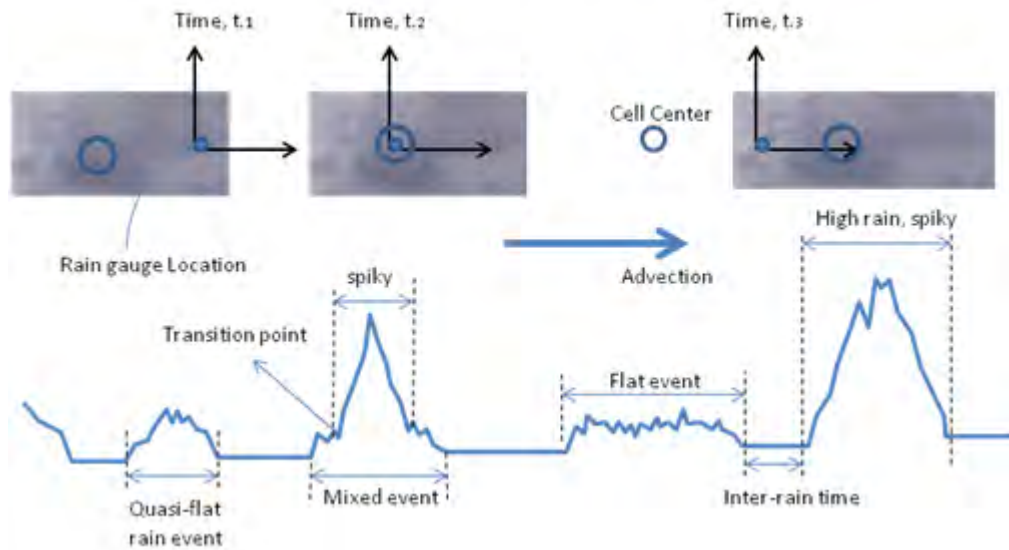
Figure 1-6 Space-time rain cell derived from a point rain-rate from a rain gauge [21]

A rain event may commence with a quasi-flat growth of rain rates at a time t.1 and develops into a spiky profile at time, t.2. If this rain event passes over a point rain rate measurement equipment, then the time taken by a portion of rain form to move from the equipment to another point can be transformed into distance if the average advection velocity of that portion of the rain form is known and is assumed to be constant [21–25]. When this procedure id repeated for all rain events in a given location, the path intersections can be used in (1-18) to compute attenuation. This technique is known as "Synthetic Storm". Fig. 1-6 illustrates the movement of a rain cell over a rain gauge. The rain cell velocity may be divided into two: for the stratiform range ($0 \leq R \leq 12$ mm/h) and the convective range of rain rates ($12 \leq R \leq 20$ mm/h and above) [37–38].

1.3 References

[1] Ippolito L. J., *Radio wave Propagation in Satellite Communication*, [Chapters 4, 5 and Appendix 6.] *Van Nostrand Reinhold Company: New York*, 1986.

[2] T. Pratt and C.W. Bostian, *Satellite Communications*, pp.345-346, A Wiley Interscience Publication, John Wiley & Sons Inc, 1988.

[3] C. K. Crane, *Electromagnetic Rain Propagation through rain*, John Wiley & Sons, Inc. 1996.

[4] M. Marcus and B. Pattan, *"Millimetre Wave propagation-Spectrum Management Implications," IEEE Microwave Magazine*, Vol. 6, pp. 54- 61, June 2005.

[5] Propagation data and prediction methods required for the design of Earth-space telecommunication systems, ITU-R Rec. P.618-9, 2007.

[6] Propagation prediction techniques and data required for the design of terrestrial line-of-sight systems," Recommendation ITU-R 530-10, 2003.

[7] A.D. Panagopoulos, P. M. Arapoglou, J. D. Kanellopoulos and P. G. Cottis, "Long Term Rain Attenuation Probability and Site Diversity Gain Prediction Formulas", *IEEE Transactions on Antennas and Propagation*, vol. 53, no. 7, July 2005.

[8] E. Matricciani, "Prediction of orbital diversity performance in satellite communication systems affected by rain attenuation," *Intern. Journal of Satellite Communications*, vol. 15, pp.45-50, 1997.

[9] Crane, R.K, "A two-component rain model for the prediction of attenuation statistics", *Radio Science,* Vol.17, N.6, 1371-1387, 1982.

[10] G.O. Ajayi and E.B.C. Ofoche, "Some tropical rainfall rate characteristics at Ile-Ife for microwave and millimetre wave application," *J. of Climate and Applied Meteor.*, vol. 23, pp. 562–567, 1983.

[11] F. Moupfouma, "Rainfall-rate distribution for radio system design," *IEEE proceedings*, vol. 134, pp. 527-537, Feb. 1987.

[12] "Specific attenuation model for rain for use in prediction methods," ITU-R, Geneva, 2005, ITU-R Rec. P.838-3.

[13] Afullo T.J.O, "Raindrop size distribution modelling for radio link design along the eastern coast of South Africa," *Progress In Electromagnetics Research B*, Vol. 34, 345-366, 2011.

[14] Olsen, R. L., D. V. Rogers, and D. B. Hodge, "The aR^b relation in the calculation of rain attenuation," *IEEE Transaction on Antennas and Propagation*, Vol. 26, 318-329,1978.

[15] Moupfouma F. "Rain induced attenuation prediction model for terrestrial and satellite-earth microwave links," IEEE, Vol.42, 539-550, 1987.

[16] Fashuyi M. O. and Afullo T. J. O, "Rain Attenuation Prediction and Modelling for Line-of-Sight Links on Terrestrial Paths in south Africa," *American Geophysical Union: Radio Science*, Vol. 42, Oct. 2007.

[17] "Radio wave propagation modelling for SatCom services at Ku-Band and above," *COST Action 255, European Space Agency*, 2005.

[18] Dissanayake A, Allnutt J, Haidara F. A prediction model that combines rain attenuation and other propagation impairment along earth-satellite paths. *IEEE Transactions Antennas Propagation* 1997; 45:1558–1564.

[19] Abdulrahman A. Y., Rahman T. A., Rahim A. S. K., Ul Islam M. R. "A new rain attenuation conversion technique for tropical regions," *Progress In Electromagnetic Research,* Vol. 26: pp.53-67, 2010.

[20] Adhikari A., S. Das, A. Bhattacharya, and Maitra A., "Improving rain attenuation estimation: modelling of effective path length using KU-band measurements at a tropical location," *Progress In Electromagnetics Research B*, Vol. 34, 173-186, 2011.

[21] Fontan F. P., Nunez A., Valcare A. and Fiebig U. C., "Converting simulated rain-rate series into attenuation series using the synthetic storm technique," *Propagation Impairment Mitigation for Millimetre Wave Radio Systems, COST Action* 280, June, 2005.

[22] Kanellopoulos D. and Kafetzis P., "Comparison of the Synthetic Storm technique with a conventional rain attenuation prediction model," *IEEE Transaction on Antennas and Propagation,* Vol. 34, 713-715, 1985.

[23] Matricciani E., Carlo Riva, "Concurrency of rain rate attenuation statistics in slant paths: Test with the Synthetic Storm Technique," *EuCAP 2007*, Edinburgh, 11-16, November, 2007.

[24] F. P. Fontan, A. Nunez, A. Valcarce and U. C. Fiebig., "Converting Simulated Rain-rate Series into Attenuation Series Using the Synthetic Storm Technique", COST Action 280, *3rd International Workshop*, June 2005.

[25] Cox, D. R. and Isham, V., "A simple spatio-temporal model of rainfall," *Proc. R. Soc*. Lond., 415(A), 317–328, 1988.

[26] Ferraris, L., Gabellani, S., Rebora, N., and Provenzale, A. "A comparison of stochastic models for spatial rainfall downscaling", *Water Resour. Res.,* 39, 1368–1384, 2003.

[27] Eagleson, P., Fenessey, N., Quiliang, W., and Rodriguez-Iturbe, I., "Application of spatial Poisson models to air mass thunderstorm rainfall" *J. Geophys. Res*., 92(D8), 9961–9978, 1987.

[28] Waymire, E., Gupta, V., and Rodriguez-Iturbe, I., "A spectral theory of rainfall intensity at the meso-beta scale", *Water Resour. Res.,* 20, 1483–1465, 1984.

[29] C. Capsoni, F. Fedi, C. Magistroni, A. Paraboni, A. Pawlina: "Data and theory for a new model of the horizontal structure of rain cells for propagation applications, *Radio Science*, Vol. 22, n°3, pp. 395-404, 1987.

[30] L. Féral, F. Mesnard, H. Sauvageot, L. Castanet, J. Lemorton: "Rain cells shape and orientation distribution in South-West of France", *Phys. Chem. Earth (B)*, Vol. 25 no.10-12, pp. 1073-1078, 2000.

[31] Paraboni A., G. Masini, C. Riva, 1998, "The spatial structure of rain and its impact on the design of advanced TLC systems", *Proc. Fourth Ka Band Utilization Conf.* Nov. 2-4, 1998, Venice, Italy, pp. 169-172.

[32] Assis Mauro S., L. A. R. da Silva Mello and Jorge L. Cerqueira, 'Rain Attenuation Research in Brazil', URSI GA 2005.

[33]   A. Pawlina-Bonati,'Essential Knowledge of Rain Structure for Radio Applications Based on Available data and Models, '*Proceedings of Radio Africa 99, Gaborone, Botswana, October 1999,* pp. 96-106.

[34] Austin, P. and Houze, R. "Analysis of structure of precipitation patterns in New England"*, J. Appl. Meteorol.*, 11, 926–934, 1972.

[35] A. Pawlina, M. Binaghi, "Radar rain intensity fields at ground level: new parameters for propagation impairments prediction in temperate regions," *Proc. of the 7th URSI Comm. F Open Symp. On Wave Propagation and remote sensing, Ahmedabad, India*, pp.217-220, Nov.1995,

[36] Olsen, R.L., Rogers, D.V., Hodge, D.B., "The aR^b Relation in the Calculation of Rain Attenuation," *IEEE Trans. On Antennas and Propagation*, vol. AP-26, no.2, March 1978, pp. 318-328.

[37] Drufuca G, Zawadzki I, "Statistics of rain gauge data", *Journal of Applied Meteorology*, Vol. 14, December, pp. 1419- 1429, 1975.

[38] S. Begum, C. Nagaraja, I. Otung, "Analysis of rain cell size distribution for application in site diversity," *IEEE Antennas & Propag.*, pp.1–5, 2006.

1.4   Research Motivation and Contributions

It has been noted that so far, the existing ITU-R standards underestimate attenuation on links situated in tropical sites. Numerous attenuation and rain rate measurement data exist but the majority were obtained from temperate locations. The data is used to determine the effective rain rate or the equivalent rain cell diameter. The use of these results so far shows that there is need for improvements in rain attenuation prediction.

The proposed approach deviates from the existing ones and is based on the fact that the physical features of a rain cell are unique for each given location thus the rain cell model so derived from local measurements gives a better comparison to the real rain cell than the integrated rain rate data from large databases. This way, the resulting rain cell size should give a better overall result when used in rain attenuation prediction.

The single improved and universal rain attenuation model will be used by network planning engineers for initial link implementation and continual mitigation applications both for terrestrial and satellite radio links. The simple model for both terrestrial and satellite radio links is desired for ease of implementation. The rain cell size is also a requirement for site diversity planning. Therefore, the rain cell size so developed will aid in link area and network area designs for Southern Africa, an important data which is currently unavailable.

1.5   Organisation of dissertation

The rest of this dissertation is organized in the following way:

Chapter two presents the methodology used to derive the rain cell size from point rain rate measurements using 1-minute integration time data. A new approach is presented where the rest of the data available in 1-hour integration time for various locations are converted and used to develop the rain cell sizes for those locations. The results are then used to map site diversity separation distances for Southern Africa.

Chapter three follows with the approach used to model rain cell area for application in network area planning by the use of the generated rain cell diameter distribution, RCDD. This is achieved by producing the rain cell number density distribution from point rain rate measurements and synthesis of the area parameters by the use of statistical method of moments.

Chapter four describes the proposed method used to estimate rain attenuation on terrestrial links. Link measurements have been used to carry out comparison tests for the proposed model. The rain attenuation is taken to follow a truncated-Gaussian rain rate growth. The proposed model has the best performance for the site. In another test, the result in chapter three for the RCDD is used to model attenuation growth and the postulation is proved to be adequate.

Chapter five gives the final contribution where the proposed attenuation prediction model for satellite links is presented and used in comparison tests with other two models. Attenuation is assumed to growth with rain rates in the test analysis. The growth of rain rates is assumed to be a truncated-Gaussian form. The proposed model gives the least RMS error in both cases.

Chapter 6 is the discussion for the conclusions and the future direction of the work presented. This is followed by the appendices of the derivations made to obtain the attenuation equations used in this dissertation.

The work in this dissertation is in the following publications:

Akuon P. O. and Afullo T. J. O., "Rain cell size statistics from rain gauge data for site diversity planning and attenuation prediction," *Proc. of Southern Africa Telecommunication Networks and Applications Conference (SATNAC),* East London, South Africa, pp.213-216, 4-7th Sept. 2011. ISBN: 978-0-620-50893-3.

Akuon P. O. and Afullo T. J. O., "Rain cell sizing for the design of high capacity radio link systems in South Africa," *Progress In Electromagnetics Research Jrnl. B*, Vol. 35, pp. 263-285, Nov.2011. These two papers are produced from this work in Chapter 2.

Akuon P. O. and Afullo T. J. O., "Path reduction factor modelling for terrestrial links based on rain cell growth," *Proc. of IEEE Africon conference*, Livingstone, Zambia, 13-15th Sept. 2011. ISBN: 978-1-61284-991-1.This is a direct publication from Chapter 4 of this work.

Akuon P. O. and Afullo T. J. O. "Negative power law attenuation estimation for rainy Earth-Space radio links," *Progress In Electromagnetics Research Symposium, Kuala Lumpur, Malaysia,* March, 2012. Chapter 5 of this dissertation forms the basis of this paper.

CHAPTER TWO

Rain Cell Sizing

2.1   Abstract

Rain cell size is an input requirement for rain-induced attenuation studies. It is useful in estimating the extent of a given radio link path that will traverse the rain medium in a given rain event. The "Synthetic Storm" approach, which requires 1-minute integration time data, is used to derive the proposed rain cell sizes for various climatic zones within South Africa. The conversion of the readily available 1-hour integration time rain rate data to the desired 1-minute rain rate is carried out first for some locations and then validated by the existing measurement data and proposed global conversion factors. By the use of rain-induced attenuation prediction equation for terrestrial links that requires rain cell size as input, contour plots of specific attenuation for two high bandwidth frequencies used in terrestrial link implementations are presented. Site diversity separation distance map is proposed as well from the link budget analysis for each location to achieve an all time link availability of 99.99% of time.

2.2   Introduction

There is a continual evolution of telecommunication technologies today partly as a result of the problems and limitations encountered in the use of high capacity radio links. Fibre optic transmission is an alternative for signal transmission praised for its high bandwidth transmission capability but is highly prone to accidental damage making it a comparatively insecure channel with rampant maintenance requirements expected. The growth in smart phones acquisition by subscribers is expected to increase the demand for services like Internet connectivity, multimedia and video-streaming, and digital television thus increasing bandwidth demand. Therefore, there is rising need to fully utilize the microwave spectrum especially the 10 GHz and above. However, these frequencies are prone to undesired signal attenuation as they pass through precipitation due to their relatively small wavelengths. While the effects of precipitation agents have remained a major disturbance of the transmitted radio signals in terrestrial and satellite systems, the effects of rainfall are more significant. Therefore, rainfall attenuation studies have been of interest, particularly to radio link planners for signal transmission at millimetre wavelengths. There is need to model rainfall more fully by determining the size of rain cells for a given rain rate threshold and the growth of rain rates in order to achieve more accurate global attenuation prediction results. This is so because, it is the rain structure that varies from one location to another. ITU-R [1] and many

other authors including [2–6] have suggested the need for determination of the rainfall rate parameter, $R_{0.01}$, to obtain precise calculations involving attenuation studies. $R_{0.01}$, (mm/h) defined as the rainfall rate exceeded for 0.01% of time in a year, helps radio system engineers to predict the expected worst case rainfall attenuation that would occur at that percentage exceedance level. Values of $R_{0.01}$ can be obtained from the available rainfall rate data in ITU-R data bank or from long term local measurements. These values are dependent on the integration time of the measurement device in use. Many researchers [7–8] have suggested the use of integration times of 1-minute as the most suitable. Rainfall studies in Africa [4–7], [9–10] and South African region [11–13] have suggested the need for adequate rainfall data at 1-minute integration time, which are scarce. However, higher integration time data (hourly, daily and even, monthly) are available from many weather stations. Thus, the scarcity of 1-minute rainfall data requires conversion from higher integration time rainfall rate data obtained from the location under consideration by the use of suitable conversion techniques [8, 14–20]. An attempt is made to predict the expected $R_{0.01}$ values for South Africa by the use of the available 1-hour integration time data. Section 2.3 describes the conversion method adopted for this work based on power law relationship which is presently recommended by the ITU-R. The results obtained for the South African rain regions are then used to determine the equivalent rain cell diameter size in section 2.4. Based on an earlier work on terrestrial link attenuation prediction, the rain cell size model is used in Chapter 4 to produce attenuation maps for the region. Chapter 3 presents the proposed separation distance mapping for site diversity in South Africa, a useful technique employed in rain attenuation alleviation methods.

2.3   Methodology and Results

2.3.1 Integration Time Rain Rate Conversion

The rain rate measurements are obtained from the communications centre in the School of Electrical, Electronic and Computer Engineering, Howard Campus, the University of KwaZulu-Natal, Durban, South Africa. The Joss-Waldvogel disdrometer set up at the centre is connected to a terminal computer which records 1-minute integration time data.

The data is collected over a period of two years (January 2009 – December 2010) with minimal equipment outages. Table 2.1 shows the number of rain events. The hourly data for Durban and all other locations were obtained from the South African Weather Service (SAWS) data bank for a period of five years. Rainfall rate conversion adopted here involves the process of converting rainfall rate values from a higher integration time to a smaller integration time.

Table 2-1 Number and duration of rain events in each threshold

Rain event threshold Number of Events	Total duration (hours)			
	$R \geq 3$ mm/h (466)	$R \geq 5$ mm/h (467)	$R \geq 12$ mm/h (225)	$R \geq 20$ mm/h (108)
Convective ($R \geq 12$ mm/h)	420	420	420	163
Stratiform ($R < 12$ mm/h)	1287	737		
Stratiform and Convective	1707	1157		

The conversion is unique to a particular region because it involves the geographical and climatic properties of a location. While notable methods of conversion have been developed [8, 10–19], it is interesting to note that some of these methods depend on the prevailing climatic factors. The rainfall rate conversion methods have been classified into three categories by Emiliani *et al.* [20] namely: physical-stochastic, empirical and analytical methods. In classifying the methods, they considered the modelling, procedural influences and physical processes involved in the rainfall rate conversion. ITU-R also specifies the power-law conversion for some countries and regional maps exist showing regional values for $R_{0.01}$ (see ITU-R 837-5). It should be noted that the ITU-R method is empirical as it considers rainfall data within a location to derive conversion parameters. Interestingly, other empirical methods including that of Flavin [14] and Segal [15] are based on power-law conversion methods. This method was used by Ajayi and Ofoche [7] to derive rain conversion parameters in several locations in Nigeria. Owolawi *et al*. have introduced various rain rate conversion methods for application in the South African region: Hybrid, Linear, Power and Polynomial. The polynomial method was tested as the best method for the ten year, 5-minute rain rate data from 21 stations in South Africa [19, 21, 27].

The power-law conversion function in ITU-R 837-5 [1] is given by:

$$R_1(P_T) = \alpha[R_\tau(P_T)]^\beta \qquad (2\text{-}1)$$

where α and β represent the conversion coefficients of the rainfall rates $R_1(P_T)$ and $R_\tau(P_T)$ at the 1-minute and τ-minute integration times respectively at equal probabilities P_T.

Studies have shown climatic variations particularly between the Eastern Coasts and Western Coasts of South Africa [18, 21–22]. In this work, we derive rainfall rate parameters α and β for Durban based on empirical data and extend this relationship to other sites in South Africa. This approach caters for the variation of climatic conditions at several locations in South Africa.

By utilizing the available 2 year, 1-minute rain rate data from the disdrometer, we simulate our conversion method, based on the power-law empirical method of Watson *et al.* [8] to determine our parameters for the various locations selected for this study. The derivation of rainfall rate conversion factors for different locations is achieved by comparing the hourly data between Durban and other cities. Through this approach, we obtain regression coefficients α' and *β'* for the relationship between Durban and those cities. Consequently, we use (2-1) to compute the conversion factor for the 1-minute and hourly measurements for Durban at equal rain rate probability exceedances. From [1] the relationship is given as:

$$R_1 = \alpha'[R_{60}]^{\beta'} \tag{2-1}$$

where α' and β' are the regression coefficients obtained for Durban.

By comparing the respective hourly data between other cities and Durban at equal rainfall rate probability exceedances, we get another set of expressions with regression coefficients α" and β" as expressed in (2-3):

$$R_{60,\ X} = \alpha''[R_{60,\ Durban}]^{\beta''} \tag{2-3}$$

where *X* represents the location being compared with Durban in the 1-hour data.

On the basis of (2-2) and (2-3), we obtain the values of α and β in equation (2-1) by multiplying the regression coefficients in (2-2) and (2-3) thereby defining unique values for each location. Firstly, we use the derived coefficients for Durban to convert the hourly-data from other towns to their equivalent 1-minute values. Thus,

$$R_{1,\ X} = \alpha'[R_{60,X}]^{\beta'} \tag{2-4a}$$

where $R_{1,\ X}$ is the 1-min rainfall rate for a given town.

But since we have derived the relationships between the hourly data for Durban and those of other towns as expressed in (2-3), the 1-minute results obtained in (2-4a) are then transformed by the coefficients α'' and β'' to obtain the exact values for those towns. This way, we assume that the transformation of the hourly data between Durban and any other town give the same results that would be obtained if 1-minute data were transformed between Durban and any of the towns. This assumption is validated later with the comparison tests in Table 2-4. Thus, the new 1-minute rain rate value for any town is given as:

$$R_{1, X..} = \alpha'' \left(\alpha' \left[R_{60,X} \right]^{\beta'} \right)^{\beta''} \tag{2-4b}$$

From (2-4b), the overall regression coefficients can then be defined such as expressed in (2-4c) and (2-5):

$$\alpha = \alpha''(\alpha')^{\beta''} \tag{2-4c}$$

$$\beta = \beta''\beta' \tag{2-5}$$

We compare the hourly rain rate data for Durban to those of the other locations since the statistics of 60-minutes resolution data for different locations are more closely related than those of 60-minutes to 1-minute data. This process is repeated for four other locations in South Africa. The Fig. 2-1 (a) shows the equiprobable plot (rainfall rate values at the same probability level) of corresponding rain rate values at 1-min integration time and 1-hour. The non-unity correlation coefficient, $R^2 = 98.95\%$ means that the conversion factor is adopted even though not all the points lie on the graph but it is considered adequate for this work. Fig. 2-1 (b) is a complementary cumulative distribution (CCDF) graph for Durban site. The graph of T = 60 minutes is the measured 5-year, hourly rainfall data for Durban and the graph of T = 1 Minute is the measured 2-year, 1-minute rainfall data. The third graph is the CDF graph for T = 60 minutes multiplied by the derived conversion factors (α' = 6.3313, β' = 0.6837). From Fig. 2-1 (b), it can be seen that the translation of the CCDF curve (T = 1 Min translated from 1 hr curve) closely follows the curve obtained from the measured time series rain rate data (T = 1 Min). The 1-min data gives better resolution with the lowest rain rate of 0.01 mm/h while for the 1-hour data, the lowest rainfall rate of 0.2 mm/h is exceeded only 3.9367% of the time in a year. This results in a substantial loss of rain rate information in the 1-hour data. Also, the length (1 707 hours) of the 1-hr series data is far less than that of the 1-min series data (40 140 minutes), thus we consider the whole year period for the 1-hr series data including the dry spell periods in a year (see Ajayi *et al*. [4, 7]) while only the rainy days for 1-min series data are considered.

The loss of data and the difference in the time period explain the reason why the distribution for the measured 1-min data is much higher than that of the 1-hr for the rain rates below 6 mm/h as depicted in Fig. 2-1 (b). Fig. 2-1 (c) shows the conversion factors between Durban and Richard's Bay for the 1-hour data. Fig. 2-2 illustrates the CCDF plots of the measured 1-hour and 1-minute data from Durban, measured 1-hour data from Richards Bay and converted 1-minute data for Richards Bay. The conversion factors for all the climatic locations considered in this work are listed in Table 2-2.
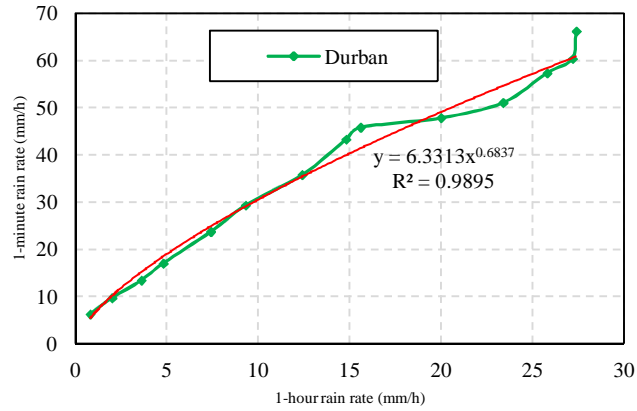
(a)
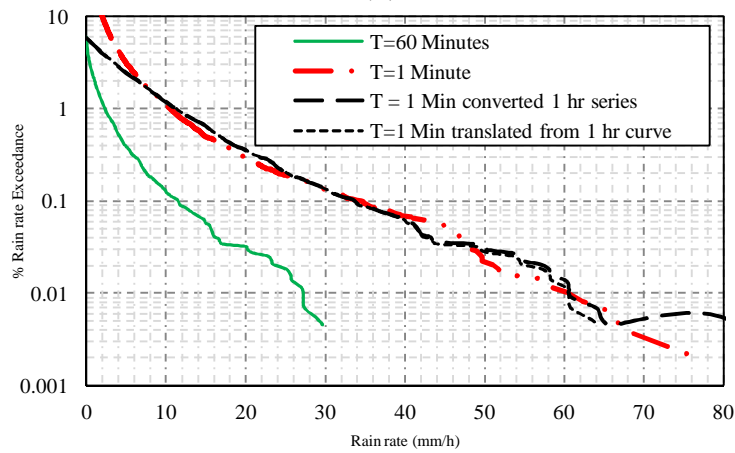
(b)
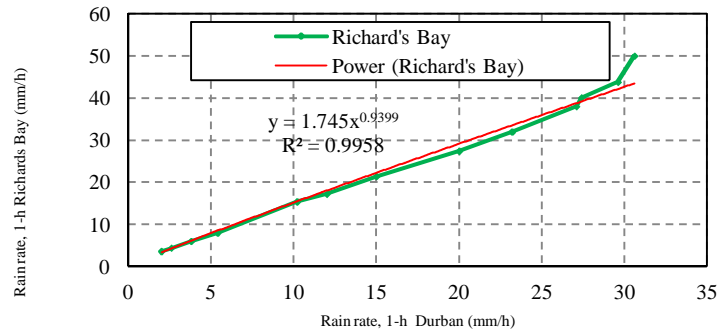
(c)

Figure 2-1 Rain rate conversion technique for Durban (a) 1-h to 1-min conversion plot for Durban (b) Rain rate % CCDF, Durban for 1-min and 1-h, (c) 1-h to 1-h conversion between Durban and Richard's Bay
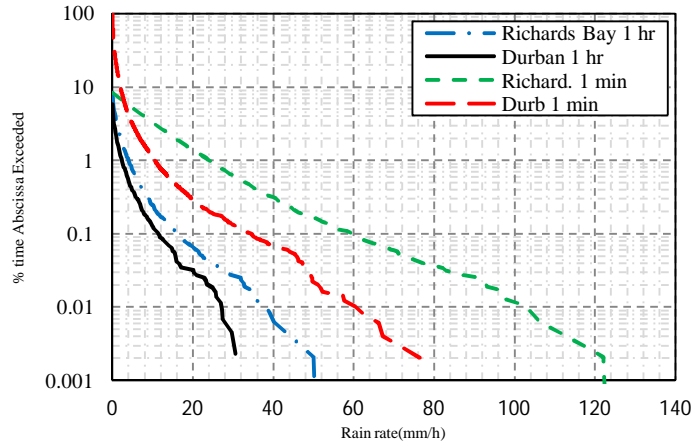
Figure 2-2 Rain rate % CCDF for Durban and Richard's Bay for 1-hr and 1-min integration time

Table 2-2 Rainfall rate integration time power law conversion coefficients for four climatic locations in South Africa

Location	Lon	Lat	α	β	R^2
Durban	29 °97'	30 °95'	6.3313	0.6837	0.9895
Pretoria	25 ° 73'	28 ° 18'	5.0935	0.6743	0.9830
Pietermaritzburg	30° 40'	29 ° 63'	6.1143	0.8393	0.9847
Richard's bay	32° 6'	28° 48'	9.8863	0.6426	0.9847
Ile-Ife Nigeria [11]	04°31'	0°30'N	11.565	0.7982	-

Since 5-year rainfall data is collected in hourly basis, the CDF of rainy days alone would result in limited statistics. In some cases, the highest recorded rainfall rate would seem to occur 0.1% of time. This means that the 1-hour statistics present significant loss of vital data required in rainfall rate modelling. In order to solve this, we have included dry spell period in each year for the 1-hour integration time data but retain the exact rainy days statistics for the 1-minute data collected from the disdrometer.

This has enabled us to achieve lower than 0.01% of time in the 1-hour data that can then be related to the 1-minute data for conversion model to be achieved. This approach of including the dry spell period in the 1-hour data was used by Ajayi *et al*. to improve the resolution of data with higher integration time and the same was applied by Sakar *et al*. in India [4]. Based on rainfall measurements in Ile-Ife, Nigeria, between September 1979 and December 1981 by the use of a fast response rain gauge with an integration time of 10 seconds, Ajayi *et al*. produced a table for the power law conversion coefficients.

By linear extrapolation, it has been determined that α = 11.565 and by logarithmic extrapolation, β = 0.7982 for conversion from 60 minutes integration time data [4, 11]. Since Ile-Ife is a tropical site, while Durban and Richard's bay are sub-tropical, it is expected that the conversion factor for Ile-Ife will be higher than those in South Africa. This is depicted in Table 2-2. In order to validate the conversion method employed in this work, the results of the proposed 1-min rainfall rate data are compared to those obtained from global coefficients as contained in the work of Emiliani *et al.* [20]. Table 2-3 lists the power law coefficients q (amplitude) and r (power) where the 1-min data is obtained from measured 60-min data. In their work, they presented the percentage relative deviation of the coefficients for different climatic zones: temperate, cold, tropical and global. In this work, we use the global coefficients.

Table 2-4 shows the results obtained from the measurements, proposed method and those obtained from the coefficients in [20]. The equiprobable rainfall rates were plotted between 1% and 0.01% of time for the proposed method as in Fig. 2-2 for the other cites and the equiprobable rainfall rate values compared to those of [20] as indicated in Table 2-4. It is evident that within the relative deviation levels of Table 2-3, the values compare closely for the rain rates between 0.1% and 0.01% of the time. At 1% of the time, the proposed method results in a more accurate prediction for the measured 1-min data in Durban. The global coefficients show a larger difference at higher percentage exceedance e.g. 1% since the compared values of rain rate of the 1-hour data (5 years) and 1-min data (2 years) vary considerably at these levels. The ITU-R P.837-5 [1] suggests that conversions from 30-min to 1-min with an average absolute difference of 5.72 mm/h for the measurements is acceptable, therefore the resulting differences in rainfall rate values in Table 2-4 should be acceptable as well.

Table 2-3 Global rainfall rate (60-min to 1-min) integration time coefficients [20]

Global coefficients	$q = 0.509$	$r = 1.394$
Max. rel. deviation	48%	17%
Min. rel. deviation	-52%	-15%

Table 2-4 Comparison of the proposed conversion factors with global coefficients

LOCATION	DATA	% of TIME		
		1%	0.1%	0.01%
DURBAN	1-h measured	2.20	11.40	27.20
	1-min measured	10.49	34.45	60.35
	Proposed (1-min)	10.85	33.42	60.56
	Emiliani *et al* (1-min)	2.63	29.20	63.65
PRETORIA	1-h measured	1.60	9.80	21.20
	Proposed (1-min)	6.99	23.73	39.93
	Emiliani *et al* (1-min)	1.65	23.40	44.20
PIETERMARITZ BURG	1-h measured	2.20	13.20	30.60
	Proposed (1-min)	11.48	46.13	89.71
	Emiliani *et al* (1-min)	2.45	39.48	88.77
RICHARD'SBAY	1-h measured	4.00	16.20	38.00
	Proposed (1-min)	24.09	59.19	102.38
	Emiliani *et al* (1-min)	6.20	54.22	124.19

2.3.2 Derivation of Rain Cell Sizes

A rain cell can be defined as the area bound by a given rain rate threshold and above. In our earlier work [21], we gave detailed procedures used in this process for Durban. As suggested by many authors, we take a circular assumption of shape to derive cell diameter size statistics for South Africa [22-25]. The same approach is used here to determine rain cell sizes for three other regions within South Africa. The point rain rate time series data is converted to distance series data by multiplying the duration taken by rain form by its appropriate advection velocity. This conversion is made for all the rain events in the measurements.

This procedure is called "Synthetic Storm" technique which was initially introduced in 1975 by Drufuca and has been used by many authors e.g. Pawlina *et al*. and Begum *et al* to derive rain cell size statistics around the world [22–25]. The data availability consists of 2 year, 1-min integration time series disdrometer data (518 rain events with rain rate of at least 3 mm/h, total of 669 hours of rainfall) and 5 year, 1-hr integration time series rain gauge data (466 rain events with rain rate of at

least 3 mm/h, total duration of 1707 hours). The rain rate thresholds used to group the data are the 3, 12 and 20 mm/h. Any given rain event exhibits a continuous change in rain rate with time as the rain moves across a given area. The drop diameters also keep on changing, a phenomenon which results to non-uniform speed of advection of rain form. However, the knowledge of an average advection velocity for each portion of a constant rain rate within one minute would be adequate. Some research has shown that intense convective rain forms move faster than less intense ones. Though the rain form is expected to move at the same speed as the wind speed for atmospheric pressure level of 700mb, this is not the case and the correlation of the two has been shown to be poor.

Radar scans have also been used to measure the translation velocity of rain cell structures which provide relatively good results. The Doppler speed detection only scans rain structures that move towards or away from the radar and these results in prediction of lower velocity values [25–26]. By the use of attenuation statistics in [21], we were able to estimate typical advection velocity of the stratiform rain forms with rain rate, $R < 12$ mm/h as 6 m/s and those of the convective rain forms as 10 m/s. The output distance data for each class are then processed statistically to find their cumulative probability distribution.

Goldhirsh [23] showed that with CDF of rain cell extensions, the rain rate-distance relationship can be derived from the graphs at a given percentile level (with power law coefficients u and v). If all the occurrences of rain events are to be taken into account, then the rain cell size model thus determined must be able to predict the largest cell area for a given rain rate threshold. This is done by plotting the graph of the equiprobable distances in the classes against the respective lower bounds of rain rates and fitting a power law relationship between those rain rates and the equiprobable cell diameters. The resulting equation produces the equivalent rain cell diameter size model. The chart of Fig. 2-3 describes the logical data exchange between the measurements and the rain cell size distribution statistics.

The data base of rain rate time series stores the data specified by different integration times and time period constraints e.g. 5 years. To convert the data to recommended 1-minute series, a viable method is iteratively chosen from a list of conversion models available. The high resolution (1-min is recommended) rain rate data is then separated into rain events. For each rain event, rain rate thresholds are chosen. There are so many cells that result from the data when rain rate thresholds below 3 mm/h are included in the study and this is likely to skew the resulting distribution. Radar scans have also shown that the cells may not obey the circular shape assumption.

The rain cells from higher rain rate thresholds are also few which may lead to unstable distribution [25-26]. We apply threshold classes for 3, 5, 12 and 20 mm/h. The rain forms are classified into two: stratiform ($R < 12$ mm/h) and convective ($R \geq 12$ mm/h). For each rain event, if the portion of rain rate is stratiform, then the distance is computed by multiplying the total time taken by that portion by a velocity value of 6 m/s. Otherwise, for convective cell areas, a velocity of 10 m/s is applied. This procedure is repeated for all the threshold values considered and the resulting distances are stored separately. The probability distribution, PDF of the distances would result in rain cell number distribution while the CDF easily predicts the rain cell size distribution.

This procedure is carried out to derive the equivalent rain cell size for Durban area by the use of the ITU-R-recommended measured 1-min integration time data. The result of the rain cell size distribution is shown in Fig. 2-4(a). After this, we derive the equivalent cell size for Durban area by the use of the measured 1-h integration time data: See Fig. 2-4 (b). However, due to the limited resolution in the data, it is hard to compare the resulting cell size distribution with those derived from the 1-min plots. For example, in the 1-h measurements, when the rainfall rate is 0.2 mm/h with a velocity of 6 m/s (21.6 km/h), the cell size generated would be 21.6 km (1 hour by 21.6 km/h).
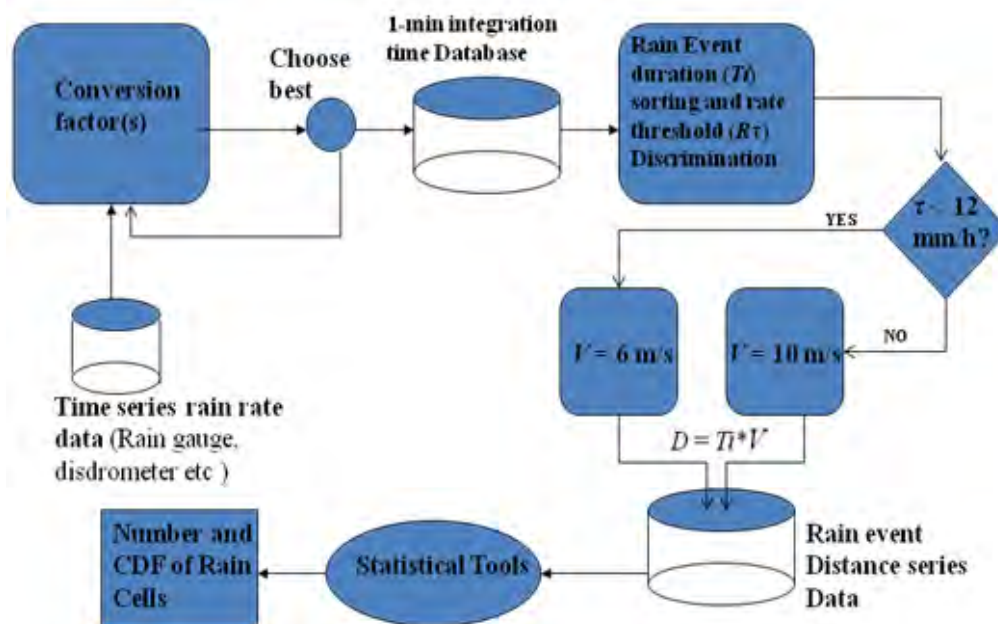
Figure 2-3 Rain cell size CDF production process from point rain rate
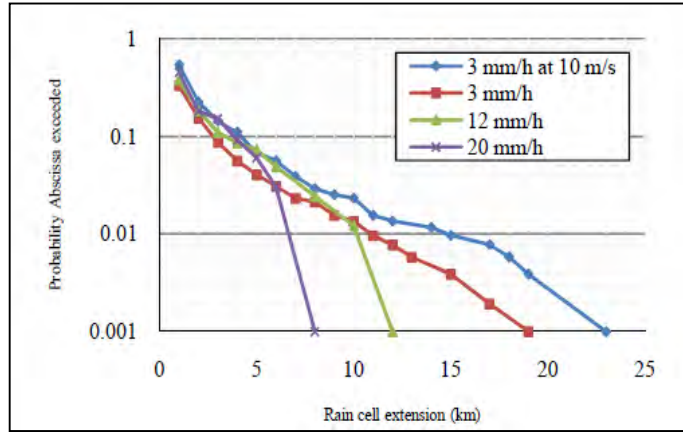
(a)
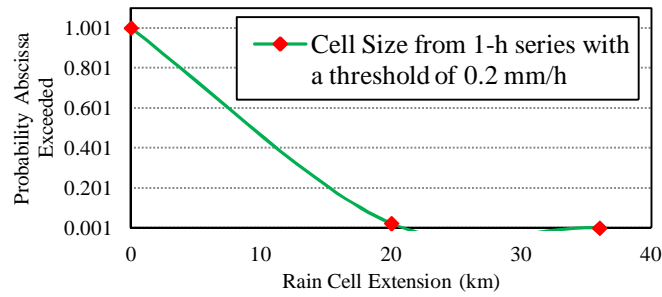
(b)
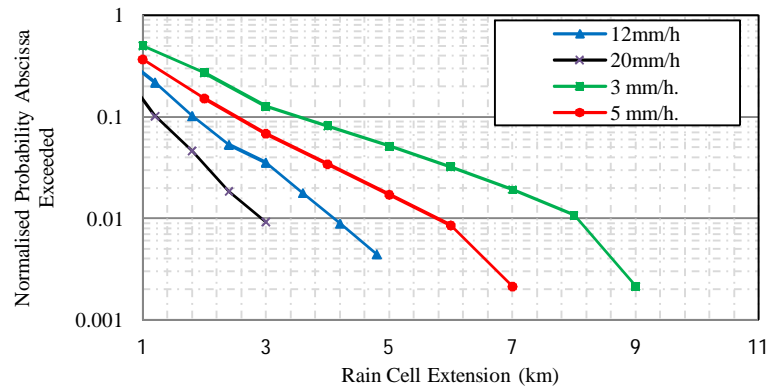
(c)

Figure 2- 4 Rain cell size CCDF for Durban (a) measured 1-min data, (b) measured 1-h series data, (c) data series converted from 1-h data

For the convective rain forms with velocity of 10 m/s (36 km/h), the cell size would be 36 km. In an attempt to resolve this, we therefore convert the 1-h time series data by the use of conversion factors in Table 2-2 to obtain the rainfall rate values that would produce the same CCDF as the measured 1-min integration time series data. Conversely, this process does not convert the 1-hour time series data into their respective 1-min time series data, but the process only enhances the rain cell extension plots of the 1-hour data by producing more points. With these new values, the new rain cell size distribution is derived for Durban area as shown in Fig. 2-4(c). Linear extrapolation is then applied to obtain the percentile level where the rain cell size will have the exact or near exact value as that generated from the 1-min data. This is determined to be the 99.99% centile. This data manipulation is repeated on the 1-hr time series data obtained from all the other locations. In summary, to achieve higher resolution in the measured 1-hour time series rain rate data, we obtain the equivalent time series data that would produce the same CDF as the 1-min data by the use of conversion values in Table 2-2. Fig. 2-4 (a) is the plot from 1-minute data: when equal advection velocity of 10 m/s is applied uniformly for all cells (see 3 mm/h at 10 m/s), the cell range is more exaggerated than if 6 m/s were used for the stratiform rain cells. Fig. 2-4 (c) illustrates the cell sizes derived from the enhanced 1-hour rain rate data for Durban showing that the largest rain cell extends up to 9 km while the smallest diameter is 2 km in range. The maximum cell has a range of 19 km with the smallest cell being 7 km.

The result is a model expressed by (2-6) [21]:

$$D = 32.673\, R^{-0.467} \tag{2-6}$$

where D (km) is the equivalent rain cell diameter and R (mm/h) is the rain rate.

When this result is compared to the available radar measurements of rain cell sizes, rain rate threshold of 5 mm/h was found to extend up to 25 km in Spinno D'Adda, Italy and Chilbolton, England. This could mean that the data collection from the disdrometer do not fully represent all the rain events in Durban. Also, we have earlier shown that the resulting rain cell diameter of (2-6) is the weighted mean intercept of the virtual radio path [30]. For worst case consideration of the largest rain cell that occurs, then we multiply the (2-6) by a factor of $\pi/2$. Thus the diameter model becomes $D = 51.32 R^{-0.467}$.

When the rain cell statistics from Fig. 2-4 (c) (plotted from the enhanced 1-hr data) is linearly interpolated to the 99.99% percentile and by the use of Goldhirsh method, the new rain cell model is deduced as [21, 23]:

$$D = 51 \, R^{-0.46} \tag{2-7}$$

This result shows that the 5 mm/h threshold extends up to 24.32 km which is close to the reported radar observations of 25 km.

Fig. 2-5 (a) and (b) show the CCDF of cell sizes and the Goldhirsh's method of conversion at 99% centile respectively with data obtained from Richard's Bay. The same extrapolation is carried out to derive the cell sizes at 99.99% centile.

The resulting model for Richard's Bay is given as:

$$D = 55 \, R^{-0.455} \tag{2-8}$$

This procedure was carried out for the eight locations and the unique coefficients for rain cell sizes are listed in Table 2-5 since other towns had the same relationships.
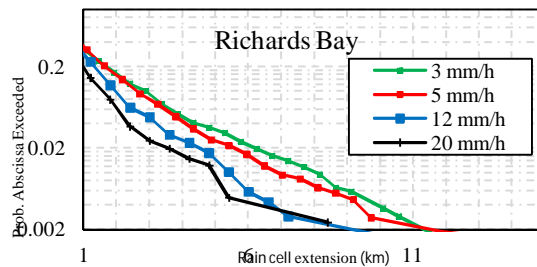
(a)
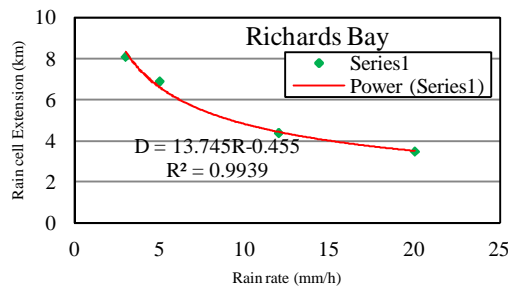
Figure 2-5 Rain cell diameters (a) CCDF for Richard's Bay (b) derivation of rain cell size at the 99% percentile

Table 2-5 Equivalent rain cell diameter coefficients for some locations in South Africa

LOCATION	LON	LAT	u	v
DURBAN	29 ^{o}97'	30 ^{o}95'	51	-0.460
PRETORIA	25 ^{o} 73'	28 ^{o} 18'	30	-0.462
PIETERMARITZBURG	30° 40'	29 ^{o} 63'	45	-0.467
RICHARD'S BAY	32° 6'	28° 48'	55	-0.455

The values for u–parameter seem to be dependent on the location while the slope– parameter, v remains somewhat constant for the region (about 0.461 on average). The rain cell sizes derived in this work do not necessarily refer to the mean cell diameter but rather the maximum cell size that passes through the point rain rate equipment. Rainfall occurs with highly intensive cells embedded in the stratiform structures where their contribution to attenuation on the radio link is obtained from the sum of the input of all the cells. The derived relationships in Table 2-5 can then be applied in attenuation prediction for the localities of interest and also in site diversity planning as long as the attenuation equation requires the rain cell size as an input. From Table 2-5, it is noted that the overall rain cell sizes at the coastal areas in the eastern part of the country for example in Durban and Richard's Bay, are larger than those of the inland areas as in the case of Pretoria and Pietermaritzburg. This may be attributed to the strong oceanic winds that tend to sweep rain across the land areas.

2.4 Site Diversity Planning

In terrestrial and satellite link planning, the received signal power level (RSL) is determined from the decibel difference between the equivalent isotropically radiated transmitter power (EIRP) and the total net path loss [31]:

$$\text{RSL} = P_t + G_t + G_r - \text{FSL} - A_g - L_r - L_t - (A_r + A_w) \tag{2-9}$$

where P_t is the transmitted power, G_t is the gain of the transmitter antenna, G_r is the receiver antenna gain, Free space loss (FSL), A_g is the attenuation due to gas, A_r is the attenuation due to rain, A_w is the wet antenna loss (both transmitter and receiver terminals), L_t is the loss in transmit-systems and L_r is the loss in the receive-systems.

The gaseous loss is mainly contributed from vapour absorption (0.16 dB/km at 22 GHz) and oxygen absorption (15 dB/km at 60 GHz). The free space loss is derived from the following [31]:

$$FSL = (32.4 + 20 \log_{10} L + 20 \log_{10} f) \tag{2-10}$$

where f (GHz) is the frequency used in the link and L is the link path length in km.

With the knowledge of the rain rate, R % at desired availability, expected rain attenuation, A (p) % can be computed. Link planners normally provide a fade margin based on clear weather conditions. In the case of a rain event, the free space loss (FSL) is expected to lessen thus providing for the signal loss in a rain medium. However, this approach leads to low link reliability during rain events and thus the provision for rain attenuation during initial link planning has become necessary. From (2-9), the rain fade margin can be alleviated by increasing the transmitter equivalent isotropically radiated power (EIRP) and the gain of the receiver. But due to large attenuation margins experienced from rain attenuation, the power and gain adjustments are not sufficient: thus site diversity comes into play.

Two sites in a geographical area may be affected equally by the same rain event that covers that area. With the knowledge of the rain cell extension length for a given rain rate threshold, the minimum distance between two diversity sites can be determined to increase diversity gain. This analysis is presented for both terrestrial and satellite radio links since both links are similar in view of site diversity apart from the fact that the link elevation angle for terrestrial case is normally small. Given two sites w and x that are to be linked by a terrestrial link, this can be done directly as a line of sight (LOS) link. To alleviate the rain fade by site diversity method, the same link can be routed via another site y, then y to w, such that x and y become the two diversity sites.

The mean attenuation for a single site; A_s is expressed as [33]:

$$A_s = \frac{1}{2}\{A_x + A_y\} \tag{2-11}$$

$$A_J(t) = \text{minimum}[A_x(t) + A_y(t)] \tag{2-12}$$

where A_x is the attenuation at site x and A_y the attenuation at site y. A_J is the joint attenuation for the two sites.

The diversity gain G_D (P) of attenuation equalled or exceeded at a given percentage of the time, P is given by:

$$G_D(P) = A_s(P) - A_J(P) \tag{2-13}$$

where A_J (p) is the joint attenuation for sites x and y.

Link reliability, Γ is the percentage of time the link is within the received threshold level despite any environmental changes. The percentage, $P\%$ for which a required margin, M_r is equalled or exceeded can be expressed as given in (2-14a):

$$P = (100\% - \Gamma) \tag{2-14a}$$

The rain fade margin, M_r

$$M_r = A(P) + \delta N - G_D(P) \tag{2-14b}$$

where A (P) is the expected single site attenuation, and δN is the (thermal) loss due to increase in temperature. Hodge [27-28] has shown that the diversity gain can be computed from a given attenuation, A and the separation distance, d:

$$G_D = G_d G_f G_E G_Z \tag{2-15}$$

$$G_d = m\left(1 - e^{-nd}\right) \tag{2-16}$$

$$m = 0.64A - 1.6\left(1 - e^{-0.11A}\right) \tag{2-17}$$

$$n = 0.585\left(1 - e^{-0.98A}\right) \tag{2-18}$$

$$G_f = 1.64e^{-0.025f} \tag{2-19}$$

$$G_E = 0.00492\theta + 0.834 \tag{2-20}$$

$$G_z = 0.00177z + 0.887 \tag{2-21}$$

where z is the baseline-to-path angle, θ is the elevation angle and f (GHz) is the frequency used.

From above, the diversity gain is expected to vary from zero to the maximum (single site attenuation) when d is large enough such that the rain at the two sites are uncorrelated. However, rainfall occurs as stratiform structure with convective rain cells altogether. Therefore there is saturation for site diversity gain, which is a value less than single site attenuation. The distance should not be too large since the next site may fall into another rain region.

From (2-14a), in order to achieve reliability at $P = 0.01\%$, the diversity gain corresponds to the rain attenuation expected to be equalled or exceeded 0.01% of the time. For Durban, the rain attenuation equalled or exceeded 0.01% of the time, is computed from (2-11) where the value of rain rate is given as 60 mm/h [29–30]. From Table 2-5, the rain rate threshold of 60 mm/h is

computed to stretch up to 7.75 km in Durban area. To maximize site diversity gain, the second redundant site *y*, should be situated at least 8 km away from the site, *x*. The rain cell size relationships therefore provide the minimum required separation distance required to achieve a given link reliability level. To determine the maximum value of *d* that will guarantee availability at equal probability, the field of the next neighbour rain cell must be known. It has been reported that thunderstorms could be separated from one another by 10-30 km [33–34]. Thus, this range of distances provides the maximum separation distance.

This approach is repeated for several stations in the South African region with the knowledge of the rain rate threshold values at the 0.01% of the time and the distance–rain rate relationships described in Table 2-5 [13, 29–30].

Since the data used for the rain rate mapping are based on 21 locations in South Africa, the results for *d* for all other locations are derived by the use of inverse distance weighting method (IDW) and implemented in the MATLAB software to determine the interpolated distance matrix for all the coordinates in South Africa. The matrix is then transformed into contour plots to depict the rain field extension areas bound by the thresholds at 0.01% of time.
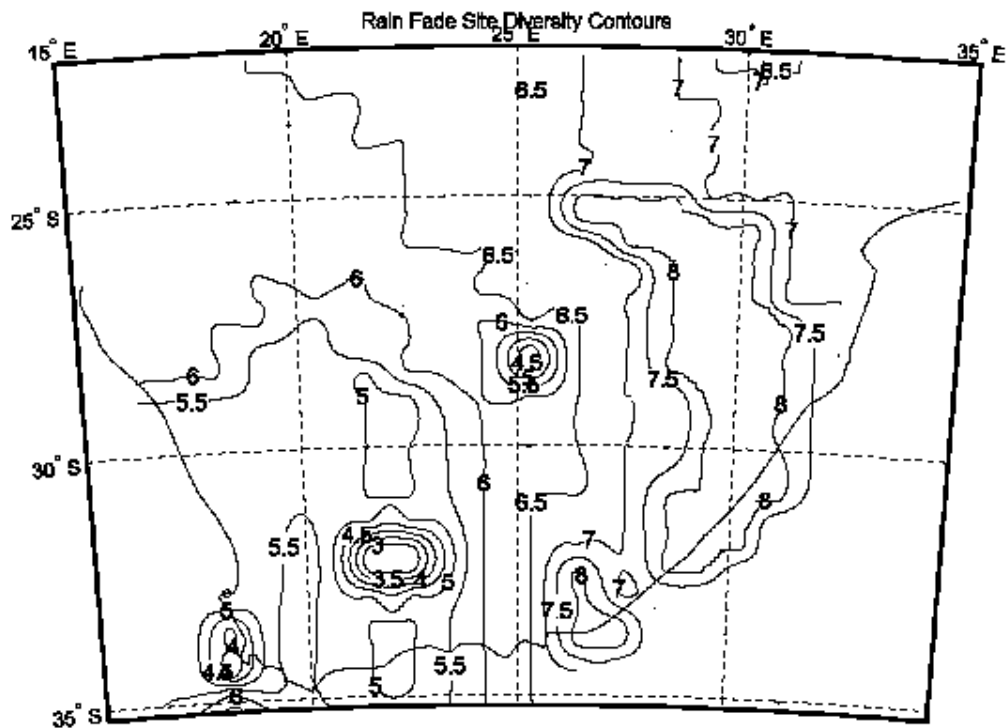
Figure 2-6 Site diversity distance plot for link reliability of 99.99% in South Africa

The result is shown in Fig. 2-6 which is applicable for site diversity planning for both terrestrial and satellite high capacity radio links. With the values of *d* given for the climatic regions of South Africa, link planners will easily apply the equations (2-11) through (2-21) to derive the optimal diversity gain. Other recent developments on site diversity topic can be found in studies involving multiple sites [35–40].

2.5 Conclusion

A method has been proposed to determine rain cell size distribution from rain gauge network with high integration time of one hour. It has been shown that attenuation statistics in a given location can be used to estimate the advection velocity of rain forms. The attenuation statistics of the terrestrial radio link were used to approximate the average advection velocity of the stratiform rain in Durban as 6 m/s. This velocity value can be used to derive cell size statistics for other regions experiencing similar climatic conditions. The equivalent rain cell diameter which is required as an input to the given attenuation prediction is found to be $D = 51R^{-0.46}$ for the rain cell area considered in this work. The rain cell sizes for the South African region have been successfully derived based on point rain rate data collected over five years. There are variations in cell sizes based on the total fractal area of observation and the size of the cells are seen to be directly proportional to the values of rain rate measurements at 0.01% of time. The applications for the cell sizes have been introduced as applied in attenuation prediction and site diversity planning. Unless 1-minute data measurements are carried out throughout the country and rain cells sizes derived, the results in this work present a viable solution to the need. Since the rain cell size derivation process is based on the assumption of velocity of advection, which varies for the stratiform and convective rain forms, comparison of rain fields from RADAR data and from a network of point rain rate equipment is recommended for further analysis. The procedure used here in the CCDF analysis is compared to the PDF analysis of Chapter 3 with similar outcomes being derived. This rain cell diameter model is applied in the work in Chapters 4 and 5 to verify the application of rain cell diameter in rain attenuation modelling.

2.6 References

[1]   "Characteristics of precipitation for propagation modelling," ITU-R, Geneva, 2007, ITU-R Rec. P.837-5.

[2]   R.K. Crane, "Prediction of attenuation by rain," *IEEE Trans. Comm.*, vol. 28, pp. 1717–1733, 1980.

[3]   R.K. Crane, *Electromagnetic Wave Propagation through Rain*. New York: John Wiley, pp 1−40, 1996.

[4]   G.O. Ajayi, S. Feng, S.M. Radicella, B.M. Reddy (Ed), *Handbook on Radio propagation Related to Satellite Communications in Tropical and Subtropical Countries,* Trieste: ICTP, pp. 7–14,1996.

[5]   J.S. Ojo, M.O. Ajewole and S.K. Sarkar, "Rain rate and rain attenuation prediction for satellite communication in Ku and Ka bands over Nigeria," *Progress in Electromagnetics Research B*, vol. 5, pp. 207-233, 2008.

[6]   F. Moupfouma, "Improvement of a rain attenuation prediction method for terrestrial microwave links," *IEEE Trans. Antennas Propag.*, vol. 32, pp. 1368–1372, 1984.

[7]   G.O. Ajayi and E.B.C. Ofoche, "Some tropical rainfall rate characteristics at Ile-Ife for microwave and millimetre wave application," *J. of Climate and Applied Meteor.*, vol. 23, pp. 562–567, 1983.

[8]   P.A. Watson, M. Gunes, B.A. Potter, B. Sasthiaseelan and J. Leitas, " Development of a climatic map of rainfall attenuation for Europe," *Post Graduate School of Electrical and Electronic Engineering, University of Bradford*, No. 327, pp. 153.

[9]   F. Moupfouma, "Rainfall-rate distribution for radio system design," *IEE proceedings*, vol. 134, pt. H, no. 6, pp. 527-537, Feb. 1987.

[10] C.T. Mulangu, P.A. Owolawi and T.J. Afullo, "Rainfall rate distribution for LOS radio systems in Botswana*," SATNAC Conference,* Mauritius, Sept. 2007

[11] M.O. Fashuyi, P.A. Owolawi and T.O. Afullo, "Rainfall rate modelling for LOS radio systems in South Africa," *Trans. of South African Inst. of Elect. Engineers (SAIEE)*, vol. 97, pp 74–81, 2006.

[12] M.O. Odedina and T.J. Afullo, "Characteristics of seasonal attenuation and fading for line-of-sight links in South Africa," *Proc. of SATNAC*, pp. 203–208, Sept. 2008.

[13] P.A. Owolawi, "Rain rate probability density evaluation and mapping for the estimation of rain attenuation in South Africa and surrounding Islands," *Progress in Electromagnetic Research*, vol. 112, pp. 155–181, 2011.

[14] R.K. Flavin, "Rain attenuation considerations for satellite paths," *Telecom. Australian Research Laboratories*, report no 7505.

[15] B. Segal, "The influence of rain gauge integration time on measured rainfall-intensity distribution functions*," J. of Atmospheric and Oceanic Tech.* vol. 3, pp. 662–671, 1986.

[16] P. Rice and N. Holmberg, "Cumulative time statistics of surface-point rainfall rate." *IEEE Trans. Commun.*, vol. 21, pp. 1772-1774, Sept. 2002.

[17] M.S. Singh, K. Tanaka and M. Lida, "Conversion of 60-, 30-, 10- and 5-minute rain rates to 1-minute rates in tropical rain rate measurement," *ETRI Journal*, vol. 29, no. 4, Aug 2007.

[18] Y. Karasawa and T. Matsudo, "Prediction of one-minute rain rate distribution in Japan," *Trans. IEICE*, J73-B-H,pp. 518-527, 1990.

[19] C. Capsoni and L. Luini, "A physically based method for the conversion of rainfall statistics from long to short integration time," *IEEE trans Antennas*, vol. 57, no. 11, 2009.

[20] L.D. Emiliani, L. Luini and C. Capsoni, "Analysis and parameterization of methodologies for the conversion of rain-rate cumulative distributions from various integration times to one minute," *IEEE Antennas Propag. Mag.*, vol. 51, no. 3, pp. 70–84, June 2009.

[21] P.O. Akuon and T.J.O. Afullo, "Rain cell size statistics from rain gauge data for site diversity planning and attenuation prediction," *Proceedings of Southern Africa Telecommunication Networks and Applications Conference (SATNAC),* East London, South Africa, pp.213-216*, 4-7th* Sept. 2011. ISBN 978-0-620-50893-3.

[22] G. Drufuca G, I. Zawadzki, "Statistics of rain gauge data," *J. of Applied Meteorology*, vol. 14, pp. 1419–1429, Dec. 1975.

[23] J. Goldhirsh "Rain cell statistics as a function of rain rate for attenuation modelling," *IEEE Trans. Antennas Propag*., vol.57, no. 5, pp. 799–801, Sept. 1983.

[24] Pawlina A. "No rain intervals within rain events: some statistics based on Milano radar and rain-gauge data," COST Action 280, 1st *International Workshop*, July 2002.

[25] S. Begum, C. Nagaraja, I. Otung, "Analysis of rain cell size distribution for application in site diversity," *IEEE Antennas & Propag.*, pp.1–5*, 2006.

[26] Emilio Matricciani, Apolonia Pawlina Bonati, "rain cell size statistics inferred from long term point rain rate: model and results," *Proc. Third Ka band utilization conference*, Sorrento, Italy, September, 1997.

[27] D. B. Hodge, "An empirical relationship for path diversity gain," *IEEE Trans. On Ant. & Propag.*, vol.24, pp.250-251, March 1976.

[28] D.B. Hodge, "An improved model for diversity gain on earth-space propagation paths," *Radio Science*, 17, pp.1379-1399, Nov-Dec, 1982.

[29] Pius Adewale Owolawi, "Characteristics of rain at microwave and millimetric bands for terrestrial and satellite links attenuation in South Africa and surrounding islands," *PhD Thesis*, July 2010,pp114-116.

[30] Akuon P. O. and Afullo T. J. O., "Path reduction factor modelling for terrestrial links based on rain cell growth," *Proc. of IEEE Africon conference*, Livingstone, Zambia, 13-15th Sept. 2011. ISBN: 978-1-61284-991-1.

[31] Freeman, R. L., *Radio System Design for Telecommunication*, 3rd edition, A Wiley Interscience Publication, John Wiley & Sons Inc,2007.

[32] Recommendation ITU-R 530-10, "Propagation Prediction Techniques and Data Required for the Design of Terrestrial Line-of-Sight Systems," Vol. 2001, P Series, *International Telecommunication Union,* Geneva, Switzerland, 2001, pp.271-295.

[33] T. Pratt and C.W. Bostian, *Satellite Communications*, pp.345-346, A Wiley Interscience Publication, John Wiley & Sons Inc, 1988.

[34] Apolonia A. Pawlina, "No Rain Intervals within Rain Events: Some Statistics Based on Milano Radar and Rain-gauge Data," Propagation *Impairment Mitigation for Millimetre Wave Radio Systems*, COST Action 280. *1st International Workshop* July 2002

[35] A.D. Panagopoulos, P. M. Arapoglou, J. D. Kanellopoulos and P. G. Cottis, "Long Term Rain Attenuation Probability and Site Diversity Gain Prediction Formulas", *IEEE Transactions on Antennas and Propagation*, vol. 53, no. 7, July 2005.

[36] V. K. Sakarellos, D. Skraparlis, A. D. Panagopoulos and J. D. Kanellopoulos, "Outage Performance Analysis of a Dual-Hop Radio Relay System Operating at Frequencies above 10 GHz", *IEEE Transactions on Communications*, Vol. 58, No 11, November 2010.

[37] A. D. Panagopoulos and J. D. Kanellopoulos "Prediction of triple-orbital diversity performance in Earth-space communication", *International Journal of Satellite Communications*, No. 20, pp. 187-200, 2002.

[38] A. D. Panagopoulos and J. D. Kanellopoulos "Adjacent Satellite Interference Effects as applied to the Outage Performance of an Earth-Space System located in a Heavy Rain Climatic Region", *Annals of Telecommunications*, No 9-10, pp.925-942, 2002.

[39] E. Matricciani, "Physical-mathematical model of the dynamics of rain attenuation based on rain rate time series and two layer vertical structure of precipitation," *Radio Science*, vol.31, pp.281-295, 1996.

[40] E. Matricciani, "Prediction of orbital diversity performance in satellite communication systems affected by rain attenuation," *Intern. Journal of Satellite Communications*, vol. 15, pp.45-50, 1997.

CHAPTER THREE

Rain Field Area Synthesis

3.1   Abstract

Rain cell diameter distribution (RCDD) is generated from point rain rate data collected over two years in Durban, South Africa. By the use of the statistical moment generators, the diameter of the average rain cell, maximal cell area and the fractional area occupied by all cells during rain events are derived. This investigation is made for minimum rain rate thresholds of 3, 12 and 20 mm/h. To achieve this, two proposed distribution models are compared: the exponential model and power law distribution model. The results of the two models show considerable agreement thus qualifying the proposed approach in detecting the rain field from point rain rate data. The maximum rain field area that can be detected from point measurements is found to be 60 km wide for rain rates of 3 mm/h and above. The application of the results in attenuation modelling is briefly introduced.

3.2   Introduction

For radio applications, the description of the area occupied by rain cells and the statistical model of rain cell size distribution is vital. This knowledge is essential in estimating the likelihood of a radio path being intercepted by a rain field, which leads to signal attenuation. For high frequency bands, intense rain forms which tend to have high concentration of rain drops with relatively large sizes compared to the signal wavelength, have serious attenuation effects [1]. A rain cell can be defined as the area in space bound by a given minimum threshold of rain rate; R_T (mm/h) [2]. Radar pictures provide a good method for detecting rain field area, which is of great value to radio planning engineering. With the knowledge of the expected rainy region for a given rain rate threshold, route diversity methods can be easily applied to alleviate rain-induced attenuation in a given area [3]. However, radar data is not as easily accessed and processed as compared to point rain rate measurements. Rain gauge and disdrometer systems are some of the equipment used for carrying out rain rate measurements. This data can then be transformed into their respective spatial distribution by the use of "Synthetic Storm" technique. This procedure involves converting the time series rain rate data into distances by the use of a desirable rain cell advection velocity. Rain events can be classified into two classes: stratiform and convective rain cells. We have earlier showed that the velocity of 10 m/s is tolerable for convective cells with rain rate, ($R > 12$ mm/h) and 6 m/s for stratiform rain structures ($R < 12$ mm/h) in Durban [3–7].

The cumulative distribution (CDF) of rain cell extensions were derived with distance ranges from 0.6 km to 19 km. The CDF enables us to describe the maximum extent of rain cell diameter for a given rain rate threshold from which rain cell size model is derived. The approach taken here deviates from the CDF statistics and the probability distribution (PDF) of the number of cells is considered to generate the rain field area from point rain rate. The total number of cells in each range bin is noted for every rain rate threshold sampled. In section V, we will show that the PDF can be used to model the rain cell size as well as the fractional rain area occupied by the cells derived from the point rain rate database.

3.3 Methodology

3.3.1 Rain Cell Patch Chord Analysis

Let's presuppose as in Fig. 3-1, that a rain gauge or disdrometer is situated at point P. The single cell maximum diameter of the rain rate threshold is denoted by D. Any rain cell that moves within the square area of width $2D$ is assumed to pass over point P. All the rain cell patches within the fractional area are generated from the "Synthetic Storm" technique. The total mean chord length of the rain patches falls within the area represented by the inner continuous line in Fig.3-1.

If the rain cell centre moves vertically through point P, the mean chord lengths is described by (3-1); if the rain cell centre moves within the area bound by the inner dotted concentric circle, the weighted mean chord lengths is derived from (3-2):

$$I = \frac{\int_0^{\frac{\pi}{2}} D\cos\theta \, d\theta}{\frac{\pi}{2}} = 2D/\pi \qquad (3\text{-}1)$$

$$I_W = \frac{D\left(\frac{2D}{\pi} + 0 + \frac{2D}{\pi} + 0\right)}{D} = 2D/\pi \qquad (3\text{-}2)$$
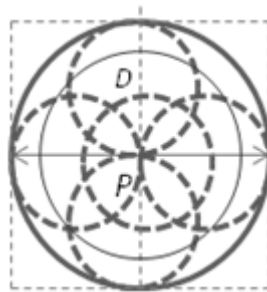
Figure 3-1 Rain cell intercept with point rain rate equipment

The inference made from (3-2) is that the mean of the lengths of rain cell patches is $2D/\pi$. For radio applications, interest is vested in the contribution of the diameter of the whole cell, D rather than the mean of the rain patch, I_w. Thus, from measurements, the distribution of rain cell patches obtained is converted to the cell diameter by the factor, $\pi/2$. By assuming a power law relationship, we have shown that the rain cell patches can be estimated by (3-3a), so the rain cell diameter distribution is determined from (3-3b) [3]:

$$D_p = \alpha R^{-\beta} \qquad\qquad (3\text{-}3a)$$

$$D = \frac{\pi}{2}.\alpha R^{-\beta} \qquad\qquad (3\text{-}3b)$$

where α and β are factors determined from the empirical rain rate (R) data and D_p is the mean diameter of the rain cell patches.

3.3.2 Rain Cell Number Density Distribution, RCDD

Today, several authors have presented results for RCDD from radar observations based on assumption of circular rain cell shape [2, 7–11]. In the present work, we consider two methods that are frequently used to express RCDD: the exponential model and power law model.

3.3.2.1 Exponential RCDD Model

The exponential form of RCDD is given as [2]:

$$N(D, R_\tau) = N_0(R_\tau)\exp[-\lambda(R_\tau)D] \qquad\qquad (3\text{-}3c)$$

where D is the equivalent rain cell diameter bound by a given rain rate threshold, R_τ, $N(D, R_\tau)$ is the total number of cells having a diameter D per unit area of observation, A (km^2), $N_0(R_\tau)$ is considered as the intercept parameter and λ is the slope factor of the distribution.

This model has been used in many rain field studies. Some of the places include England [8] in 1963 by Dennis and Fernald, Illinois [9], Virginia [9] in 1978 by Konrad and Niamey [10] in 1995 by Tenorio *et al*. It has been argued that when the range of distances fall within 0 to 18 km, then the slope factor, λ exhibits little deviation for all rain thresholds in the distribution. The values for the slope factor λ were noted to vary from 0.27 in Illinois radar observations to 0.5 with most observations giving an average value of 0.35 [8–10]. Statistical moments provide a simpler method for obtaining desired parameters in data analysis. The nth raw moment of the exponential distribution is given as [3]:

$$m_n(R_\tau) = N_0(R_\tau) \int_{D_{min}}^{D_{max}} D^n \exp[-\lambda(R_\tau)D] \, dD \qquad (3\text{-}4a)$$

Integrating (3-4*a*) with respect to the rain cell diameter, *D* results in:

$$m_n(R_\tau) = N_0(R_\tau) \frac{n}{\lambda^{n+1}} \left[-e^{-\lambda D} \left(\frac{\lambda^n D^n}{n} + \lambda^{n-1} D^{n-1} + (n-1)\lambda^{n-2} D^{n-2} + \cdots + (n-1)! \right) \right]_{D_{min}}^{D_{max}}$$

$$(3\text{-}4b)$$

In radio applications and for the exponential model, only the first three moments may be used i.e. 0, 1 and 2nd moments. From (3-4*b*), we see that assuming that the minimum cell diameter is zero instead of 0.6 km, $\lambda(R_\tau) = 0.35$ and integrating it to infinity introduces a small increase of 10% only in m_0. Therefore, (4*b*) can be reduced to be of the simpler form:

$$m_n(R_\tau) \approx N_0(R_\tau) \frac{n!}{\lambda^{n+1}} \qquad (3\text{-}4c)$$

This form of equation is easier to implement in software computation algorithm than that of (3-4*b*).

Nevertheless, we have employed (3-4*b*) to derive our statistical parameters instead of the reduced expression given in (3-4*c*) to avoid the approximation.

3.3.2.2 Power law RCDD Model

The general power law model is expressed as [11–12]:

$$N(D, R_\tau) = N_0(R_\tau) D^{-\lambda(R_\tau)} \qquad (3\text{-}5)$$

where the parameters bear the same meanings discussed earlier.

It has been noted that the power law model is well suited for RCDD since it is more accurate in catering for the rain cell clusters rather than individual rain cell. Kuo *et al*. and Machado *et al*. noted that the cirrus cloud has the slope parameter value that varies from -1.91 to -2.51, in spite of the rain rate threshold [11–12].

The raw moment functions of the power law expressions are given in (3-6) and (3-7):

$$m_n(R_\tau) = N_0(R_\tau) \int_{D_{min}}^{D_{max}} D^n D^{-\lambda(R_\tau)} \, dD \qquad (3\text{-}6)$$

$$= \frac{N_0(R_\tau)}{(n-\lambda+1)} \left[D_{max}^{(n-\lambda+1)} - D_{min}^{(n-\lambda+1)} \right] \qquad (3\text{-}7)$$

3.4 Analysis of Statistical Parameters

The parameters required for rain field analysis for radio applications are discussed. These include the total cell number, the average diameter of rain cells, the cell area and total fractional area detectable from point rain rate [2].

A. Total number of cells, $N_T(R_\tau)$

$$N_T(R_\tau) = \int_0^\infty N(D, R_\tau)dD = m_0 \tag{3-8}$$

B. Average diameter of cells (km), $< D >$

$$< D > = \frac{1}{N_T(R_\tau)} \int_0^\infty D.N(D, R_\tau)dD = \frac{m_1}{m_0} \tag{3-9}$$

C. Average cell area (km^2), $< a >$

$$< a > = \frac{1}{N_T(R_\tau)} \frac{\pi}{4} \int_0^\infty D^2.N(D, R_\tau)dD = \frac{\pi}{4} \frac{m_2}{m_0} \tag{3-10}$$

D. Diameter of the average cell (km), D_0

$$D_0 = \sqrt{\frac{1}{N_T(R_\tau)} \int_0^\infty D^2.N(D, R_\tau)dD} = \sqrt{\frac{m_2}{m_0}} \tag{3-11}$$

E. Fractional area occupied by the cells (km^2), F_A

$$F_A = \frac{\pi}{4} \int_0^\infty D^2.N(D, R_\tau)dD = \frac{\pi}{4} m_2 \tag{3-12}$$

F. Fractional length of cells (km), F_D

$$F_D = \sqrt{\int_0^\infty D^2.N(D, R_\tau)dD} = \sqrt{m_2} \tag{3-13}$$

3.5 Data Analysis

The data used was collected from a disdrometer located at the School of Electrical and Electronics and Computer Engineering in the University of KwaZulu-Natal. The two year 1-minute point rain rate data was converted to represent rain fall patches which were assumed to be the diameter of the rain cells. We did not consider rain cells below 3 mm/h and those beyond 20 mm/h since they could introduce errors in the distribution. More details about conversion of rain rates time series into their respective distances have been discussed elsewhere by the authors [3]. Fig. 3-2 (a), (b) and Fig. 3-3 illustrate the PDF plots of the rain cell number density against the rain cell diameters.
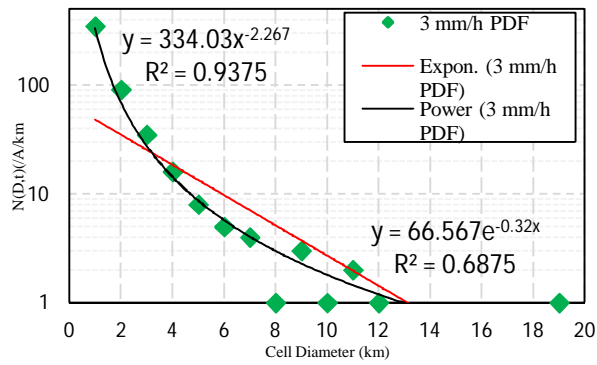
(a)
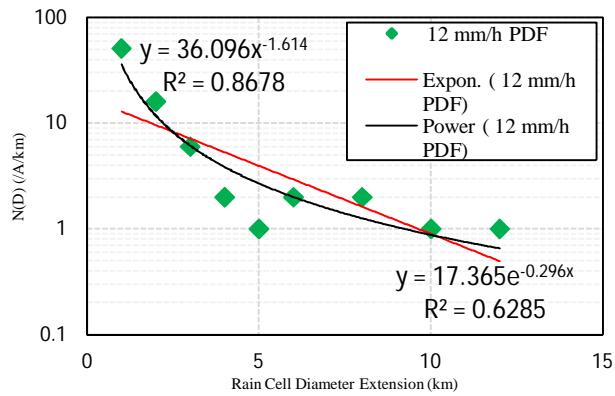
(b)

Figure 3-2 (a) Rain cell number density distribution for rain rate threshold of 3 mm/h, (b) rain cell number distribution for rain rate threshold of 12 mm/h
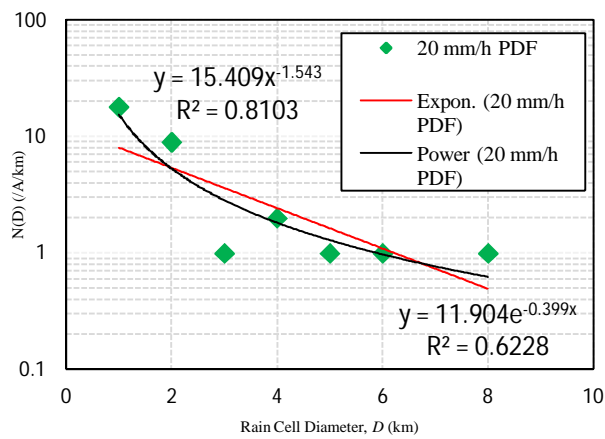
Figure 3-3 Rain cell number density distribution for 20 mm/h rain rate threshold

3.6   Results and Discussion

From the distributions described in Figs. 3-2 through 3-4, the parameters listed in Table 3-1 have been derived. From Fig. 3-1, and by applying the power law model of (3-3a) and (3-3b), we have the mean rain patches described by $31.837R^{-0.468}$ and the resulting rain cell diameter distribution given as $D = 50R^{-0.468}$. This result is comparable to the one we derived from the CDF analysis where $D = 51R^{-0.46}$ [3]. From Fig. 3-1 we note that the fractional area length is twice the rain cell diameter, D. The percentage error, e_m in predicting the fractional area or simply the fractional diameter by the use of power law and exponential model have been computed and recorded in Table 3-1 according to (3-14):

$$e_m \ = \ \frac{|(F_{Dp}/2)-D_m|}{D_m} * 100 \qquad (3\text{-}14)$$

where F_{Dp} is the predicted value and D_m is the expected value for each model for each rain rate threshold.

The expected value, D_m is computed from the expression, $D = 50\ R^{-0.468}$ for each rain rate threshold. The predicted values are those calculated from the statistical parameters. From the results, we can see that the power law model gives a better estimation than the exponential model for the whole range of rain rate measurements i.e. at least 3 mm/h.

Table 3-1 Rain field area parameters for Durban, South Africa

Parameter	Exponential law			Power law		
	3 mm/h	12 mm/h	20 mm/h	3 mm/h	12 mm/h	20 mm/h
N_{TM}	518	82	33	518	82	33
N_{0M}	347	51	18	347	51	18
N_{TP}	208.021	58.665	29.834	257.310	49.147	22.642
N_{0P}	66.567	17.365	11.904	334.03	36.096	15.409
λ	0.32	0.296	0.399	2.267	1.614	1.543
$<D>$	3.125	3.378	2.506	2.647	4.026	4.230
$<a>$	15.340	17.928	9.867	10.649	24.224	26.403
D_0	4.419	4.778	3.544	3.682	5.554	5.798
D_m	28.820	17.898	12.246	28.825	17.898	12.246
F_A	3191.016	1051.767	294.370	2740.208	1190.529	597.800
F_D	63.7407	36.58093	19.3476	59.0648	38.92485	27.59332
e_m (%)	10.58	2.19	-21	2.454	8.74	12.66

Where $N_{0M,}$ *is* the measured y-intercept value for the number of cells, $N_{T\,P}$ is the predicted total number of cells, N_{0P} is the predicted y-intercept value for the number of cells, λ is the slope factor and N_{TM} is the measured value for the total number of cells.

3.6.1 Correlation of RCDD in other locations

The method is applicable in RCDD generation for other locations as long as the rain rate relationship between two locations is known. This is helpful and eliminates the problems that arise due to lack of rain rate data for most locations.

The power law expression in (3-5) is manipulated thus:

$$N(D,R_\tau) = N_0(R_\tau)\left[\alpha R^{-\beta}\right]^{-\lambda(R_\tau)} \tag{3-15a}$$

$$N(D,R_\tau) = N_0(R_\tau)[xD^y]^{-\lambda(R_\tau)} \tag{3-15b}$$

where $R = (D/\alpha)^{-1/\beta}$ and x and y are the rain rate correlation factors of the two locations while α and β are the power law parameters for the rain cell size.

The results in (3-15*a&b*) enable the correlation of RCDD of two locations whose rain rate relationship is known since the slope factor at a given rain rate is taken to be a constant.

3.7 Conclusion

Even though radar data provide exact rain cell occurrence in space, the point rain rate analysis presents the distribution of the rain cells as they reach the ground. Radar rain cell data obtained from a range bound within 60 km is well catered for by this method and comparison tests can be performed to ascertain the rain cell extensions observed from space borne devices and radar. Since 1-min rain rate and rain cells data from radar are rare, the RCDD for neighbouring locations can be correlated from the rain rate time series data. This work finds application in radio network deployments that require knowledge of rain cell size information like radio cell area coverage. These may include the average diameter of rain cells and total cell area. The separation distance between two diversity sites can as well be estimated from this work. To further validate the parameters in Table 3-1 the value of the slope factor, $\lambda = 2.267$ of the power law model is used in Chapter 4 (Figure 4-8) in attenuation prediction for terrestrial links, and improvements in the results are noted. Also, the rain cell size obtained here complements the work in Chapter 3.

3.8 References

[1] "Propagation Prediction Techniques and Data Required for the Design of Terrestrial Line-of-Sight Systems," ITU-R*,* Geneva, 2005, ITU-R Rec. P.530-11.

[2] Sauvageot H. and Mesnard Frederic, "The relation between the area-average rain rate and the rain cell size distribution parameters," *Journal of Atmospheric Science*, vol.56, pp. 57-70, Jan. 1999.

[3] P. O. Akuon and T. J. O. Afullo, "Rain cell size statistics from rain gauge data for site diversity planning and attenuation prediction," *Proc. of Southern Africa Telecommunication Networks and Applications Conference (SATNAC),* East London, South Africa*,* pp.213-216*,* 4-7th Sept. 2011. ISBN: 978-0-620-50893-3.

[4] P. O. Akuon and T. J. O. Afullo, "Path reduction factor modelling for terrestrial links based on rain cell growth," *Proc. of IEEE Africon conference*, Livingstone, Zambia, 13-15th Sept. 2011. ISBN: 978-1-61284-991-1.

[5] A. Pawlina-Bonati, "Essential knowledge of rain structure for radio applications based on available data and models," *Proc. of Radio Africa 99, Gaborone, Botswana,* pp 96–106, October 1999.

[6] G. Drufuca G, I. Zawadzki, "Statistics of rain gauge data," *J. of Applied Meteorology*, vol. 14, pp. 1419–1429, Dec. 1975.

[7] A. Pawlina Bonati, E. Matricciani, "Rain cell size statistics inferred from long term point rain rate: model and results," *Proc. Third Ka Band Utilization Conf.*, Sorrento, Italy, pp. 299–304 Sept., 1997.

[8] A. S. Dennis and F. G. Fernald, "Frequency distributions of shower sizes," *J. Appl. Meteor.,* vol.2**,** pp**.**767–769, 1963.

[9] T. G. Konrad, "Statistical models of summer rain showers derived from fine-scale radar observations," *J. Appl. Meteor.,* vol. 17**,** pp. 171–188, 1978.

[10] R. S. Teno´ rio, H. Sauvageot, and S. Ramos-Buarque, "Statistical studies of rain cell size distribution using radar data during squall line episodes in West Africa," *Proc. Third Int. Symp. on Hydrological Applications of Weather Radar,* Sao Paulo, Brazil, 518–526,1995.

[11] K. S. Kuo, R. M. Welch, and S. K. Sengupta, "Structural and textural characteristics of cirrus clouds observed using high spatial resolution LANDSAT imagery," *J. Appl. Meteor.,* vol. 27**,** pp.1242–1260, 1988.

[12] L. A. T. Machado, and W. B. Rossow, "Structural characteristics and radiative properties of tropical cloud clusters," *Mon. Wea. Rev.,* vol. 121**,** 3234–3260, 1993.

CHAPTER 4

Attenuation Prediction for Terrestrial Links

4.1 Abstract

A new path length reduction factor that accounts for the growth and occurrence of multiple rain cells along a propagation path of a given terrestrial link is introduced in this work. In addition, the mathematical and empirical derivations that were used to come up with this new factor are outlined. This model is investigated by comparing it to other well-known models by utilizing attenuation statistics from a 19.5 GHz terrestrial link experiment carried out in Durban, South Africa. The predicted and measured attenuation values are then compared for the three models. Evaluation of the three models is then carried out by calculating their attenuation percentage error values. It is seen that the proposed model performs well over the ITU-R model in the terrestrial link thus validating it as a good model for rain attenuation predictions in the Southern Africa region.

4.2   Introduction

Path reduction factor in rain attenuation studies is the ratio of the effective path length of a link where the rain rate is considered as uniform, to that of the actual link length. It accounts for the inhomogeneity of the spatial form of rain along a given path. It is therefore important in prediction of attenuation on links. Sufficient fade margin allocation lowers the probability of link outages due to rain which is a major problem at frequencies above 10 GHz [1]. There are indications that in equatorial climates which experience larger raindrop mean diameters than those of the temperate climates, the occurrence of rain phenomena on the radio links is a vital cause for frequencies above 7 GHz [2]. Various path reduction factor models exist that are used for prediction of rain attenuation; those evaluated in this work are the ITU-R [3, 5] model, Moupfouma model [4] and the proposed model. The path length factor is calculated by dividing the actual attenuation (predicted by a model or measured) by the product of the actual path length and the specific attenuation. ITU-R P.530-11 [5] outlines the steps used for calculation of rain attenuation, A(dB) thus:

$$A = \gamma L_{\text{eff}} = aR^b L_{\text{eff}} \qquad (4\text{-}1)$$

where the coefficients a and b are dependent on the drop-size distribution of rain, polarization, frequency and temperature and γ (dB/km) is the specific attenuation given in [3].

L_{eff} is the effective path length given by (4-2):

$$L_{\text{eff}} = r.L \qquad (4\text{-}2)$$

where r is the path reduction factor which varies according to the temporal variation of rain rate and its spatial distribution.

Effective path length is the length of the link where the attenuation for any given time percentage is only as a result of a point rainfall rate that coincides at that time percentage. That is the reason why the rain intensity is assumed to be constant over the effective path length [4]. ITU-R P.530-11 [5] gives a path reduction factor at 0.01% of the time defined by (4-3):

$$r_{0.01} = 1/(1 + L/D_0) \qquad (4\text{-}3)$$

where $D_0 = 35 \exp(-0.015R_{0.01})$ for $R_{0.01} \leq 100$ mm/h and $D_0 = 35 \exp{-1.5}$ for $R_{0.01} > 100$ mm/h.

$R_{0.01}$ is the rain rate value exceeded for 0.01% of the time and D_0 is the rain cell diameter. $A_{0.01}$ is the attenuation value exceeded for 0.01% of the time as given in (4-4):

$$A_{0.01} = \gamma L_{\text{Eff}} = \left(aR_{0.01}^b L.r_{0.01}\right) \qquad (4\text{-}4)$$

The predicted attenuation values for other percentages of the time are then derived from (4-5):

$$A_p/A_{0.01} = 0.12p^{-(0.546+0.043\log p)} \qquad (4\text{-}5)$$

Moupfouma [4] presented a path length factor defined as functions of the frequency, the percentage of time the given year and the actual path length. The Moupfouma reduction factor model, r is shown in (4-6):

$$r = 1/\left(1 + 0.03L^m \left(\frac{P}{0.01}\right)^{-\beta}\right) \qquad (4\text{-}6)$$

where m is dependent on the frequency of the link and path length, L. The variable, β is defined as the range $0.36 \leq \beta \leq 0.6$ based on the probability level P (%) and on L.

4.3 Methodology

In order to have a mathematical model of rainfall, some knowledge is required on the physical nature of rain. In this attempt, we considered various factors which include: occurrence of rain in the form of cells, rain cell shapes, rain cell movement, growth of rain rates within a cell and rain cell size statistics. The ITU-R model in (4-3) does not account for the growth of rain into multiple cells.

Moupfouma model as given in (4-6) requires knowledge of the probability level of interest and therefore does not support the direct use of full rain rate data which is readily available. The approach used was initially introduced by Hansson [6] who estimated a rain cell movement on a path by defining a time accumulation factor (ACCF). His work was later redefined by Bryant *et al.* [7] by using a different definition of probability of interception of path by rain cells.

From appendix A.2 (see equation A.2-17), the weighted mean intercept, *I* is given as:

$$I = \frac{2}{\pi} L \left(1 + \frac{1.047}{\xi_\theta}\right)\left(\frac{1}{\xi_\theta L/D + 1}\right) \tag{4-7}$$

where *L* is the path length, ξ_θ is the elevation coefficient (see appendix A.1, equation A.1-4) and *D* is the equivalent rain cell diameter function.

The ellipsoidal factor of $\varrho = 2.047$ is as a result of the rain cell interception with path where $\xi_\theta \approx 1$ for terrestrial links (due to low elevation angles) and *I* relates to the path length and rain cell diameter dimensions. Fig.4-1 illustrates how the coefficient of elevation changes with link elevation angles.

4.3.1 Rain Cell Size Model

With *D* as the equivalent rain cell diameter that will provide annual 99.99% of the time link availability and *R*, the rain rate , the rain cell diameter is expressed as:

$$D = 51R^{-0.46} \tag{4-8}$$
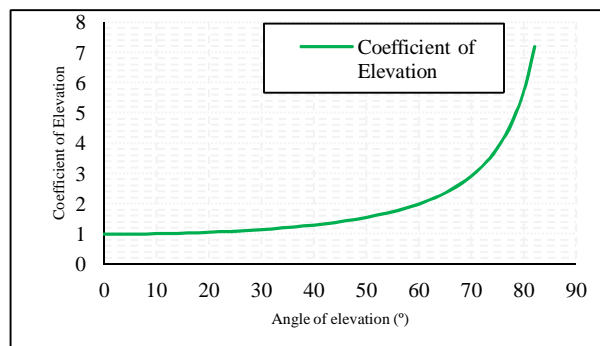
Figure 4-1 Variation of Coefficient of Elevation, ξ with elevation angle, θ

The rain cell diameter distribution obtained in this analysis is compared to other existing models: Bryant *et al.* model [7] (Lae site, PNG, tropical ITU-R zone P), Mauro Assis and Timoteo da Costa model [15] (ITU-R data bank for radio links in temperate regions) and ITU-R model [5].

Durban being a subtropical climatic zone, the rain cell diameter distribution is seen to lie between those of the temperate and tropical zones. This is illustrated in Fig.4-2.

4.3.2 Growth of Rain Rate within Rain Cells

There exist models that have classified rain cells into typical shapes like Gaussian by Eagleson *et al.,* "HYCELL" by Féral *et al.* that estimates a rain cell to have Gaussian inner core for convective and outer exponential shape for stratiform rain [16]–[18]. In 1998 Paraboni *et al.* also presented a modified exponential shape to account for minimal rain rates [19].
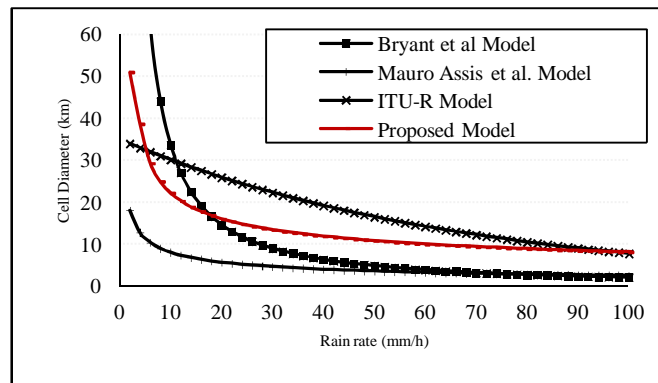
Figure 4-2 Equivalent rain cell diameter distribution models
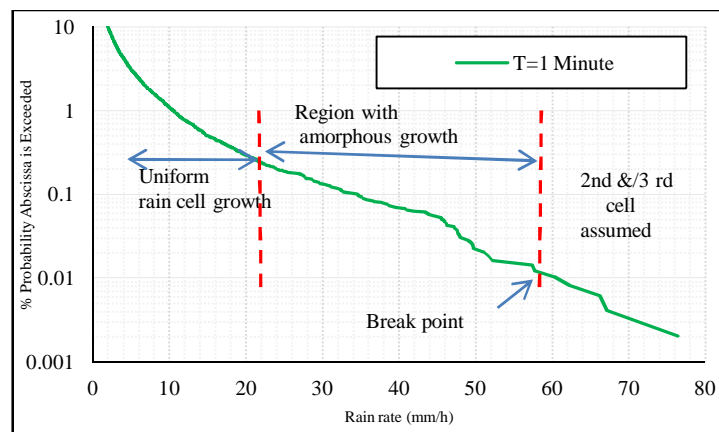
Figure 4-3 Rain rate cumulative distributions for Durban, South Africa

Another work on rain cell shape was done by Mauro Assis *et al.* in Brazil by presenting a truncated exponential shape which works well in predicting rain attenuation in short path lengths since the path length reduction factor has a value greater than one [20].

From measurements, as shown in the exceedances plot of Fig. 4-3 and rain event plot of Fig. A.3-1, we see that the uniformity in the exponential growth of rain rates changes at the rain rate of about 19 mm/h and the change in rain rate becomes amorphous with few changes until the maximum rain rate in the rain event is attained.

At the maximum rain rate within the cell, the rain cell breaks and then the rain rates decay to zero in the case of a single rain event as shown in Fig. A.3-1 otherwise a second cell is assumed to occur whose effect is depicted in Fig. 4-3 at the break point. This means that at the onset of a rain event, a rain cell sets up, which grows towards a multiple cell event with a uniform exponentially growth to a point where an amorphous growth then starts. We refer to this as the point of inflexion, of which from the two year, (2009-2010) 1-minute rainfall data from disdrometer measurements (located at Centre of Excellence, Howard College, in the University of KwaZulu-Natal, Durban , 29º97'S, 30º95'E), tends to be at $1/\pi$ of the peak of the rain events [14]. After this point, the changes in rain rate are not uniform, the rain rate increases abruptly to a higher value, implying that the effect of attenuation reduces per unit rain rate increase. Thus, in the region between the point of inflexion and the rain rate at the break point, R_b (just before the rain rate exceeded for 0.01% of time in a year, $R_{0.01}$), the change in rain cell growth rate decays till it gets to zero at the peak point. Beyond the breakpoint, a second cell is assumed to be set up which introduces more attenuation effects and the growth factor used at $R_{0.01}$ is that of the second cell. The point of inflexion equals R_b/π and R_b may be taken to be $R_{0.01}$ where it is not known.

The rain rates growth factor within rain cells ς is defined by:

$$\varsigma = \varsigma_m \exp - \left(\frac{(R - R_i)^2}{2\zeta^2} \right) \tag{4-9}$$

where R is the rain rate, R_i the rain rate at the point of inflexion (R_b/π), ς_m is the peak factor at R_i, and ζ determines the width of the curve shape.

$$\varsigma_m = \exp \left(\frac{0.693 \times R_b/\pi}{R_b} \right) = 1.24681 \tag{4-10}$$

$$\zeta = (R_b - R_b/\pi) = 0.6817 \, R_b \tag{4-11}$$

With low rain rates below 3 mm/h, small-sized rain drops are coalesce and water is likely to collect on the antenna terminals thus causing signal attenuation.

We cater for this by introducing a truncated-Gaussian growth factor, ς_1 which accounts for attenuation for minimal rain rates in the first cell by modifying the coefficient ς_m in (4-9) thus:

$$\varsigma_1 = 1 + \left(\varsigma_m - 1\right) \exp - \left(\frac{(R-(R_b/\pi))^2}{2\zeta^2}\right) \tag{4-12}$$

For rain rates above break point, the effect of the second cell on attenuation may be accounted for by the growth factor of the second cell. The maximum inflexion is estimated to be at 95% of the first cell in the case where any rain rate value above break point, $R_2 \geq R_b$, thus:

$$\varsigma_2 = 1 + \left(0.95\varsigma_m - 1\right) \exp - \left(\frac{(R_2-R_b)^2}{2\zeta^2}\right) \tag{4-13}$$

For a third rain structure, for this work, we propose a factor of the maximum inflexion, $\varsigma_3 = \varsigma_m$. This may only be applicable in some parts of tropical rainfall zones like Malaysia and Indonesia [2] where $R_3 \geq R_b$ and $\varsigma = n\varsigma_2$. n denotes the number of cells after the breakpoint. Fig.4-4 illustrates the growth factor of rain rates for two rain cells.

From (4-7), rain attenuation for terrestrial links can then be defined by:

$$A = \frac{\gamma L}{\cos\theta} \varsigma \frac{2}{\pi} \left(1 + \frac{1.047}{\xi_\theta}\right) \left(\frac{1}{\xi_\theta L/D+1}\right) \tag{4-14}$$

where A (dB) is the attenuation, γ is the specific attenuation (dB/km), and θ, the elevation angle, ς is the factor introduced by the growth of rain rates within the cell; it takes the values ς_1 or $n\varsigma_2$.
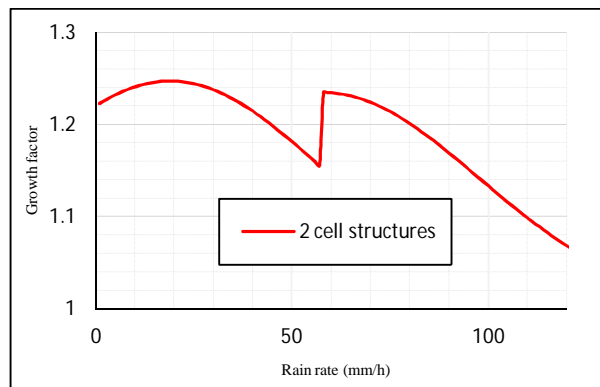
Figure 4-4 Illustration of rain rate growth factors within rain cells in Durban, South Africa

The proposed model has a reduction factor, r for terrestrial links of length L (km) and low elevation angles of less than ten degrees defined by (4-15) where the value 1.303 is the constant derived from (4-14) and the value of D is given in (4-8). The coefficient of elevation is ignored since for low elevation angles encountered in terrestrial link installations which may be less than ten degrees, the value is closer to unity as is seen in Fig. 4-1.

$$r = 1.303 \, \varsigma \, \frac{1}{1+L/D} \tag{4-15}$$

$$\varsigma_{0.01} = \varsigma_1; \text{ otherwise [7] for } R_{0.01} \geq 110 \text{ mm/h,}$$

$$\varsigma_{0.01} = n\varsigma_2$$

4.4 Results and Discussion

A horizontally polarized terrestrial link performance in Durban, South Africa was recorded for a period of one year. The path length was 6.73 kilometres and transmitting at a frequency of 19.5 GHz. During the same year, rain rate measurements were taken for Durban and a similar rain rate cumulative distribution is shown on the graph of Fig. 4-3. Details of this link are available in other publications [20–22]. Path length reduction factors for virtual links of length between 1 and 30 kilometres are also compared for the three models and another for Lin [23] at 0.01% of the time. The proposed reduction factor is seen to compare very closely to the ITU-R model (see Fig. 4-5) at the set parameters and has a value more than unity for path lengths shorter than seven kilometres i.e. path length equals or less than the rain cell diameter. The predicted attenuation values are calculated for the three models (ITU-R, Moupfouma and the proposed model) and compared to the measured attenuation data as given in Fig. 4-6.

Figure 4-5 Path reduction factor for different terrestrial path lengths at $R_{0.01}$ of 60 mm/h, Frequency = 19.5 GHz in Durban, South Africa
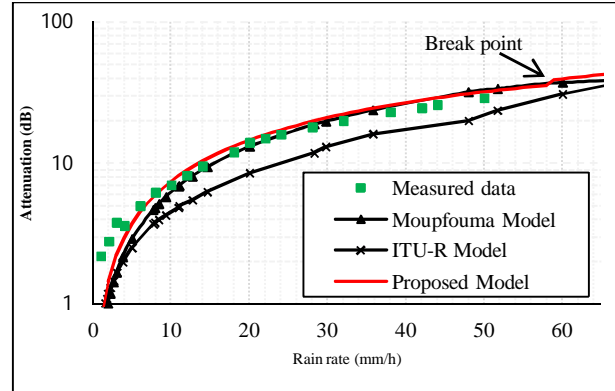
Figure 4-6 Model comparison of predicted and measured attenuation in Durban, South Africa

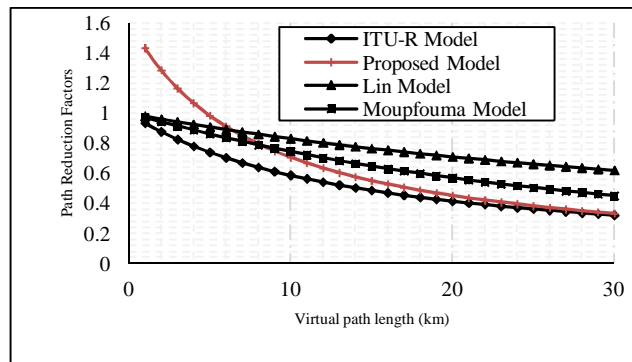The percentage errors, e_m between the measured and predicted attenuation values are computed for all the models and for every rain rate according to (4-16):

$$e_m = \frac{|A_p - A_m|}{A_m} * 100 \qquad (4\text{-}16)$$

where A_p is the value of the predicted attenuation and A_m is the measured attenuation for each model at a given % of the time.

The error results are presented in Fig. 4-7 for comparison purposes. The model with the least percentage error value is taken as the best model in this evaluation method. We note that ITU-R model underestimates the rain attenuation for Durban for the relatively low rain rates experienced in the subtropical location. The proposed model and the Moupfouma model give better prediction results of rain attenuation and the proposed model does not depend on the scaling factor from the values at the 0.01% of the time as is the case with ITU-R model and Moupfouma model. However, all the three models have almost equal prediction near the 0.01% rain rate value. At 70 mm/h, the ITU-R model overestimates the measured values while the other two show saturation trend in attenuation of about 40 (dB). It is only the proposed model that clearly shows the deviation point at the breakpoint where attenuation abruptly changes to a higher value at the break point rain rate value, which we discussed earlier. This is indicated in the graph of Fig. 4-6. The larger percentage errors on the predicted values at lower rain rates can be attributed to the effects of minimal rain rates experienced between 0 and 3 mm/h (rain water deposit on the antenna leading to wet antenna losses at both the transmit-end and receive-end) or non-uniformity in path attenuation. The rain drops at low rain rates are believed to fill the path more fully than larger rain drops which are sparsely localised in nature thus increasing their path reduction factor for low rain rates.
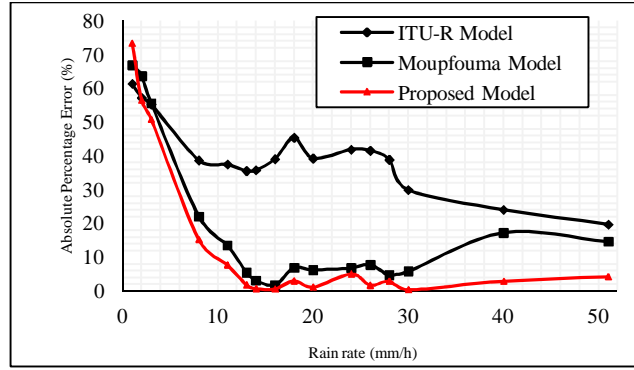
Figure 4-7 Absolute percentage errors for the three models
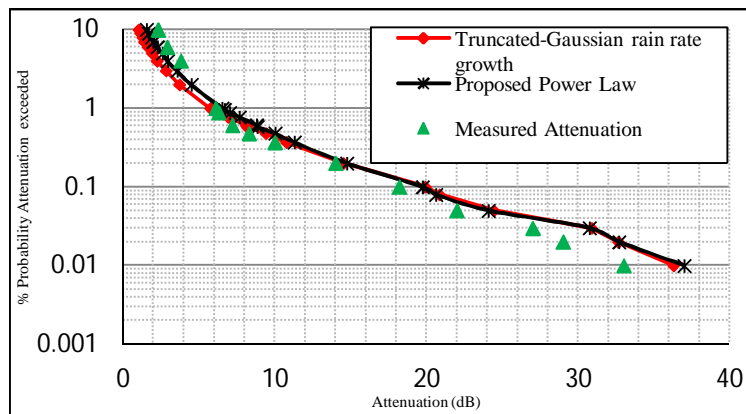
Figure 4-8 Attenuation prediction from two growth factors

From the error analysis, there is an underestimation in the low rain rate region by all the models. The growth of rain rates alone is not sufficient to predict the growth in attenuation. The decay factor of the power law form of the RCDD in Chapter 3 is used to estimate the attenuation growth for rain rates below the break-point. The growth is expressed as:

$$\varsigma = 1 + R^{-\frac{1}{\lambda}} \quad ; \quad \lambda = 2.267 \tag{4-17}$$

where R is the rain rates.

When this is used in the attenuation model in (4-14), the result shows an improvement in attenuation for low rain rates as depicted in Fig. 4-8 (see proposed power law graph). With the model presented here for attenuation prediction in terrestrial links, link planning can be achieved with more accurate estimations. Figs. 4-9 and 4-10 show the mapping of specific attenuation using ITU R values [3] for 15 GHz and 26 GHz frequencies in South Africa. The contours are generated in MATLAB software from measured $R_{0.01}$ values in South African cities [24].
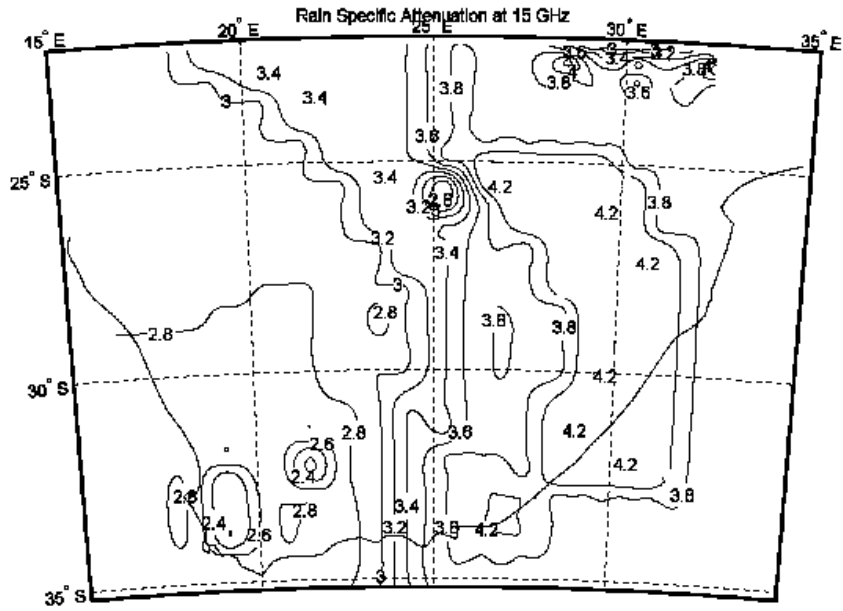
Figure 4-9 Rain-induced specific attenuation contours for horizontally polarized microwave link of 15 GHz frequency at 0.01% of the time
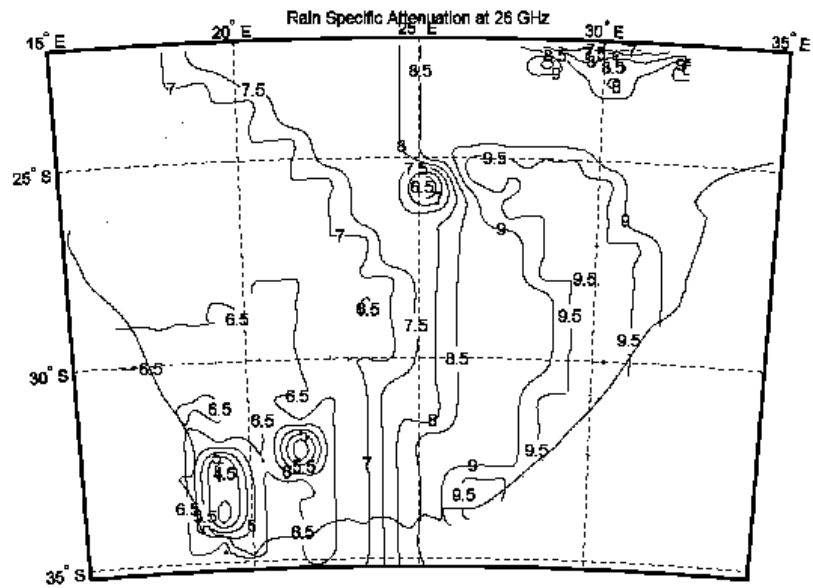
Figure 4-10 Rain-induced specific attenuation contours for horizontally polarized microwave link of 26 GHz frequency at 0.01% of the time

4.5   Conclusion

The rain rate data obtained for Durban were successfully used to investigate the performance of proposed path reduction factor model by determining the rain cell size distribution. The proposed reduction factor model is not limited to values less than one and is therefore useful in predicting attenuation on short links where the rain cell can occur over a whole length of link. The truncated-Gaussian growth factor model has incorporated the physical nature of rainfall in space and time and has been used to show that it is good in attenuation prediction for the terrestrial link. Suitability of the proposed model for other regions of different climatic conditions is to be investigated further. The start point of the second cell accounts for the increase in attenuation encountered at R_b, which then saturates though the nature of the growth of the second rain cell after this point requires further investigations. There is poor prediction for low rain rates by all the models and further description of path should be investigated to solve this feature. Nonetheless, the postulation and application of RCDD decay factor to model the growth in attenuation seems to improve the error.

4.6   References

[1] R. K. Crane, "A two-component rain model for the prediction of attenuation statistics," Radio *Science,* vol.17, pp. 1371–1387, 1982.

[2] F**.** Moupfouma and J. Tiffon, "Raindrop size distribution from microwave scattering measurements in equatorial and tropical climates,'' *Electronic Letters,* vol. 18, pp. 1012–1014, 1982.

[3] "Specific attenuation model for rain for use in prediction models," ITU-R, Geneva, 2005, ITU-R Rec. 838-3.

[4] F. Moupfouma, "Improvement of a rain attenuation prediction method for terrestrial microwave links," *IEEE Trans. on Ant. and Prop.*, vol. 32, pp. 1368–1372, 1984.

[5] "Propagation Prediction techniques and data required for the design of Terrestrial Line-of-Sight systems," ITU-R, Geneva, 2005, ITU-R Rec. P.530-11.

[6] L. Hansson, "New concept used to predict slant path rain attenuation statistics," *Proc. IEEE.* Vol.137, pp.89-93, Apr. 1990.

[7] Bryant, G. H., I. Adimula, C. Riva, and G. Brussard, "Rain attenuation statistics from rain column diameters and heights," *Int. J Satellite Commun.*, vol. 19, No. 3, pp. 263–283, 2001.

[8] A. Pawlina-Bonati, "Essential knowledge of rain structure for radio applications based on available data and models," *Proc. of Radio Africa 99, Gaborone, Botswana,* pp 96–106, October 1999.

[9] G. Drufuca G, I. Zawadzki, "Statistics of rain gauge data," *J. of Applied Meteorology*, vol. 14, pp. 1419–1429, Dec. 1975.

[10] A. Pawlina Bonati, E. Matricciani, "Rain cell size statistics inferred from long term point rain rate: model and results," *Proc. Third Ka Band Utilization Conf.*, Sorrento, Italy, pp. 299–304, Sept., 1997.

[11] M. Binaghi and A. Pawlina Bonati, "Statistical dependence of rain occurrence in multiple site case modelled with dynamical radar derived parameters," *Proc. ISAP 92, Int. Symp. On Antennas and Propag.,* pp. 1053–1056, Sapporo (Japan), Sept. 1992.

[12] S. Begum, C. Nagaraja, I. Otung, "Analysis of rain cell size distribution for application in site diversity," *IEEE Antennas & Propag.*, pp.1–5, 2006.

[13] C. Capsoni and L. Luini, "A physically based method for the conversion of rainfall statistics from long to short integration time," *IEEE Trans. Antennas Propag.*, vol.57, no. 11, pp. 3692–3696, Nov. 2009.

[14] Akuon P. O. and Afullo T. J. O., "Rain cell size statistics from rain gauge data for site diversity planning and attenuation prediction," *Proc. of Southern Africa Telecommunication Networks and Applications Conference (SATNAC),* East London, South Africa*,* pp.213-216*,* 4-7th Sept. 2011. ISBN: 978-0-620-50893-3.

[15] A. Timoteo da Costa and M. S. Assis, "The concept of path length factor in the prediction of rain attenuation in terrestrial links," *XXVIIth General Assembly of URSI,* Maastricht, the Netherlands, Aug. 2002.

[16] P. Eagleson, N. Fenessey, W. Quiliang and I. Rodriguez-Iturbe, "Application of spatial Poisson models to airmass thunderstorm rainfall," *J. Geophys. Res.*, vol. 92, pp.9961–9978, 1987.

[17] L. Féral, F. Mesnard, H. Sauvageot, L. Castanet, J. Lemorton, "Rain cells shape and orientation distribution in South-West of France," *Phys. Chem. Earth (B)*, vol. 25, pp. 1073–1078, 2000.

[18] L. Féral, F. Mesnard, H. Sauvageot, J. Lemorton, "HYCELL-A new hybrid model of the rain horizontal distribution for propagation studies," *Radio Sci.*, vol. 38, Issue 3, pp. 23–1, 2003.

[19] A. Paraboni, G. Masini, C. Riva, "The spatial structure of rain and its impact on the design of advanced TLC systems," *Proc. Fourth Ka Band Utilization Conf.,* Venice, Italy, pp. 169–172, Nov 4, 1998.

[20] K. Naicker and S. H. Mneney, "Propagation measurements and modelling for Terrestrial Line-of-Sight links at 19.5 GHz," *IEEE Africon, Gaborone, Botswana,* vol. 01, pp.95–100, Sept. 2004.

[21] M. O. Fashuyi and T. J. O. Afullo, "Characteristics of seasonal attenuation and fading for line of site links in South Africa," *Proc. Of SATNAC,* pp. 203-208, Sept. 2008.

[22] M. O. Odedina and T. J. Afullo, "Characterization of rain attenuation and its Application to terrestrial communication systems in South Africa," *Proc. of the 6th IASTED Conf. on Antennas, Radar and Wave Propag.*, Banff, Alberta, Canada, July 2009.

[23] S. H. Lin, "Nationwide long term rain statistics and empirical   calculation of 11GHz microwave rain attenuation," *The Bell System Tech. J.*, Vol.56, No. 9, pp.1581–1604, 1997.

[24] P. A. Owolawi, "Rain rate probability density evaluation and mapping for the estimation of rain attenuation in South Africa and surrounding Islands," *Progress in Electromagnetic Research*, vol. 112, pp. 155–181, 2011.

Chapter 5

Attenuation Prediction for Satellite Links

5.1   Abstract

The slant path attenuation model is presented that is derived from physical postulation of rain cell shape and rain rate growth within the cell. The model is extended for use beyond the break-point where the birth of multiple rain cell structures is depicted. The break-point of rainfall rates in the initial cell is close to the rain rate value exceeded for 0.01% of the time. The rainfall growth rate is modelled with a truncated-Gaussian characteristic- resulting in multiple growth factors that describe growth in the first rain cell and the possible multiple cell structures beyond the break point. The elevation coefficient for possible slant path elevation angles is shown based on mathematical analysis, validated by use of empirical data analysis, and used to show that it modifies the rain cell diameter and the ellipsoidal path curvature. The two physically derived results together with a rain cell size distribution model obtained from 5-year rainfall data in the sub-tropical zone, Durban (29º97'S, 30º95'E) South Africa are then used to derive the slant path attenuation model based on mean path intercept approach. By the use of comparison tests with ITU-R, Bryant *et al* and the proposed models, the predicted attenuation values for satellite links located in tropical climatic zones of varying elevation angles are compared with the measured values. The proposed model has the best performance from the test variables used.

5.2   Introduction

Technologies emerge today some of which are as a result of the problems and limitations encountered in the use of satellite links which are set up at microwave frequencies. Fibre optic transmission is an alternative for signal transmission praised for its high bandwidth transmission capability but is highly prone to physical damage making it a comparatively insecure channel with rampant maintenance requirements expected. Though there are fewer satellite earth stations in GSM technology today, the future of Long-Term Evolution (LTE) technology adopted by the Next Generation Networks group (NGN) will see the introduction of more Internet Protocol (IP) based network elements even in the access network. Growth in cell phones acquisition will see an increase in the demand for services like Internet connectivity, multimedia and video-streaming, and digital television thus increasing bandwidth demand. Therefore, there is rising need to fully utilize the microwave spectrum especially the 10 GHz and above.

However, these frequencies are prone to undesired signal attenuation as they pass through precipitation due to their relatively small wavelengths. The precipitation of rain significantly introduces signal fading through scattering and absorption processes by the rain drops [1–4]. This scenario necessitates a provision for the expected signal fading along the path as it encounters a rainy medium. Unless an optimal value is set, the transmitted signal power may be either too high (leading to a waste in the bandwidth) or too little, (resulting to frequent rain induced signal losses). To address this issue, the ITU-R organization has put in place recommendations used in predicting expected optimal attenuation in rain medium for satellite links [4].

Other authors have also come up with models from varying approaches that are used for the same purpose: measurement of specific attenuation as a function of rain rate (e.g. Ajayi model [3], SAM model [5], Flavin model [6]), prediction of rain attenuation in the path based on point rain rate and those based on attenuation exceedance percentages (e.g. DAH model [7], Crane Global model [8], ITU-R model [2], Bryant model [9]). For rain induced attenuation models, various input parameters are required to compute the predicted attenuation values. These include: the earth station height, antenna elevation angle, frequency of transmission, rain height, polarization angle and constants, point rain rate, rain rate at a given percentage probability level and rain rate break point.

Other popular models include Assis- Einloft model, Australian model, Brazil model, Crane two-component model, EXCELL model, Garcia-Lopez model, ITU-R 618 model, Karasawa model, Leitao-Watson model, Matricciani model, Misme-Waldteufel model [18], SAM model, and Svjatogor model. The details of these models are well described in COST-255 project [10]. Most studies have indicated that the most critical prediction is required for the high rain rate region i.e. between the rain rate exceeded for 0.01% of the time in a year, $R_{0.01}$ and above since this provision would ensure at least 99.99% availability of the link [2,7–9].

There is a break point in the cumulative distribution (CD) of rainfall rates, R at a value that has been determined to be closer to the $R_{0.01}$ in some tropical zones [11–14]. In 2001, Bryant *et al* noted in their four year measurements at Lae, New Guinea (PNG), that rain rate at break point, R_b seems not to fluctuate with annual variations in CD of rainfall. New studies have associated this break point of rain rates with the increase in attenuation on the link at equal probability, and this new finding proved useful in the development of the modified ITU-R model by Ramachandran *et al* in 2006 [14].

5.3   Methodology

5.3.1 Some Slant Path Models and Parameters

We consider some models that are related to the approach that we have used to come up with the proposed model. The standard ITU-R [4] model recommends a general formula for use in prediction of rain–induced attenuation in earth-space microwave links situated anywhere.

The model is good, periodically updated for better accuracies and seems to work well in areas where a single structure of rainfall event occurs over a wide area. This occurrence of wide rain cell diameters has been found to be dominant in temperate climatic zones, upon which the empirical data used to derive the rain rate and rain cell diameter relationship was based. For tropical zones, the ITU-R model is reported to underestimate the measured attenuation. It does not account for the sudden increase in attenuation at break point and consequent saturation that seems to occur at higher rain rates which is a common scenario in the tropical regions [11–14]. However, the model was tested by Paraboni in 1995 and found to be the best of the models and is applicable in many areas [15]. Bryant *et al*'s model makes no assumption on rain rate shape, performs quite well in the 0.01% of time exceedances region for tropical sites, and utilizes the full rain rate to estimate attenuation due to rain on satellite links [9]. The model derives a relationship between the rain rate and the rain cell diameter which was modelled from rainfall data from Lae, PNG site. The model adopts the supposition of occurrence of multiple cells at higher rain rate values whose number grows exponentially with rain rate, R and considerably accounts for the sudden increase in attenuation caused by the rising break in the rain rate CD. They gave a result for the rise in rain column heights that is dependent on the rain rate, a vital factor for slant path attenuation estimations. The model performs better than the standard ITU-R model for the overall test sites [9].

In 2007 Ramachandran *et al* derived an ITU-R modified attenuation model which depicts the break point in attenuation and saturation, but does not represent the full rain rate characteristic. It performs better around the region of the rain rate value exceeded 0.01% of time for most tropical regions than the ITU-R and Crane models, and notably for Lae site. The prediction for other tropical sites by the model around the 0.01% exceedance region may still require fine tuning in the modification [14]. On the other hand, the proposed model incorporates a supposition of rain rate growth shape within an initial rain cell that follows the lower rain attenuation caused by mid rain rate values in the region between 10% and 0.01% of time exceedances points.

For the region between 0.009% and below (rain rates higher than the rain rate at break point), at least a modification is required to account for the rising break in the distribution of rain rate and attenuation that occurs [10-14]. This is achieved by postulating an evolution of a second rain cell at the break point which may grow in the same form as the initial rain cell but also dependent on the geometry of the path inclination to the horizontal plane. The rain event after the break point is convective in nature which implies a more rapid decay than the first rain cell, and larger rain drops which may result in more wave reflections [17].

The derivation of the rain rate growth shape and rain cell diameter size distribution from Durban data are available in other earlier work carried out by the authors [11, 16]. The direction of this work therefore is to formulate a feasible representation of rainfall phenomena as it occurs in space, by considering two factors: (1) a physical rain cell form (shape and size) that would intercept a slanting signal path and (2) its mean effect on microwaves signal at any obtainable frequency of transmission. For the shape, we consider the rain height model as suggested by [9] which is a function of rain rate, truncated-Gaussian rain rate growth factor [11] and rain cell size distribution model [15]. The rain rate growth model takes into account a possible incidence of a second and or third rain cell structure in a given rain event beyond the break point which then decays with time thus buttressing the scenario of saturation in attenuation measurements seen at about the 0.001% of time point .

 It has also been suggested that changes in specific attenuation and link outage threshold may cause saturation [9, 14]. For the second point, the signal attenuation experienced through the rain medium is as a result of the sum of scattering and absorption processes of microwave signals as the waves go through rain drops. The study of rain drop size distribution is important since it may significantly vary from a geographical area to another, which would in turn change the magnitude of specific attenuation [1-4, 8]. We have assumed that the coincidence of different drop size distributions for the same rain rate, the consequent effects of signal absorption, reflections and scattering, and hence the change in specific attenuation, is nominal after the break point. In this way we avoid the complex mathematical analysis of dynamically changing rain drop cross sections beyond the break point. In this study, the use of frequency and polarization factors contained in ITU-R 838-3[1] to compute specific attenuation is considered adequate.

5.3.1.1 Earth-Space Slant Path

The slant path can be represented as shown in Fig. 5-1 where the region above region *A* represents the frozen precipitation, region *B* is liquid precipitation (rain), H_s is station height, H_r is the rain isotherm height at 0°C , H'_r , $L's$, L'_G are the multiple cell rain height, slant path and horizontally projected length, respectively; L_s is the slant path in rain, L_G is the projected horizontal path length and *S* is the Earth-space path.

ITU-R Rec. P.839-3 has details of the steps used for computing the slant path [19]: The freezing rain height H_{fr} (km) is obtained from the absolute value of location site latitude φ (degrees):

$$H_{fr} = 5.0 \text{ km}, \quad \text{for} \quad 0° \le \varphi < 23° \tag{5-1a}$$

$$H_{fr} = 5.0 - 0.075(\varphi - 23°) \text{ km}, \quad \text{if} \quad \varphi \ge 23° \tag{5-1b}$$

The length of the slant-path, *Ls*;

$$L_S = \frac{H_r - H_s}{\sin \theta} \quad \theta \ge 5 \tag{5-2a}$$
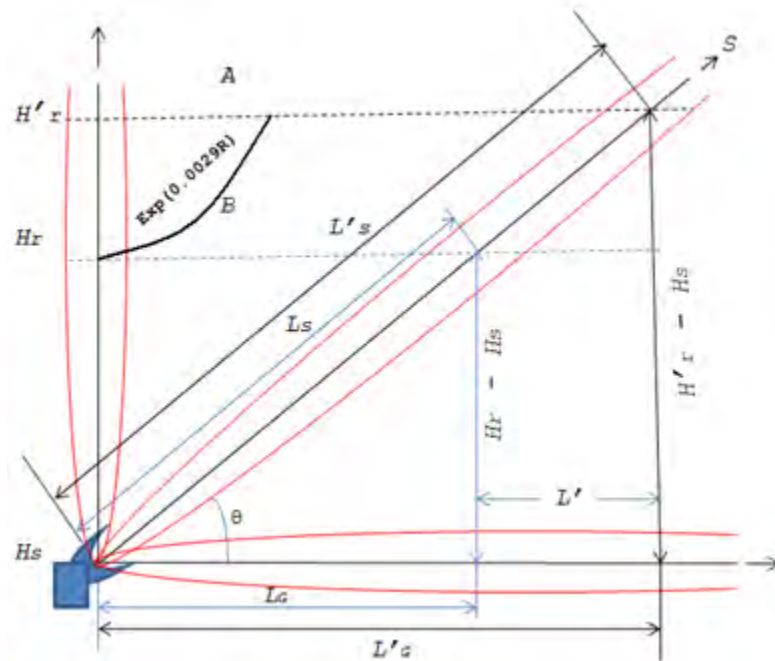

Figure 5-1 Derivation of path parameters from radio link orientation

Here, θ is the angle of elevation and H_s(km) is the earth station height. For smaller elevation with angles less than 5°, the slant path is estimated by [19]:

$$L_s = \frac{2(H_r - H_s)}{\left(\sin^2\theta + \frac{2(H_r - H_s)}{R_e}\right)^{0.5} + \sin\theta} \quad \theta < 5 \qquad (5\text{-}2b)$$

$$\text{the earth radius, } R_e = 8500 \text{ (km)} \qquad (5\text{-}3)$$

Then the horizontal path length is calculated from:

$$L_G = L_s \cos\theta \qquad (5\text{-}4)$$

The same procedure is applied for the slant path of the multiple cell structures that are assumed to occur beyond the first break point.

5.3.1.2 Rain Cell Diameter and Height Models

In order to relate the extent of path that will be in rain, we determined the rain cell size distribution model described by (5-5) for any given rain rate, R with D as the rain cell diameter [16]. This was achieved by the use of the 5-year hourly rainfall data collected by a network of rain gauges in the South African sub-tropical zone, Durban and 2-year 1-minute integration time data from disdrometer set up at the Centre of Excellence in the University of KwaZulu-Natal. The result is based on the work of Drufuca, Pawlina-Bonati and Begum *et al.*, where rain events are taken as cells that move across a given area at an average velocity. The rain rates for 12 mm/h and below which are considered stratiform are assigned an advection velocity of 6 m/s, while those above the 12 mm/h are assigned a velocity of 10 m/s. By the use of these advection velocities, the durations of threshold rainfall rates are converted to their corresponding cell extension distances from where equiprobable values of those distances are related to the rain rates from graphical plots. This method of conversion is called "Synthetic Storm" [11, 19-21]. From (5-5), we see that a rain event of 5 mm/h and above occupies an equivalent path that is 24 km long, while a rain rate of 60 mm/h can stretch over 7.7 km. This information is an input requirement for path attenuation prediction and is also useful in site diversity planning.

For example, a given link can be rerouted or be provided a back up by configuring it to another geographical link separated by 8 km whenever rainfall of 60 mm/h intensity occurs.

$$D = 51R^{-0.46} \qquad (5\text{-}5)$$

It has been established that rain varies in its vertical structure. Some tropical regions that experience high rainfall rates have been shown to have rain heights that increase with rain rates up to about 10 km [9, 22].

This implies that the cumulative distribution of rain rate alone is not sufficient to estimate the attenuation; knowledge of rainfall distribution beyond the 0ºC isotherm height is also vital. Bryant *et al* through empirical analysis deduced a formula for the rain height that increases as the rain rate increases. A relationship for the change in value for the rain freezing height at high rain rates in tropical regions was deduced to be of the form [9]:

$$H_{fr} = 4.5 + 0.0005R^{1.65} \qquad\qquad (5\text{-}6)$$

In exponential form, though with reduced accuracy, it can be re-written as:

$$H_{fr} = 4.2\, e^{0.0029R} \qquad\qquad (5\text{-}7)$$

The exponent estimates the growth in height from the freezing height point as indicated in Fig. 5-1.

5.3.1.3 Angular Coefficient of Elevation

With low elevation angles, it is expected that the horizontal path would be more prone to more attenuation activity than in the path of higher elevation angle as noted in temperate zones. We reason that this is because of the larger rain cell diameter that stretches over the path for rain rates below the break point. This can be seen from the equation of the rain cell size distribution described in (5-5): convective cells have smaller diameter than those of the stratiform. For some tropical zones, it has been noted that attenuation due to rain increases with high elevation angles. This supports the proposal that the effect of rain from an equal rain height on slant paths increases according to the elevation angle in tropical zones [23-24].

This can be attributed to the "birth" of multiple cell activity in tropical zones. In the case of the vertical structure of rain, the rain cell diameter is expected to be less from the rain height and grows as it meets the atmospheric wind turbulence at lower heights. This elevation dependent scenario was empirically verified by [9] who gave an expression for the elevation coefficient for elevation angles between 0 and 90 degrees. This effect can be modelled and determined mathematically by the illustration of the figure in Appendix A-1.
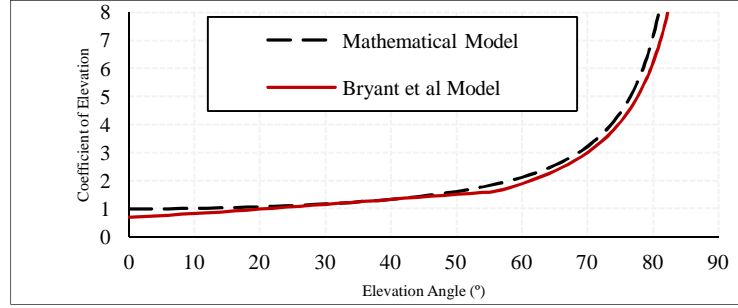
Figure 5-2 Comparison for variation of coefficient of elevation, ξ with elevation angle, θ

This mathematical model is compared to the empirical model obtained by [9] from ITU-R data bank (comprised 1300 years of beacon measurements from 213 site locations) and the result is shown in Fig.5-2. The empirical results are described by equations in appendix B.2 and B.3. It is seen that this mathematical model presents a continuous curve that relates very closely to the values obtained from the empirical model. Therefore the path is intercepted more by rain in the lower elevation angles than it is when the elevation angle is higher-a significant result for attenuation studies in temperate zones which experience single rain structures in rain events.

5.3.2 Proposed Rain Cell Growth factor

The growth factor for the rainfall rates ς_1 in the first rain cell for terrestrial links is given by a truncated-Gaussian shape [11]:

$$\varsigma_1 = 1 + \left(\varsigma_m - 1\right) \exp - \left(\frac{(R - (R_b/\pi))^2}{2\zeta^2}\right) \qquad (5\text{-}8)$$

where R is the point rain rate, R_b is the rain rate where the rain cell is assumed to break into multiple structure, ς_m is the peak growth rate, (R_b/π) is the rain rate at the peak growth rate (point of inflexion) and ζ determines the width of the curve shape where:

$$\varsigma_m = \exp\left(\frac{0.693 \times R_b/\pi}{R_b}\right) = 1.24681 \qquad (5\text{-}9)$$

$$\zeta = (R_b - R_b/\pi) = 0.6817 R_b \qquad (5\text{-}10)$$

The truncate is introduced to compensate for the effect of "minimal" rainfall rates. When a rainfall event starts, small drops collect on the antenna terminals both at the transmit and receive ends. The signals are absorbed by those drops causing loss of signal power.

A rain event is proposed to start as a stratiform event and grows with uniform exponential growth after which it becomes amorphous. In this region, the intensity is expected to peak randomly to any value until a maximum value is attained for that event after which the rain rates decay and rainfall stops. If in the same event there occurs another rapid increase in intensity, then that is considered as a different rain cell structure culminating into a multiple cell rainfall event. Therefore, the effect of any other rain cell structure on attenuation which is a common occurrence in tropical climate may be accounted for after the break point by the growth factor of the second cell; ς_2 .This is achieved by replacing R in (5-8) with $R_2 - (R_b - R_b/\pi)$ where R_2 is any rain rate value above break point, $R_2 > R_b$ in the second cell. The slope of the growth of the second cell is determined from Fig.4-3 to have a value equal to 95 % of that of the first cell:

$$\varsigma_2 = 1 + \left(0.95\varsigma_m - 1\right) \exp - \left(\frac{(R_2 - R_b)^2}{2\zeta^2}\right) \qquad (5\text{-}11)$$

Since it has been noted that in tropical zones, attenuation increases with higher elevation angles [23-24], we introduce a factor in the growth of the second cell structure to compensate for this variation. The amplitude of the inflexion point of the second cell is modified by the sine of the elevation angle to account for the vertical variability in the second rain cell with respect to the path inclination as the second cell develops from the frozen precipitation (this is a logical approach). Therefore for slant path, the growth of the second cell is described by:

$$\varsigma_2 = 1 + \left[\left(0.95\varsigma_m - 1\right) \sin \theta\right] \exp - \left(\frac{(R_2 - R_b)^2}{2\zeta^2}\right) \qquad (5\text{-}12)$$

Thus the attenuation effect of the rain column height is experienced more on a highly elevated path than it would be on a low lying path in the tropical zones due to this cell multiplicity.

From the knowledge of the break point rainfall rate values for a desired location, the growth of rain rates can be determined from (5-8) and (5-12). Fig.5-3 illustrates the graphical representation of the growth of rain rates for some locations in tropical zones around the globe. In the parentheses are the break point rain rate followed by the elevation angle of the link.

The break points have been taken to be the value of rain rates exceeded for 0.01% of the time in a year for locations whose break points are not available from measurements. Note the effect of low elevation angles at the break point for Bangkok (54.8º) and Nairobi (56.9º) in the second rain cell structure. The vertical reduction in attenuation is accounted for by the sine of the angle of elevation in the second rain cell. Since the value of attenuation at 0.01% of time is taken to occur after the break point, the highly elevated sites experience more attenuation at equal probability.
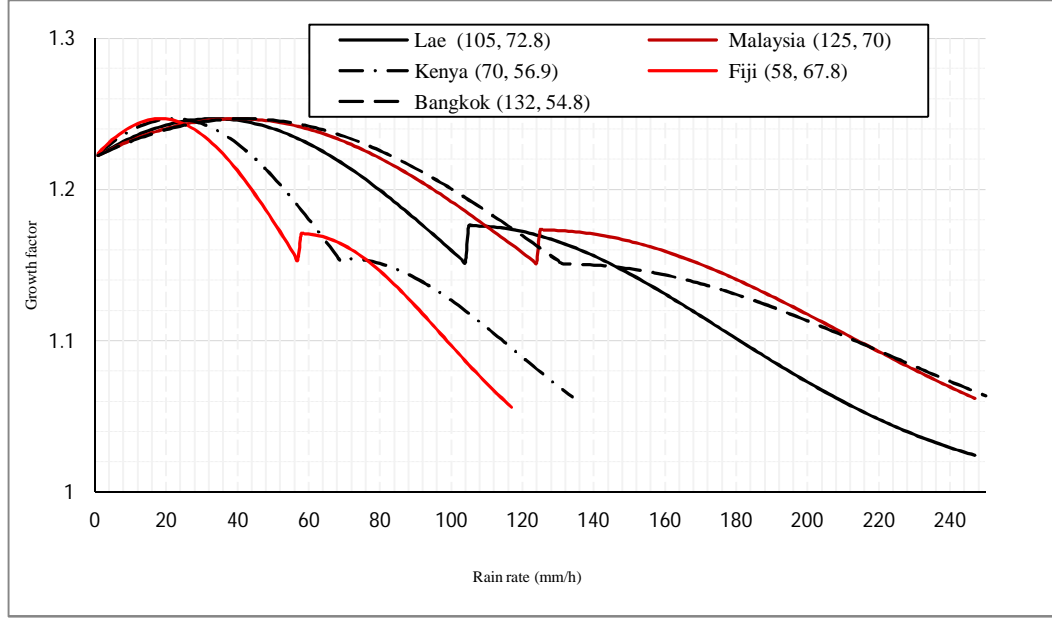
Figure 5-3 Rain rate growth within rain cells for the selected tropical sites depicting second cell growth forms with equal maximum amplitude of the first cell

5.4 Slant Path Attenuation

From our earlier work, we found that the mean intercept, I of the path in rain for a microwave path is described by [11]:

$$I = \frac{2}{\pi} L_G \left(1 + \frac{1.047}{\xi_\theta}\right) \left(\frac{1}{\xi_\theta L_G/D + 1}\right) \tag{5-13}$$

where the variables bear the same meanings described earlier.

From (5-13) we see that the mean intercept reduces with higher elevation angles as is physically expected. However, for application in satellite links which are slanting with respect to the horizontal plane, the attenuation due to rain on the link is experienced only up to the rain height as shown in Fig.5-1. As the rain height increases, so is the mean intercept of the path since the slant path equally increases. Therefore, the value of L changes with the rain height which is a function of the rain rates as described in (5-6a).

The slant path rain attenuation is the product of the specific attenuation (dB/km) and the effective path length,L_e. And since L_e can also be expressed as the mean length intercepted by a rain cell, we have:

$$A = (\gamma L_e) \tag{5-14}$$

$$A = \left(\gamma \frac{L_G}{cos\theta}\right) \frac{2}{\pi} \varsigma \left(1 + \frac{1.047}{\xi_\theta}\right)\left(\frac{1}{\xi_\theta L_G/D+1}\right) \qquad (5\text{-}15)$$

where A (dB) denotes the attenuation, γ is the specific attenuation (dB/km), $D(R)$ (km) is the diameter of the rain cell which is a function of rain rate, $L (R)$ (km) is the horizontally projected path length and θ, the elevation angle. ξ_θ is the elevation coefficient, and ς is the factor introduced by the growth of rain rates within the cell.

By definition of the path reduction factor by ITU-R [2], and from (5-15) we deduce the overall slant path reduction factor, r as:

$$r = \varsigma \frac{2}{\pi}\left(1 + \frac{1.047}{\xi_\theta}\right)\left(\frac{1}{\xi_\theta L_G/D+1}\right) \qquad (5\text{-}16)$$

From rain rate cumulative distribution (CD) exceedances plots in tropical zones, there is evident break away point in the rain rate just before the rain rate exceeded at 0.01% of time. At this break point, we assume the occurrence of a second rain cell above the initial one. The rain rate growth factor at this point rises to 95% of the value experienced at the point of inflexion of the first cell (this may not be true in all cases).
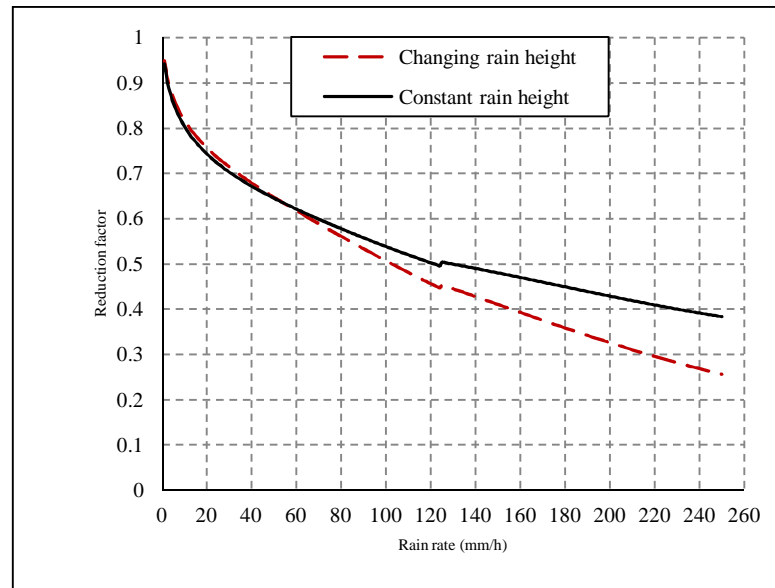

Figure 5-4 Path reduction factor variation with path lengths and rain rate for Johor-Bahru, Malaysia indicating the break points in the prediction at $R_b = 125$ mm/h, $\theta = 70°$

The slant path reduction factor at the 0.01% of time $r_{0.01}$ is therefore the product of (5-16) and ς_2 of (5-12) since it occurs in the second cell i.e. for the attenuation beyond R_b, the growth of rain rates takes the form given by the curve of the second cell.

This estimation is suggested for further investigations since the second cell may not fully follow the growth of the first one. This characteristic of the break point is depicted in Fig.5-3 and Fig. 5-4.

Fig. 5-4 shows the reduction factor modelled for a satellite link in Johor-Bahru Malaysia which has a break point rain rate value of 125 mm/h and elevated at 70º. The break point and increase in attenuation is depicted on the slope of the curve after 125 mm/h rain rate. The overall effect on the reduction factor by assuming a constant rain height of $H_r = 4.86$ km rather than an increasing height described by (5-6a): $H_r = 4.5 + 0.0005R^{1.65}$ is also shown. Assuming a constant rain height results in an under estimation of 19.34 % for signal attenuation compared to the increasing height for Johor Bahru at the break point rain rate. More investigations are therefore required to determine the effective rain height for tropical zones to be adopted by the ITU-R.

Having noted this, the standard ITU-R model stipulated by ITU-R Rec. P.618-9 [4] was used with the height model of (5-6a) to reduce the error margin and the improvement is noted in the model in the tropical zones bound by 24ºN or 24ºS latitudes.

5.5   Results and Discussion

5.5.1 Prediction Based on Full Rain Rate

In order to show the applicability of the proposed model for full rain rate distribution, the graph of Fig.5-5 is plotted for the full rain rate prediction for Lae in Papua New Guinea using Bryant *et al* model and the proposed model. The two models are compared to show that the proposed model can sufficiently be used to give prediction for full rain rate range apart from the break point and the value exceeded at 0.01% of time. Ramachandran *et al* by the use of the modified ITU-R model [14] noted an attenuation saturation of 22.7 dB for PNG which can be seen in Fig. 5-5 in the graph of the proposed model at 0.001% of time (150 mm/h). The proposed model is seen to grow slowly after the break point which is as a result of the decay in rain rate growth and the effect of the vertical reduction factor.
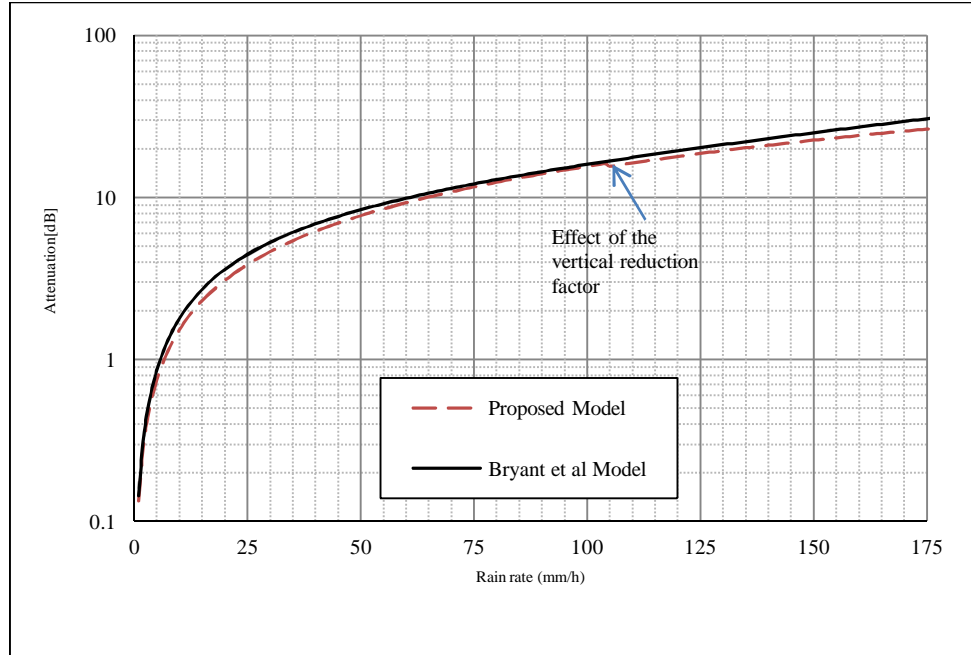
Figure 5-5 Attenuation break point as described for Lae site in Papua, New Guinea (PNG)

5.5.2 Prediction based on $R_{0.01}$

The proposed set of slant path attenuation equation is given below:

Path Reduction Factor	$r_{0.01} = \varsigma \dfrac{2}{\pi}\left(1 + \dfrac{1.047}{\xi_\theta}\right)\left(\dfrac{1}{\xi_\theta L_G/D + 1}\right)$	(5-17)
Rain rate and Attenuation Growth	$\varsigma = \varsigma_2 \text{ or } \varsigma_2\varsigma_3$ $\varsigma_2 = 1 + \left[(0.95\varsigma_m - 1)\sin\theta\right]\exp-\left(\dfrac{(R_2 - R_b)^2}{2\zeta^2}\right)$ $\varsigma_3 = \varsigma_m$, $\varsigma_m = 1.24681$, $\zeta = 0.6817 R_b$	(5-18a) (5-18b)
Elevation Coefficient	$\xi_{\theta,} = 1/\eta; \quad \eta = 1.0175 - 0.0029\theta - 0.0001\theta^2$	(5-19a)

The height and diameter models are described by:

$$D = 51R^{-0.46} \tag{5-19b}$$

$$H_R = 4.5 + 0.0005R^{1.65} \tag{5-19c}$$

These models are for tropical locations bound by latitudes 24ºN or 24ºS, otherwise the ITU-R P.839-3 [22] is used to determine the mean isotherm rain height. The measured value of $R_{0.01}$ (mm/h) from long term data is then used to find specific attenuation, $\gamma_{0.01}$ (dB/km), where the value of measured $R_{0.01}$ is not available, ITU-R P. 837-5 [35] is used, thus:

$$\gamma_{0.01} = \alpha R^{\beta}_{0.01} \tag{5-20}$$

We use (21) to determine the attenuation at the 0.01% of time.

$$A_{0.01} = \gamma_{0.01} L_s \ r_{0.01} \tag{5-21}$$

Only the statistical values at 0.01% of time for rain attenuation are compared since there is more desire to see the applicability of the model to all tropical zones at the high rain rates of the CD, and the other reason is the inaccessibility of attenuation data CD for all the stations we desired to analyze. However, we have used Lae site as in Fig. 5-5 to show that our model works well for all the rain rate ranges a part from the 0.01% of time value in the tropical stations as well.

5.5.3 Results for Sampled Tropical Links

We have provided the prediction results for attenuation due to rain at the 0.01% of time by the use of the three prediction models (ITU-R model, Bryant *et al* Model and the Proposed Model). The key interests are the deviation of the predicted values from the measured values at different elevation angles, frequencies and rain rates. In the samples tested are elevation angles between 20.1° and 89°. The frequencies of the links used are those between 11.2 GHz (KU) and 39.6 GHz (Q) bands. This is the reason why Spinno d'Adda site in Italy which lies out of the equatorial tropics at (45.4ºN, 9.5ºE) is included in this work. The rain rates fall between 75 mm/h and 132 mm/h for the break point values. Whenever the measured break point rain rate is not available, the value of $R_{0.01}$ is assumed. Having noted the difficulty that arises in modelling the changes in rain structures beyond the break point, the reduction factor of (5-16) is used for the range of rain rates before break point where $\varsigma = \varsigma_1$ otherwise we use ς_2 at the break point and thereafter. For uniformity purposes, all the station heights above the sea level were neglected since not all information was available. The specific attenuation values were derived based on the polarization and frequency dependent parameters (α, β) given in ITU-R P.838-3 [1]. The values (α, β) were interpolated for specific frequencies implemented on the sample links with the given polarization angles in Table 5-1. Table 5-2 presents the calculated results.

Table 5-1 Link parameters used in the calculations

Station	Frequency (GHz)	Pol.	Elevation angle (º)	$R_{0.01}$(mm/h)	α	β
Malaysia, UTM-Johor [27]	12.594	V	70	125	0.028605	1.10585
Malaysia, USM [38]	12.255	V	40.1	130	0.02455	1.1216
Lae, PNG [9]	12.749	V	72.8	110	0.03063	1.12000
Suva, Fiji [33]	11.61	C	68.7	63	0.02093	1.14165
Surabaya [9]	11.2	C	20.2	120	0.01752	1.18820
Bangkok [31]	12.75	V	54.8	137	0.0300	1.12000
Nairobi [32]	11.6	C	56.9	75	0.02093	1.14165
Indonesia [31]	12.32	V	64.7	125	0.02455	1.1216
Nigeria [29]	11.6	C	48.3	135	0.02093	1.14165
Spinno d'Adda [9,36]	39.6	C	37.7	38	0.3304	0.9346
	18.7	V	37.7	38	0.05978	1.08221
Bangladesh [34]	12	V	61.8	132	0.0168	1.1218
	20	V	61.8	132	0.0691	1.065
Brazil Rio de Jeneiro	11.452	C	62.8	80	0.02093	1.17602
Belem [37]	11.452	C	89	125	0.02093	1.17602

Table 5-2 Measured and calculated attenuation values at 0.01% of the time: 3 models

Station	$A_{0.01}$ (dB) Measured	$A_{0.01}$ Proposed Model (dB)	$A_{0.01}$ ITU-R Model (dB)	$A_{0.01}$ Bryant *et al* Model
Malaysia, UTM-Johor [27]	25	22.65	17.053	17.702
Malaysia, USM [38]	23.5	24.546	19.696	18.66
Lae, PNG [9]	17.1	16.95	16.758	17.34
Suva, Fiji [33]	9.7	9.717	8.636	7.93
Surabaya [9]	28.5	29.18	28.12	15.86
Bangkok [31]	23.4	26.33	20.78	22.98
Nairobi [32]	8.1	10.69	10.89	9.41
Indonesia [31]	21.9	21.5	17.15	16.74
Nigeria [29]	20.8	21.787	17.49	18.41
Spinno d'Adda [9,36]	37.2	43.577	51.047	38.67
	14.4	16.83	14.63	11.97
Bangladesh [34]	13.8	13.04	11.3	12.96
	39.2	40.66	32.3	40.4
Brazil Rio de Jeneiro	13.1	12.32	10.905	12.109
Belem [37]	20.1	18.03	18.30	17.387

Elevation angle dependence: Given the link set up in Surabaya with low elevation of 20.2°, we expect that if the rainfall event is a single cell, then the length of the link intercepted by a rain cell would be longer compared to a highly elevated link, which is due to the longer horizontally projected path below the rain height level. Also, the low elevation angle has less reduction effect on the rain cell diameter and signal ellipticity since the elevation coefficient is almost unity as seen from (5-13). The proposed model is seen to give a result very close (97%) to the measured value at Surabaya; the same close (95.5%) result is obtained for Malaysia, USM with the link at 40.1° despite the expected error sources. The other two models underestimate the measurements. For high elevations, all the three models perform well for the given ranges of rain rates and frequencies especially in Belem, Brazil with elevation at 89°. In the second case when the occurrence of rainfall takes place in the form of multiple cell structures after the break point, which is a common phenomenon in tropical regions, the highly elevated link may experience higher attenuation compared to low lying links. This scenario can be explained with the results from Malaysia, Johor Bahru site and Indonesia. There is significant underestimation by the other two models despite the fact that they perform fairly well for other high rain rate sites like Belem in Brazil (125 mm/h), Bangladesh (127 mm/h) and Nigerian (130 mm/h) sites which all have high elevated links.

Therefore the conjecture in the proposed model of shape and multiplicity for rain cell structures after the break point is good enough to give better prediction results for regions with more than double rain cells. The value of growth factor used for the two sites is $\varsigma_2 \varsigma_3$.

Frequency dependence: In deriving the mean intercept in (5-16), the assumption made was to make the changing ellipsoidal curvature of the link path which is inversely proportional to the square-root of frequency, to be constant in view of a rain field. The other variable factor that is frequency dependent would be the propagation coefficients, α and β. The proposed model gives 16% over-estimation of measured value for attenuation at the Ka-band frequency of 18.7 GHz used in Spinno d'Adda, Italy site and notably the average break point rain rate is quite low (38 mm/h). For the Q-band frequency of 39.6 GHz, the proposed model results to 17 % overestimation. At all the other KU-band frequencies between 11 GHz and 13 GHz with all other factors notwithstanding, the proposed model gives results within 85% and 99% of measured values. Good results are also obtained from the other two models.

5.5.4 Error Estimations

Some sites whose polarizations were not obtained were assumed to be circular or vertical. For circular polarization, the values of the coefficients are derived from equations in appendix A.1. This assumption and the interpolations made to determine the coefficients for the different frequencies may introduce some errors. The values of the rain rates at 0.01% of time $R_{0.01}$ and rain rate at break point, R_b were taken to be equal at some instances; this caused the proposed model to overestimate the reduction factor though by a small margin of 1.2%. The station height above the sea level was assumed to be minimal in all the sites. ITU-R P.311-13 [39] stipulates the error analysis method used to determine the percentage errors in the prediction results:

Percentage error is calculated as,

$$e_i = \frac{A_{pi} - A_{mi}}{A_{mi}} * 100 \% \quad (i = 1 \text{ to N}) \tag{5-22}$$

$$\text{for: } |A_{pi} - A_{mi}| < 1, E_i = 0 \tag{5-23}$$

where A_{mi} is the measured value, A_{pi} is the predicted value, N is the total number of sites sampled

Standard deviation for the distribution of error is,

$$\sigma_{ei} = \sqrt{\frac{1}{N}\sum_{i=1}^{N} e_i^2 - (\mu_{ei})^2} \tag{5-24}$$

Mean square error (MSE) for each point of % time exceedances:

$$\mu_{ei} = \frac{1}{N}\sum_{i=1}^{N} e_i \tag{5-25}$$

Root Mean Square Error (RMS) is the obtained from the standard deviation and the MSE defined as:

$$\delta_{ei} = \sqrt{\mu_{ei}^2 - \sigma_{ei}^2} \tag{5-26}$$

ITU-R P.311-13, stipulates that best model has lowest standard deviation and RMS for the points analyzed. Table 5-3 shows the results of the error analysis.

Table 5-3 Error tests for the models

Parameters	Models	Percentage of time (0.01%)
μ_{ei}	Proposed Model	8.52
	ITU-R Model	14.52
	Bryant *et al.* Model	15.72
σ_{ei}	Proposed Model	8.14
	ITU-R Model	10.00
	Bryant *et al.* Model	12.47
δ_{ei}	Proposed Model	0.62
	ITU-R Model	10.52
	Bryant *et al.* Model	9.58

5.6   Conclusion

The focus of this work is to fully model rain as a birth of a distinct cell or cells that grow and die with time. The approach is based on physical modelling of the various features of rain and link path as they contribute to the attenuation. Therefore, the accuracy of the overall model can be increased by continual optimization of any of these aspects, making it an adaptive and simple model.

We have shown that up to three rain structures occur in some tropical sites like in Malaysia and Indonesia. It is worthwhile to note that the value of ζ may be climate dependent, as it changes the growth rate value of the rain cell : convective cells grow and die rapidly while stratiform cells as encountered in temperate climates, have a slower rain rate growth. However, the value of ζ for the truncated-Gaussian growth which is given in (10) as, $\zeta = 0.6817R_b$, is empirically determined and is adequate since the difference in growth rates is compensated for in the growth of the second cell where the rain form is highly convective.

A single input of R_b or $R_{0.01}$ for a link planning engineer is sufficient to estimate the optimal fade margin provision by the use of this proposed model. This has made it easy to determine attenuation due to point rain rate which is applicable in seasonal attenuation mitigation: Cumulative rain rate distributions require long term data with very short integration time (preferably 1- minute) to achieve accurate measurements and also vary per given location. The full range of elevation angles is catered for by the proposed model and the rain cell diameter distribution obtained from the subtropical climate data is useful in the satellite link prediction without any modification.

It is worthy to note that in the proposed approach used in this work, emphasis lies in the way the rain rates are proposed to grow within the rain cell. This is coupled with the fact that multiple rain cells occur after the rain rate exceeded 0.01% of the time is attained. Therefore ultimate improvements in the attenuation prediction may be achieved iff the best mathematical model is used to describe the growth of rain rates and rain cells.

The growth equation in (5-18$a\&b$) is the truncated-Gaussian form. This can be replaced by any other expression that would best describe the growth. Thus, from Chapter 3 (see page 46, Table 3-1), we use the result obtained for the slope factor, $\lambda = 2.267$ in the power law growth model to describe this scenario. The same analysis in the truncated-Gaussian model is used to deduce the growth form for satellite links and this is described by:

$$\varsigma_{0.01} = 1 + nR^{-\frac{1}{\lambda \sin \theta}} \quad ; \quad \lambda = 2.267 \tag{5-27}$$

where $n \geq 2$ is the number of rain cells after the break point in a given tropical site.

The multiplicity of cells is noted in high rainfall areas like in Indonesia and Johor, Malaysia where the number of cells, $n = 5$ is used. Table 5-4 below shows the results obtained from this method:

Table 5-4 Measured and calculated attenuation values at 0.01% of the time: 4 models

Station	$A_{0.01}$ (dB) Measured	$A_{0.01}$ Proposed Gaussian Model (dB)	$A_{0.01}$ Proposed Power Law Model (dB)	$A_{0.01}$ ITU-R Model (dB)	$A_{0.01}$ Bryant et al Model
Malaysia, UTM-Johor [29]	25	22.65	22.393	17.053	17.702
Malaysia, USM [28]	23.5	24.546	22.717	19.696	18.66
Lae, PNG [19]	17.1	16.95	16.958	16.758	17.34
Suva, Fiji [24]	9.7	9.717	10.205	8.636	7.93
Surabaya [19]	28.5	29.18	27.00	28.12	15.86
Bangkok [22]	23.4	26.33	25.02	20.78	22.98
Nairobi [23]	8.1	10.69	10.737	10.89	9.41
Indonesia [22]	21.9	21.5	20.822	17.15	16.74
Nigeria [21]	20.8	21.787	20.45	17.49	18.41
Spinno d' Adda [19,26]	37.2	43.577	43.37	51.047	38.67
	14.4	16.83	16.75	14.63	11.97
Bangladesh [25]	13.8	13.04	12.59	11.3	12.96
	39.2	40.66	39.26	32.3	40.4
Brazil Rio de Jeneiro	13.1	12.32	12.40	10.905	12.109
Belem [27]	20.1	18.03	17.90	18.30	17.387

Table 5-5 gives the error values as were earlier defined.

Table 5-5 Error tests for the four models

Parameters	Models	Percentage of time (0.01%)
μ_{ei}	Proposed Gaussian Model	8.52
	Proposed Power Law Model	8.33
	ITU-R Model	14.52
	Bryant *et al.* Model	15.72
σ_{ei}	Proposed Gaussian Model	8.14
	Proposed Power Law Model	7.96
	ITU-R Model	10.00
	Bryant *et al.* Model	12.47
δ_{ei}	Proposed Gaussian Model	0.62
	Proposed Power Law Model	0.60
	ITU-R Model	10.52
	Bryant *et al.* Model	9.58

From the mean error values for all the 15 sites, the proposed model overestimates the measured values by 8.33 %, however the ITU-R model results in an underestimation with 14.52 % in error followed by the Bryant *et al.* model with 15.72 % in error. The standard deviations for the error distribution are 7.96, 10 and 12.47 respectively. The power law model has the least RMS error of 0.60 for the sites sampled for this study.

Other forms of mathematical estimation of the rain cell distribution may also be used to estimate the attenuation decay factor along satellite path links and the results compared with the current form so as to obtain the best model. With the current approach, the determination of the exactness of ς, is taken to be the measure towards achieving the long term solution in attenuation prediction. And this is dependent on local rainfall characteristics. Integrated long-term rain rate data have significant errors.

A.5.1 ITU-R P.618-9 Model

5.A.1. Horizontal path reduction factor, for 0.01% of the time

$$r_{h0.01} = \frac{1}{1 + 0.78\sqrt{\frac{L_G \gamma_{R_{0.01}}}{f} - 0.38[1 - \exp(-2L_G)]}}$$ (A1)

$$\vartheta = \tan^{-1}\left(\frac{h_r - h_s}{L_G r_{0.01}}\right)$$ (A2)

The adjusted relative slant path, $L_{(sr)}$

$$L_{(sr)} = \begin{cases} \frac{L_G r_{0.01}}{\cos\theta} & \text{for } \vartheta > \theta° \\ L_s & \text{for } \vartheta \le \theta° \end{cases}$$ (A3)

5.A.2. Vertical path adjustment factor, for 0.01% of the time

$$r_{v0.01} = \frac{1}{1 + \sqrt{\sin\theta}\left(31(1 - e^{-(\theta/(1+\chi))})\frac{\sqrt{L_{(sr)}\gamma_{R_{0.01}}}}{f^2} - 0.45\right)}$$ (A4)

$$\chi = \begin{cases} 36° - |\varphi| & \text{for } |\varphi| < 36° \\ 0 & \text{for } |\varphi| \ge 36° \end{cases}$$ (A5)

The effective path length,

$$L_E = L_{(sr)} r_{v0.01} \quad \text{(km)}$$ (A6)

5.A.3 Attenuation for any other % exceedance (p)

$$A_p = \left(\frac{p}{0.01}\right)^{-(0.655 + 0.033 \ln(p) - 0.045 \ln(A_{0.01}) - z(1-p)\sin\theta)} \quad \text{(dB)}$$ (A7)

$p \ge 1\%$ $z = 0$

$p < 1\%$ $z = 0$ for $|\varphi| \ge 36°$

         $z = -0.005\,(|\varphi| - 36)$ for $\theta \ge 25°$ and $|\varphi| < 36°$

         $z = -0.005\,(|\varphi| - 36) + 1.8 - 4.25\sin\theta$, for $\theta < 25°$ and $|\varphi| < 36°$

5.A.4 Circular polarization

$$k = [k_H + k_V + (k_H - K_v)cos^2\theta \cos 2\tau]/2$$

$$\alpha = [k_H\alpha_H + k_V\alpha_V + (k_H\alpha_H - K_v\alpha_V)cos^2\theta \cos 2\tau]/2k$$

$$\text{where } \tau = 45°$$

A.5.2 Bryant *et al*. Model

The parameters of the model equations are summarized below:

5.B.1. Attenuation equation

$$A = \frac{D_m k_n k\gamma}{\cos\theta} \frac{L/D}{\xi L/D + 1} \tag{B1}$$

$$\text{where } k = 1.57, k_n = \exp(0.007R)$$

5.B.2. Coefficient of elevation

$$\xi = \frac{1}{\sqrt{2}}\exp(\sin\theta), \text{ for } \theta \le 55° \tag{B2}$$

$$= 1.1 \tan\theta , \theta > 55° \tag{B3}$$

5.B.3. Rain cell diameter and height models

$$H_R = 4.5 + 0.0005R^{1.65} \tag{B4}$$

$$D_m = 340R^{-1.2} \tag{B5}$$

5.7   References

[1] International Telecommunications Union, "Specific attenuation model for rain for use in prediction models," *Recommendation P. 838-5*, ITU-R Recommendation, 2005.

[2] International Telecommunications Union, "Propagation prediction techniques and data required for the design of terrestrial line-of-sight systems," *Recommendation P.530-13*, ITU-R Recommendation, 2005.

[3] Ajayi, G. O., "Some aspects of tropical rainfall and their effect on microwave propagation," *International Journal of Satellite Communication;* 8(3):163-172, 1990.

[4] International Telecommunications Union, "Propagation data and prediction methods required for the design of Earth-Space telecommunication systems," *Recommendation. P.618-9,* ITU-R Recommendation, 2007.

[5] Strutzman W.L., Dishman W. K. "A simple model for the estimation of rain-induced attenuation along Earth-space paths for millimetre wavelengths," *Radio Science*, 17(6):1465-1476, 1982.

[6] Flavin R. K., "Rain attenuation considerations for satellite paths," Report No. 7505, *Telecomm. Australia Research Laboratories*, 1981.

[7] Dissanayake A., Allnutt J., Haidara F., "A prediction model that combines rain attenuation and other propagation impairment along earth-satellite paths," *IEEE Transactions Antennas Propagation*, 45: 1558–1564, 1997.

[8] Crane R. K. *Electromagnetic wave propagation through rain.* Wiley: New York" 1996.

[9] Bryant G. H., Adimula I., Riva C., and Brussard G., "Rain attenuation statistics from rain column diameters and heights," *International Journal of Satellite Communications* 2001, 19(3):263–283, 2001.

[10] "Radio wave propagation modelling for SatCom services at Ku-Band and above," *COST Action* 255 report, 2005.

[11] Akuon P. O. and Afullo T. J. O., "Path reduction factor modelling for terrestrial links based on rain cell growth," *Proc. of IEEE Africon conference*, Livingstone, Zambia, 13-15th Sept. 2011. ISBN: 978-1-61284-991-1.

[12] Pan QW, Bryant GH. Effective rain column diameters and rain column heights in the tropics. *Electronics Letters*, 30(21):1800–1802, 1994.

[13] Moupfouma F. More about rainfall rates and their prediction for radio systems engineering. *Proceedings of the Institute of Electrical and Electronics Engineering Part H*, 134(6):524-537, 1987.

[14] Ramachandran V., Kumar V., " Modified rain attenuation model for tropical regions for Ku-Band signals," *International Journal of Satellite Communication*, 25: 53-67, 2006.

[15] Paraboni A. "Testing of rain attenuation prediction methods against the measured data contained in the ITU-R data bank," *ITU-R Study Group 3 Document, SR2-95/6*, Geneva, Switzerland, 1995.

[16] Akuon P. O. and Afullo T. J. O., "Rain cell size statistics from rain gauge data for site diversity planning and attenuation prediction," *Proc. of Southern Africa Telecommunication Networks and Applications Conference (SATNAC),* East London, South Africa, pp.213-216, 4-7th Sept. 2011. ISBN: 978-0-620-50893-3.

[17] Pan Q.W., Allnutt J.E., "Seasonal and diurnal effects on Ku- band site-diversity performance measured in the rainy tropical region," *Proceedings of the Institute of Electrical and Electronics Engineering, Antennas and Propagation Society International Symposium*, 3:113–116, 2001.

[18] Mime P., Waldeteufel P., "A model for attenuation by precipitation on a microwave earth-space link," *Radio Science*, 15(3): 655-665, 1980.

[19] Drufuca G., Zawadzki I., "Statistics of rain gauge data," *Journal of Applied Meteorology,* vol.14, 1419–1429, 1975.

[20] Pawlina-Bonati A., "Essential knowledge of rain structure for radio applications based on available data and models," *Proceedings of Radio Africa 99,* Gaborone, Botswana, 96–106, 1999.

[21] Begum S., Nagaraja C., Otung I., "Analysis of rain cell size distribution for application in site diversity," *Proceedings of the Institute of Electrical and Electronics Engineering Antennas & Propagation,* pp. 1–5, 2006.

[22] International Telecommunications Union, "Rain height model for prediction methods," *Recommendation P.*839-3, ITU-R Recommendation, 2001.

[23] Bowthorpe B. J., Andrews F. B., Kikkert C. J., Arlett P. L., "Elevation angle dependence in tropical region," *International Journal of Satellite Communication*, 8: 211-221,1990.

[24] Pan Q.W., Bryant G.H., McMahon J., Allnutt J. E., Haidara F., "High elevation angle satellite to earth 12 GHz propagation measurements in the tropics," *International Journal of Satellite Communication,*19(4): 363-384,2001.

[25] Migliora C. G. S., Dugamari J., "Rain rate and attenuation measurements in Brazil," *URSI Commission F. Open Symposium on Regional Factors in Prediction Radiowave Attenuation due to Rain,* Rio de Janeiro, Brazil, 8-13,1990.

[26] Hansson L., "New concept used to predict slant path rain attenuation statistics," *Proceedings of the Institute of Electrical and Electronics,* 137:89-93, 1990.

[27] Abdulrahman A. Y., Rahman T. A., Rahim A. S. K., Ul Islam M. R., "A new rain attenuation conversion technique for tropical regions," *Progress In Electromagnetic Research*, 26: pp.53-67, 2010.

[28] Baptista P., Ed., *Ref. Book Attenuation Measurement Prediction, 2ndWorkshop Olympus Propagation Experiments*, Noordwijk, The Netherlands, Eur. Space Agency WPP-083, 1994.

[29] McCarthy D. K, Allnutt J. E, Salazar W., Omeata E. C., Owolabi B. R., Oladiran T, Ajayi G. O., Raj T. I. and Zaks C., "Results of 11.6 GHz radiometric experiment in Nigeria," *Electronics Letters* 1992; 28(3):316–317.

[30] Mandeep, J. S., "0°C Isotherm height for Satellite communication in Malaysia," *Journal of Advances in Space Research*, 43(6): 984-989, 2008.

[31] Igarashi K., Minakoshi H., Watari S., Kawamura M., Ojima T., Hemmakorn N., Sang-in A., Srisupasitanon W., Sastrokusmo U., Hassan S. I. S, Reyes R., Maitava K., Sasaki M., Minode T., Yoshimura Y., "Satellite signal propagation experiments in the equatorial region and a development of satellite communication network in Asian pacific region," *Forum on The results of the POST-PARTNERS Experiments*, Tokyo, Japan, 2002.

[32] McCarthy D. K., Allnutt J. E., Salazar W. E., Sitati W., Okoth M., Mutungi J., Odhiambo C. D., Zarks C., "Results of 11.6 GHz Radiometric experiment in Kenya," *Electronics Letters* , 28(3): pp. 316–317, 1992.

[33] Kumar V., Ramachandran V., "Rain attenuation measurement at 11.6 GHz in Suva Fiji," *Electronics Letters*, 40(22):1429-1431,2004.

[34] Islam, M. R. , Rahman, M.A., Anwar F., Rashid M. M., "Performance investigation of earth-to-satellite microwave link due to rain fade in Bangladesh," *Computer and Information Technology, ICCIT 200,. 11th International Conference,* pp.773-778, 2008.

[35] International Telecommunications Union, "Characteristics of precipitation for propagation modelling," *Recommendation P.837-5*, ITU-R P Sers., 2007.

[36] Paraboni A., Riva C., Capsoni C., Codispoti G., Zuliani L. *et al.,* "Propagation and Radar measurements performed in Spinno d'Adda and the Italian planning for the Alphasat TDP5 scientific experiment," *Proceedings of the Institute of Electrical and Electronic,* Antennas and Propagation, Berlin EuCAP, 911-915, 2009.

[37] Couto de Miranda E., Pontes M. S., Mello L. A. R. da Silva, "Rainfall induced satellite beacon attenuation on three 12 GHz links in equatorial and tropical Brazil," *IEEE Ant. & Propagation Society International Symposium*, 4:1892-1895, 1998.

[38] Mandeep J. S., Allnut J. E., "Rain attenuation predictions at KU-band in south east Asia," *Progress In Electromagnetics Research, PIER; 76*: 65–74, 2007.

[39] International Telecommunications Union, "Acquisition, presentation and analysis of data in studies of tropospheric propagation," *Recommendation P.311-13*, ITU-R P Sers., Oct. 2009.

CHAPTER SIX

Conclusion and Future Work

6.1 Conclusion

Rain cell size model has been obtained that is a function of rain rate. The rain cell diameter is described by the function $D = 50\ R^{-0.46}$. This means that stratiform rain event with rain rate of at least 3 mm/h extends up to a maximum of 30 km whilst convective rainfall with rain rate of at least 20 mm/h covers a rain region of 12.6 km in horizontal dimension. Site diversity can be employed as a fade mitigation technique by making sure that any two diversity sites are separated by this distance. The maximum size of the rain field area measured by the point rain rate equipment is found to be 60 km in diameter. It has been shown that the rain cell population per given rain rate decays from small diameters to those with larger diameters. The decay factor is found to be 0.32 for the exponential form and -2.267 for the power law form. This observation can be used to estimate the decay in horizontal path reduction factor for rain events. RADAR scans of rain field area can therefore be used to further confirm the results found in this work. The rain cell size model so generated has been used in attenuation prediction for the terrestrial link and is seen to be very accurate. The same rain cell size model has been used in attenuation prediction for satellite links located in 15 tropical sites in various parts of the world and results in the best performance. The objective of this dissertation to develop and test a scalable rain attenuation model for terrestrial and satellite radio links that has a single rain cell size model as an input has been achieved.

6.2 Future Work

The rain cell size model obtained in this work has proved to be adequate in attenuation prediction. Some confirmation with RADAR data will be good. The rain cell size mapping made for other locations in South Africa is based on data conversion techniques discussed in chapter 2. If rain rate measurements from these other locations are availed, more precise rain cell sizes can then be developed for those locations.

The non-uniformity in rain attenuation has been modelled to vary as rain rates: truncated-Gaussian model. This results in underestimation for attenuation in the lower rain rates regions. It is desirable to model this non-uniformity by considering the spatial distribution of rain drops. This will enable the generation of more accurate path reduction factor as used in rain attenuation prediction. An attempt has been made here by modelling the radio links with a power law form but further investigation is deemed necessary for other mathematical forms.

APPENDICES

A.1   Derivation of Angular Coefficient of Elevation

Consider a link of length, L_s being intercepted by a rain cell of diameter, D as shown in Fig. A-1. By assuming that the same path is being inclined above the initial level, the length of the link in rain reduces for an equal instance of rain height. The intercepting diameter reduces by an elevation index, η described by:

$$\eta = \frac{D_i}{D} \tag{A.1-1}$$

where D_i is the path length in rain at any instance of elevation and D is the actual rain cell diameter at a small elevation angle, θ degrees.

The reduction ratio of the path in rain due to higher elevation angles is proved to be a trigonometric equation expressed as:

$$\eta = \frac{\cos\ (\theta + \Delta\theta_i)}{\cos\theta} \tag{A.1-2}$$

which reduces to be the fractional sum of the sine and the cosine of the elevation angle described by:

$$\eta = (-\tan\theta \sin\Delta\theta_i\ + \cos\Delta\theta_i) \tag{A.1-3}$$

where $\Delta\theta_i$ is taken as a small change in the elevation angle which is incremented in the range $0° \leq \Delta\theta_i \leq 90°$. Thus the solution of (A.1-3) for small continuous angular increments from 0 to 90° becomes:

$$\eta = 1.0175 - 0.0029\theta - 0.0001\theta^2 \tag{A.1-4}$$

with a correlation coefficient of $R^2 = 0.9993$ and where $\eta = 1/\xi_\theta$.
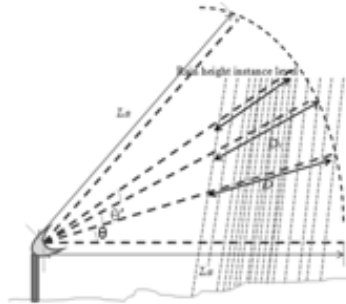

Figure A-1 Illustration of the variation of rain cell diameter with the elevation angle

A.2   Derivation of Mean Path Intercept with Rain Cell

A.2.1 Rain Cell Geometry and Model Parameters

A radio link of projected horizontal path, *ST*, *L* (km) long and a rain cell of diameter *D* (km) as shown in Fig. A.2-1 is assumed. A rain cell centre is considered to move within the oval such that it always intercepts the path *ST*. The interception at the maximum radius of the first Fresnel zone is also illustrated with the dotted lines *ST* which are projected on lines *IG* and *KC* for clarity.

This is illustrated in Fig. A.2-1. The interception with the maximum radius of the first Fresnel zone is also illustrated with the curve lines IG in the lower and CK in the upper part.

A.2.1.1 *Rain Cell Centre along Line WY over the Length XZ*

Let the rain cell intercept the path such that ST is as shown in Fig. A.2-1.

$$ST = 2\frac{D\cos\theta}{2} = D\cos\theta \tag{A.2-1}$$

The mean interception for all angles, i.e. from 0 to $\frac{\pi}{2}$ is equal to

$$ST = \frac{\left\{\int_0^{\frac{\pi}{2}} D\cos\theta \, d\theta\right\}}{\frac{\pi}{2}} = \frac{2D}{\pi} \tag{A.2-2}$$
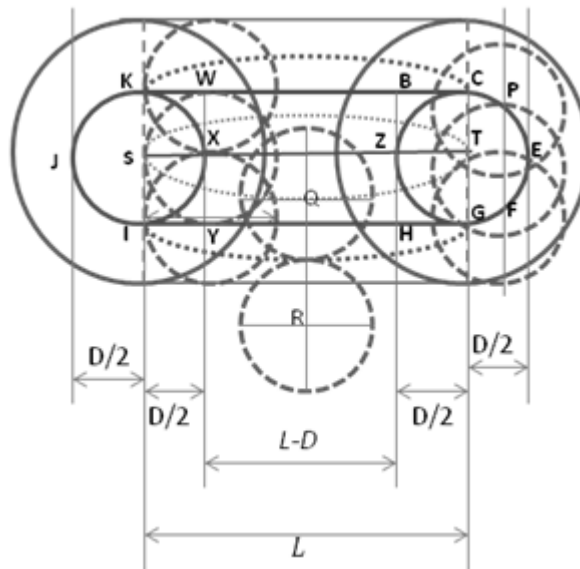

Figure A.2-1 Rain cell centre movement to intercept the path, *ST*

A.2.1.2 *Rain Cell Centre along Line PF over Length ZE*

On the vertical line through T, the overall interception moves from $\frac{2D}{\pi}$ *to* 0.
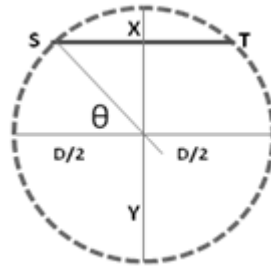

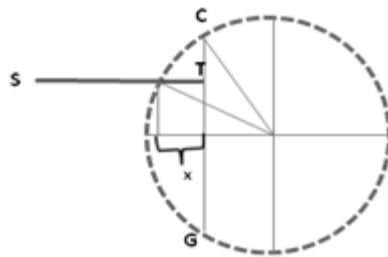Figure A.2-2 Path interception by a single rain cell over the length *L-D*

Figure A.2-3 Path interception at the oval ends

The mean interception for the whole end therefore becomes D/π over the projected *D*length. The other oval end has the same intercept.

The overall weighted mean interception thus becomes (see Fig.A.2-1):

$$I = \frac{\left\{(L-D)\left(\frac{2D}{\pi}\right)+D\left(\frac{D}{\pi}\right)+D\left(\frac{D}{\pi}\right)\right\}}{L+D} \tag{A.2-3}$$

$$= \frac{2D}{\pi}\left(\frac{L}{L+D}\right) \tag{A.2-4}$$

A.2.1.3 *Effect of Fresnel Ellipsoid*

For practical purposes, only the first Fresnel zone will be considered. The rain cell will intercept the path even if it is not on *ST* due to the Fresnel effect. This is shown in figure 2 above with the line *QR* touching the dotted curve line *IG*. The equation of an ellipse can be given by

$$Ax^2 + Bxy + Cy^2 = 1 \tag{A.2-5}$$

The circumference is given as in (A.2-6):

$$C = 4a \in (\varepsilon) \tag{A.2-6}$$

where $\in (\varepsilon)$ is the complete elliptic integral of the second kind. The exact infinite series is defined by:

$$C = 2\pi a[1 - \left(\tfrac{1}{2}\right)^2 \in^2 - \left(\tfrac{1.3}{2.4}\right)^2 \tfrac{\in^4}{3} - \left(\tfrac{1.3.5}{2.4.6}\right)^2 \tfrac{\in^6}{5} - \cdots$$ (A.2-7)
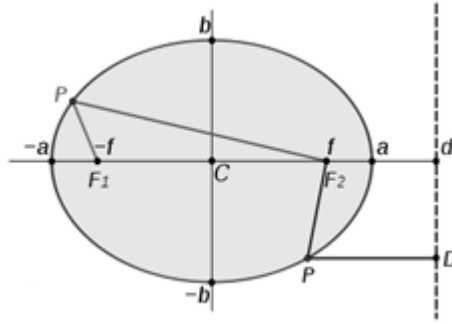

Figure A.2-4 An ellipse with a as major axis radius and b as minor axis radius

This can be simplified further by "vanishing" the denominator by the factor, $f(d)$;

$$f(d) = \tfrac{27}{1024} \left(\tfrac{a-b}{a+b}\right)^8$$ (A.2-8)

Therefore the expression for the circumference reduces to:

$$C \approx \pi(a + b)\left\{1 + \frac{3\left(\tfrac{a-b}{a+b}\right)^2}{10+\sqrt{4-3\left(\tfrac{a-b}{a+b}\right)^2}}\right\}$$ (A.2-9)

The maximum radius of the first Fresnel zone,

$$b = \sqrt{\frac{n\lambda aa}{a+a}}$$ (A.2-10)

$$= 8.657 \sqrt{\frac{L}{f}} \; [m]$$ (A.2-11)

where f is the frequency (GHz) used and L (km) is the path length.

For telecommunications radio link applications, where a $\gg b$, the circumference is given by:

$$C = \pi a \left(1 + \frac{1}{3}\right) \ or \ \pi a \left(1 + \frac{3}{11}\right) \tag{A.2-12}$$

Since approximations have been introduced, the circumference is chosen to be, $C = (4/3) \, \pi a$. The next step is to find the mean intercept that will be introduced when the rain cell cuts into the path of length given by $L = \pi a (2/3)$ i.e. half the circumference. This length is dependent on the path length and the frequency used in the radio link. The maximum interception occurs at the centre of the ellipsoid where $a = L/2$ and D/L is the ratio of the interception of the rain cell to the ellipsoidal length.

$$I_e = (2/3)\pi a \frac{D}{L} = \pi D/3 \tag{A.2-13}$$

where $a = L/2$.

The mean interception for all angles (see Fig. A.2-5) from 0 to $\pi/2$ is given as:

$$\frac{\left(\frac{1}{2}\right)\left(\frac{\pi D}{3}\right)}{\frac{\pi}{2}} = D/3 \tag{A.2-14}$$

The resulting weighted mean interception, I will become:

$$= \frac{\left\{(L-D)\left(\frac{2D}{\pi}\right)+D\left(\frac{D}{\pi}\right)+D\left(\frac{D}{\pi}\right)+L\left(\frac{2D}{3}\right)\right\}}{L+D} \tag{A.2-15}$$

$$= \frac{2D}{\pi}\left(1+\frac{\pi}{3}\right)\left(\frac{L}{L+D}\right) \tag{A.2-16}$$
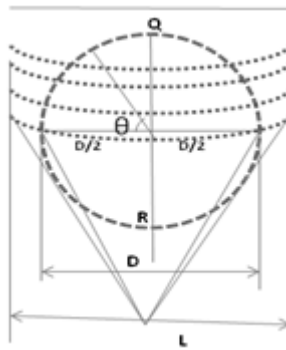

Figure A.2.5 Rain cell intercept with the radio link ellipsoidal path

From above, the effective path intercept that takes the effects of link elevation angle into account is given by:

$$I = \frac{2}{\pi}L\left(1 + \frac{1.047}{\xi_\theta}\right)\left(\frac{1}{\xi_\theta L/D+1}\right) \qquad \text{(A.2-17)}$$

A.3   Proposed Rain Attenuation Growth Factors at 0.01% of the time

A.3.1   Truncated-Gaussian Attenuation Growth

The proposed rain rate growth factor at 0.01% of the time is of the form:

$$\varsigma = 1 + n(\varsigma_m - 1)\sin\theta \exp - \left(\frac{(R-(R_b/\pi))^2}{2\zeta^2}\right) \qquad \text{(A.3-2)}$$

where *n* is the number of cells after the break point and other factors bear the same meanings discussed in this dissertation.

The vertical rain rate variability factor, *sin* θ is taken to be equal to 1 for the terrestrial links.

A.3.2   Power Law Attenuation Growth

$$\varsigma = 1 + nR^{-\frac{1}{\lambda\sin\theta}} \quad ; \quad \lambda = 2.267 \qquad \text{(A.3-3)}$$

where *n* is the number of cells after the break point and other factors bear the same meanings discussed in this dissertation.

The vertical rain rate variability factor, *sin* θ is taken to be equal to 1 for the terrestrial links.

Fig.A.3 shows the plot of a single rain event in Durban, South Africa where, with the onset of a rain event, rain rates grow to a peak of about 60 mm/h and then decays with time.
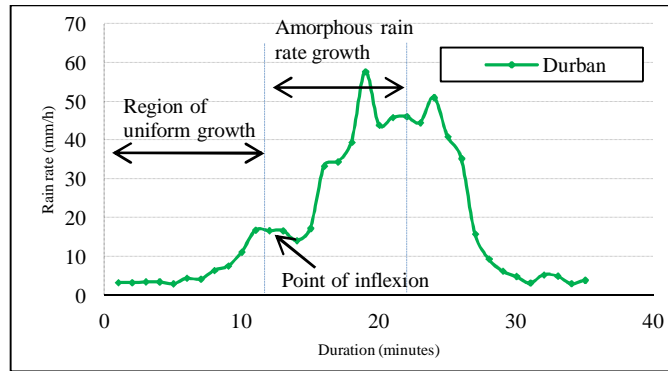
Figure A.3 Rain rate profile for a single rain event in Durban, South Africa.

A.4   MATLAB Code for Inverse Distance Weighting (IDW)

Get the world map and specify the coordinates for South Africa

```
worldmap([-35.2 -22],[15 35])

S = shaperead('landareas','UseGeoCoords',true);
geoshow([S.Lat],[S.Lon],'Color','black');
```

Locate and load the data needed for plotting:
The files are named Diversity, LatSA, LonSA, Disttwo, Spatten1 and Spatten2

```
load Diversity
whos -file Diversity. mat
Y=LatSA;
X=LonSA;
Z = Disttwo;% then Z = Spatten1; Z = Spatten2;
```

Divide the coordinates into smaller grids; apply the INVDIST command to compute the new values

```
[R,T] = meshgrid(16.3:.03125:32.3,-35.2:.0625:-22.2);
[XI,YI,ZI] = griddata(X,Y,Z,R,T,'invdist');
```

Plot the contours of the new values with appropriate line and color property with the values displayed on the contour lines

```
h = geoshow (YI,XI,ZI,'DisplayType','contour'...
  'LineColor','blue');
set(h,'ShowText','on','TextStep',get(h,'LevelStep')*1)
c = 'contour';
clabel(c,h,'LabelSpacing',300,'FontSize',11,...
    'color','r','Rotation',0);

title('Rain Fade Site Diversity Contours')
title('Rain Specific Attenuation at 15 GHz')
title('Rain Specific Attenuation at 26 GHz')
```